THE LYMAN AND WERNER PHOTOABSORPTION BANDS OF MOLECULAR HYDROGEN

by

W. Fabian B.Sc. (Hons)
Department of Physics

A thesis submitted for the degree of
Doctor of Philosophy
at the
University of Adelaide

August, 1971

CONTENTS

SUMMARY

This thesis describes the measurement of absolute oscillator strengths for a number of Lyman and Werner bands of molecular hydrogen in the spectral region 900 to 1100 Angstroms.

In spite of its astrophysical significance and quite precise theoretical calculations, there have been only a few accurate transition strength measurements for molecular hydrogen. There have been to date no optical intensity measurements for the Werner bands, and the recent measurements for several Lyman bands are not in good agreement with the theoretical calculations. The only experimental oscillator strengths which generally agree with theory are those inferred from inelastic electron scattering results. Consequently, there have been to date, no consistent experimental oscillator strengths which may be critically compared with theoretical calculations or used with confidence in astrophysical calculations.

Experimental absorption measurements were made with a fully automated photoabsorption system incorporating photon counting techniques and on-line digital data reduction and storage. The design and operation of this system is described in detail. A one metre near normal incidence monochromator operated in first order with a resolution of about

0.3 Angstroms was used as the dispersing instrument. The monochromator was fitted with a gas discharge lamp operated in a pulsed mode by a thyratron triggered power supply and used with either helium or argon, the continua of which covered most of the required spectral region.

Absolute oscillator strengths were derived from the measured absorption by using a curve of growth analysis. This was simplified by using low pressures where only Doppler broadening is significant. Measurements were made for as many rotational lines as possible for the Lyman and Werner band systems, and band oscillator strengths were obtained from the rotational line strengths using theoretical line strength factors (Hönl-London factors).

The results obtained are in excellent agreement with the electron scattering results and in reasonably good agreement with recent theoretical calculations. From the consistency between the present results and the electron scattering results, it also appears that the theoretical calculations are correct for the Lyman bands, but consistently too high for the Werner bands.

PREFACE

This thesis contains no material which has been accepted for the award of any other degree or diploma in any University. To the best of the author's knowledge and belief it contains no material previously published or written by another person, except where due reference is made in the text.

W. Fabian
August, 1971

ACKNOWLEDGEMENTS

The work described in this thesis was done in association with Mr B.R. Lewis.

The author would like to thank Dr D.G. McCoy for his assistance with the design and construction of the electronics for the photoabsorption system, particularly the digital divider and stepping motor drive and control for the monochromator. The author would also like to thank Professor J.H. Carver for his suggestions during the writing of this thesis.

Finally, the author would like to thank his supervisor, Dr L.W. Torop for his help and encouragement during the work and his suggestions during the writing of this thesis.

CHAPTER I

1. Introduction

In recent years there have been considerable advances in the use of numerical techniques for generating potential curves and molecular wavefunctions. In particular, very accurate calculations have been performed for the ground state and a number of excited states of the hydrogen molecule (e.g. Kolos & Wolniewicz 1965, 66, 69, Wolniewicz 1966, and others), with good agreement between the theoretical eigen values and the observed energy levels. A comprehensive review of theoretical calculations for H_2 up to 1968 has been given by Kolos (1968). More recently, tabulation of the potential curves and extensive references to theoretical calculations for the various states of H_2 have been given by Sharp (1971). There have also been a number of calculations of Franck-Condon factors (Halmann & Laulicht 1968, Spindler 1969 (a) (b) and (c), Allison & Dalgarno 1969, Villarejo et al. 1968, 1969) and electronic transition moments (Rothenberg & Davidson 1967, Browne 1969, Wolniewicz 1969) from which transition probabilities (oscillator strengths) for a number of band systems have been calculated (Allison & Dalgarno 1969, 1970).

It has been pointed out by a number of authors, (e.g. Ehrenson & Phillipson 1961, Peek & Lassettre 1963) that the

oscillator strength is far more sensitive to small variations in the eigenfunctions than the corresponding eigenvalues. Consequently a comparison of theoretical against experimental oscillator strengths is a far more sensitive test of the accuracy of the theoretical wavefunctions than a comparison of eigenvalues against measured energy levels. There have, however, been only a few experimental oscillator strength measurements against which the theoretical values can be compared.

This thesis describes the measurement of oscillator strengths for a number of Lyman and Werner bands of molecular hydrogen. The present results are significantly more accurate than the previous optical measurements (Haddad et al. 1968, Hesser et al. 1968) and are in close agreement with the recent electron scattering results of Geiger & Schmoranzer (1969). Both the present results and the electron scattering results approximately agree with the recent theoretical calculations of Allison & Dalgarno (1970).

1.1 The Ultra-violet Spectrum of Molecular Hydrogen

The far ultra-violet spectrum of molecular hydrogen consists of a number of band systems belonging to transitions between the electronic ground state and several excited states. The first successful analysis of a part of the spectrum was made by Witmer (1926) when he recognized that

the enhanced emission spectrum of hydrogen in argon [first observed by Lyman (1911)] was a v'' progression (v'=3 of the B state).

During the period 1926-1935 a large number of authors studied the ultra-violet spectrum of molecular hydrogen (Werner 1927, Hori 1927, Dieke & Hopfield 1927, Richardson 1930, Jeppesen 1933 and others) and classified it into two groups of transitions, now known as the B-X and C-X systems, giving rise to the Lyman and Werner band systems respectively. The D-X system was also observed in absorption by Hopfield (1930). This system was subsequently observed in emission by Jeppesen (1938). A comprehensive review of the known spectrum and structure of molecular hydrogen up to 1934 is given by Richardson (1934).

Most of the ultra-violet spectroscopic work on molecular hydrogen since this period has consisted of more accurate high dispersion studies resulting in more accurate wavelength measurements and improved molecular constants [e.g. Herzberg & Howe 1959, Herzberg & Monfils 1960, Monfils 1961 (a) and (b), 1965, Namioka 1964 (a) and (b), 1965 and others]. There have also been reported a number of other states with band systems involving the ground state [i.e. $(1s\sigma np\sigma)^1\Sigma_u^+$ and $(1s\sigma np\pi)^1\Pi_u$ states other than the B, C and D states mentioned already]. The $(1s\sigma 3p\sigma)B'\,^1\Sigma_u^+$ state was first reported by Dieke (1958), the $(1s\sigma 4p\sigma)B''\,^1\Sigma_u^+$ and $(1s\sigma 4p\pi)D'\,^1\Pi_u$ states by Monfils [1961 (a) and (b)] and more recently similar

states with n ranging up to 12 have been reported by Takezawa (197C).

Consequently the wavelengths of most of the transitions in the vacuum ultra-violet region of the spectrum have now been tabulated with high precision. However, in spite of these extensive spectroscopic measurements, there have been only a few measurements of transition probabilities for these band systems.

1.2 Experimental Transition Probabilities

Molecular transition probabilities can be experimentally determined by a number of different techniques. The following is a brief summary of the various techniques and the molecular hydrogen transition probabilities obtained by them.

Since the intensity of emitted or absorbed radiation is directly related to the transition probability (oscillator strength) and the number density of emitting or absorbing molecules, intensity measurements are the most direct means of measuring the oscillator strength. There are, however, two other widely used techniques, namely, the measurement of inelastic differential cross sections for high energy electron scattering and the measurement of excited state lifetimes. The widely used anomalous dispersion or "hook" method of Rozhdestvenskii is confined to atomic oscillator

strength measurements and is not applicable to molecular measurements because the line separation is generally too small. The need for an interferometer also limits this technique to lines above 1400Å (Zaidel & Schreider 1970).

Oscillator strengths for molecular hydrogen have been obtained by all of the above mentioned techniques except emission intensity measurements. Emission studies are difficult because the number densities of molecules in the excited states cannot be determined unless the molecules are excited in a predictable manner such as thermal excitation. Also, with the uncertainties in the absolute efficiencies of spectrometers, absolute emission intensity measurements cannot be made. Consequently, many emission intensity measurements are only relative and need to be normalized in some way to give absolute values. In the case of molecular hydrogen, there have been no reported oscillator strengths obtained from emission intensity measurements.

With absorption studies, on the other hand, the number density of molecules in the ground state is readily measured (pressure), and the absolute intensity is not required since the oscillator strength is related to the integrated absorption coefficient. In principle, the integrated absorption coefficient can be obtained by

numerically integrating the measured absorption coefficient over the frequency (or wavelength) range of the absorption line. Unfortunately, ultra-violet absorption lines are generally quite narrow and usually narrower than the resolution width of the dispersing instrument. For example, a typical line in the vacuum ultra-violet may have a width of 0.001Å, and an instrument with a comparable resolution at 1000Å would need to have a resolving power of 10^6. To actually measure the absorption coefficient over the line, however, a resolving power well in excess of 10^6 would be required. The highest resolving power attainable with present dispersing instruments is $\sim 10^6$ (with echelle gratings used in high orders). Resolving power limitations of dispersing instruments are discussed by Samson (1967). Consequently, for such narrow lines, the correct absorption coefficient cannot be measured directly and an alternative technique must be used.

One such technique is the use of high gas pressures such that the lines under investigation are pressure broadened to the extent that they are much wider than the instrument resolution width. This technique has been used on oscillator strength measurements for several bands of N_2 (Ching et. al. 1967), NO [Bethke 1959 (a)] and the Schumann-Runge bands of O_2 [Bethke 1959 (b)] with considerable success. However,

this technique is applicable only to spectral regions where a pressurized cell with windows can be used (i.e. above the Lithium Fluoride cutoff at 1050Å), and cannot therefore be used for the Werner and most of the Lyman absorption bands of H_2.

There is, however, an alternative absorption technique known as the curve of growth or equivalent width method. The curve of growth refers to the growth of the integrated absorption (equivalent width) with the amounts of absorbing material (length or pressure of the absorbing gas column). If the shape of this growth curve is known, the measured equivalent width can be related to the integrated absorption coefficient. This technique has been used for several Lyman bands by Haddad et al. (1968) and Hesser et al. (1968). The results obtained by this technique should, in principle, be accurate; however, the above mentioned Lyman band results are not in good agreement with theory or with each other. Possible sources of error in both works are discussed in Chapter 6.

The most reliable experimental Lyman and Werner band oscillator strength determinations to date have been made by high energy inelastic electron scattering measurements (Geiger et al. 1964, 1966, 1969). In the limiting case of forward scattering where the electron momentum change is

small, the Born approximation for differential cross sections can be reduced to yield optical transition matrix elements (e.g. Geiger 1964). The only limitation of this technique is the difficulty in measuring absolute differential cross sections. Geiger's measurements are only relative and have been normalized to the theoretical elastic scattering cross section of H_2. In view of the results, however, this normalization appears to be accurate. Differential inelastic cross sections for the H_2, B and C states have also been reported by Roscoe (1941); however, individual vibrational levels were not resolved in this work and the measured cross sections represent the differential cross sections summed over the entire band system and therefore cannot be used for a comparison with the present results.

The remaining technique of excited state lifetime measurements offers one distinct advantage over the other oscillator strength measurement techniques, namely, independence of the number density of excited molecules. Lifetime measurements, which have been extensively used for oscillator strength determinations of many unstable molecules and ions which can only be produced in discharge, can be obtained by a number of different techniques such as the phase shift technique described by Lawrence (1965) or the Hanle method described by Lurio et al. (1964). However these

measurements alone cannot be used for the determination of individual band oscillator strengths. The reciprocal of the lifetime is equal to the emission transition probabilities summed over all the decay channels, consequently the branching ratios for decays into the lower levels needs to be known or measured before the individual transition probabilities can be determined. For many molecules, the lower state has a continuum into which the excited molecule can decay. If the transition probability between the upper level and this continuum is large, the measured lifetime and branching ratios for discrete levels will give incorrect transition probabilities. Allison & Dalgarno (1969) have pointed out that the transitions from the $v' > 7$ levels of the B state of H_2 to the continuum of the ground state can give transition probability errors of a factor of 2 or more from lifetime measurements.

Average lifetime measurements of the $v' = 3, 4, 5, 6, 7$ levels of the B state and $v' = 0, 1, 2, 3$ of the C state of H_2 have been obtained by Hesser (1968) using the phase shift technique. These results, however, cannot be used to determine individual band oscillator strengths without assuming the relative transition probabilities (branching ratios).

1.3 Present Measurements

The present experimental oscillator strengths have been obtained with absorption measurements and the curve of growth analysis. In principle, this technique appears to be the most reliable, since the integrated absorption can be related to the oscillator strength without recourse to other measurements for normalization or branching ratios. The experimental equivalent width can be readily related to the integrated absorption coefficient by choosing experimental conditions where the growth curve is that of a Doppler line only, and can therefore be determined. The validity and experimental conditions required for the Doppler curve of growth are discussed in detail in Chapter 3.

Experimentally, the only difficulty with the use of this technique is the need to make measurements under conditions where the observed absorption is very small. This limitation is caused by the relatively poor resolution of the dispersing instrument used (McPhersons model 225 1 metre normal incidence vacuum ultra-violet monochromator) and is not inherent in the technique. The problem has been largely overcome by the development of a fully automated digital absorption recording system which, in principle, is limited in accuracy only by the counting statistics. The system is described fully in Chapter 4.

With the above mentioned system, absorption measurements were taken for a large number of rotational lines of the Lyman and Werner bands of H_2. The results for both band systems appear to be in good agreement with the electron scattering results of Geiger and Schmoranzer (1969) and also in close agreement with the theoretical calculations of Allison & Dalgarno (1970). Experimental electronic transition moments are also compared with the theoretical calculations of Wolniewicz (1969). The results are presented and discussed in Chapter 6.

CHAPTER 2

2. The Spectra of Diatomic Molecules

This chapter is a brief summary of the quantum mechanics of diatomic molecules and the interpretation of the intensity of the observed spectrum. It is not within the scope of this chapter to give a detailed account of any particular aspect of the theory as this can be found in any of a number of books on molecular structure (e.g. Herzberg 1950). The discussion of transition strengths is, however, given in some detail because there appears to be some ambiguity and variety in the notation used for band strength and Hönl-London factors. There also appears to be discrepancy in the interpretation of these terms and it is therefore necessary to define the terms used in the present work. The notation for the section on transition strengths has been taken from Nicholls & Stewart (1962).

Although much of the discussion in this chapter is applicable to other molecules, it is intended only to cover the case of absorption by homonuclear diatomic molecules, particularly molecular hydrogen. Consequently, examples relating to H_2 have been given where applicable.

2.1 The Nature of Molecular Spectra

The observed spectrum of a diatomic molecule is considerably more complex than that of an atom because the

molecule has two modes of excitation not present in atoms, namely vibration and rotation. Each electronic state possesses a set of rotation-vibration levels corresponding to the nuclear motions, and an electronic transition will, in general, be accompanied by a change in the rotation and vibration of the molecule, giving rise to a large number of discrete lines in the spectrum. These lines are grouped into bands corresponding to transitions between given vibration levels in each electronic state. The bands are classified according to the vibrational quantum number v in the upper and lower state. A band is termed ($v'-v''$) for a transition from the v'' vibrational level of the lower state to the v' level of the upper state. In absorption, the observed bands are simplified because all the vibrational levels of the lower state (ground state) are not populated. In fact, at room temperature only the lowest vibrational level (i.e. $v''=0$) is populated, giving rise to a progression of ($v'-0$) bands.

The rotational lines within a band appear as branches (see Section 2.4.3) determined by the difference in the rotational quantum number J between the upper and lower states, where J is the quantum number of the total angular momentum. The nature of the coupling between the nuclear rotation, electronic angular momentum and spin to give

the resultant J, are discussed in detail by Herzberg (1950).

2.2 The Born-Oppenheimer Approximation

The solution of Schrödinger's equation for the molecular system will yield wavefunctions which will depend on both the electron and nuclear coordinates. However, according to the Born-Oppenheimer approximation (1927), the much more rapid electron motions can be treated separately from the nuclear motions and the total wavefunction can be written

$$\psi = \psi_e \psi_{vr} \qquad \ldots\ldots \quad 2.1$$

where ψ_e is the electronic wavefunction for the electrons (in nuclei fixed coordinate system) and ψ_{vr} is the wavefunction of the vibrating and rotating nuclei. The wavefunction can be further simplified by considering the vibration and rotation separately. This yields (Pauling & Wilson 1934)

$$\psi_{vr} = \frac{1}{r} \psi_v \psi_r \qquad \ldots\ldots \quad 2.2$$

where $\frac{1}{r} \psi_v$ is the vibrational wavefunction (and depends only on the nuclear separation r) and ψ_r is the rotational wavefunction.

The above approximations are fairly good for most molecules, however equation (2.2) becomes inaccurate for light molecules (e.g. H_2) where the centrifugal force has a

significant effect on the nuclear vibration. This rotational interaction with the vibrational motion is often referred to as centrifugal distortion. In such a case, the rotation-vibration wavefunction ψ_{vr} can still be separated according to equation (2.2) except that the vibrational wavefunction now has a rotation dependent term in it (as shown for example by Pekeris 1934).

In a more rigorous approach, the electron and nuclear spin wavefunctions should also be considered in the expression for the total wavefunction. The inclusion of these spin wavefunctions and their effect on the observed transitions will be considered in Section 2.3.2.

2.3 Classification and Symmetry of Molecular States

2.3.1 Classification of Electronic States

The classification of electronic states of a molecule have been discussed in detail by Herzberg (1950 Chapter 5) and the following is a brief summary of the notation used.

Electronic states are denoted by the symbols Σ, Π, Δ .... etc. according to the magnitude of Λ, where Λ is the quantum number of the component of the electronic angular momentum along the internuclear axis. The states are designated Σ, Π, Δ .... as $\Lambda = 0, 1, 2$ .... respectively. A given electronic state is further qualified according to

the following notation.

1) The multiplicity (or electron spin degeneracy) given by (2S+1) where S is the quantum number of the total electron spin. For the two electron H_2 molecule, S is either 0 or 1 giving rise to multiplicities of 1 (singlet states) and 3 (triplet states).

2) +, -. These symbols apply only to Σ states and refer to the symmetry with respect to reflection through a plane containing the internuclear axis. For states with $\Lambda \neq 0$ the component of the electronic angular momentum can, for the same Λ, be in either direction along the internuclear axis (Λ represents only the magnitude of this angular momentum). Thus states with $\Lambda \neq 0$ are two-fold degenerate and each of the degenerate sublevels have opposite symmetry. Consequently the +, - classification becomes redundant for these states.

3) The symbols g, u which refer to the symmetry with respect to inversion about a centre of symmetry and apply only to homonuclear molecules.

The classification of some of the molecular hydrogen states can be seen from the energy level diagram shown in Fig. 2.1. The diagram shows only the electronic levels.

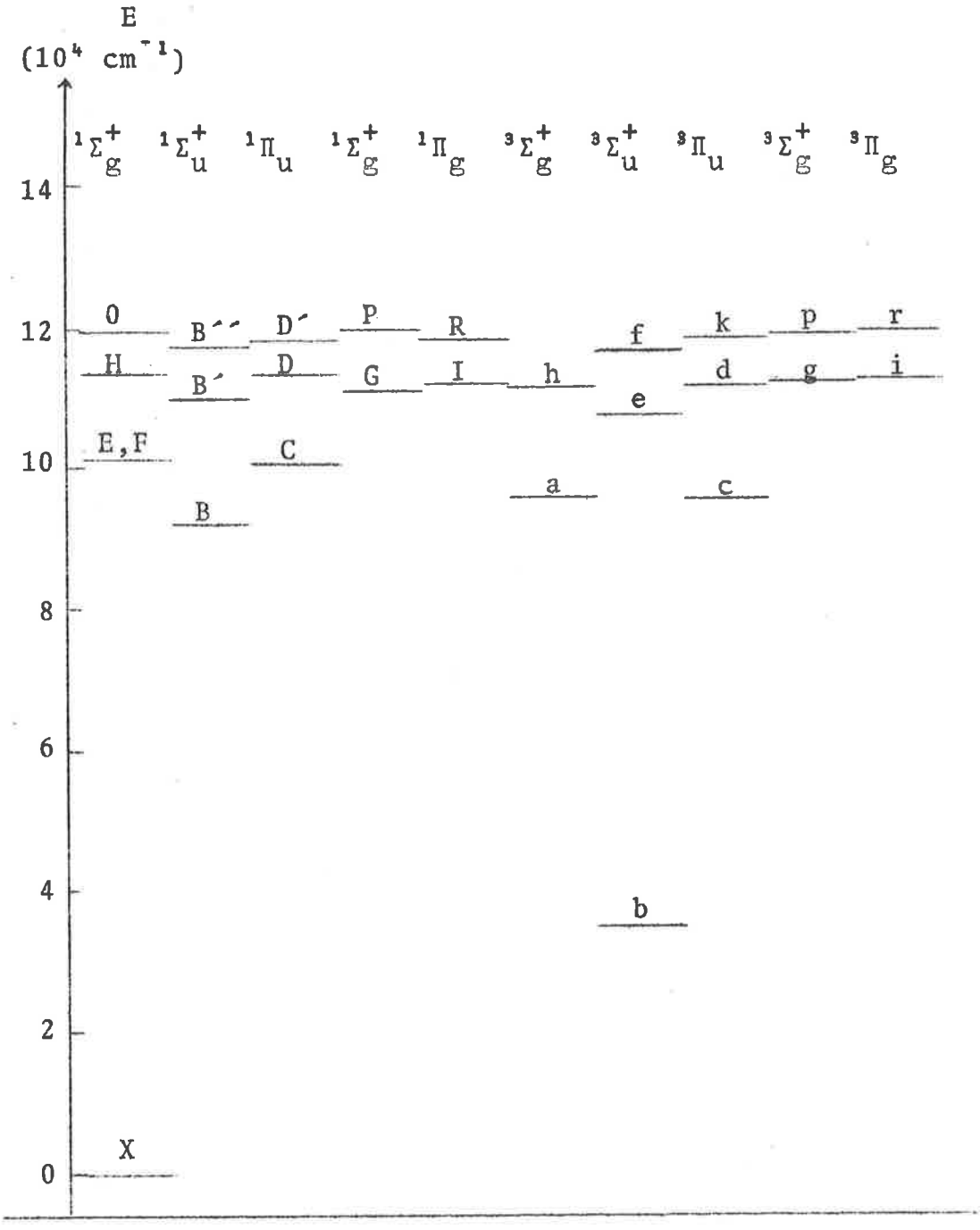

Fig. 2.1. Energy level diagram for H_2. (after Varsavsky 1966; the B´, B´´ and D´ levels not given by Varsavsky have also been included)

It can be seen from this diagram that the ground state of H_2 is classified as a $^1\Sigma_g^+$ state. To distinguish between different states with the same classification, the states are also labelled alphabetically, the ground state being labelled $X^1\Sigma_g^+$

2.3.2 Symmetry of Molecular Wavefunctions

Symmetry properties of the molecular eigenfunctions are important for the determination of selection rules and their understanding is therefore essential in the interpretation of the observed spectra. Comprehensive discussions of these symmetry properties are given in texts on molecular structure (e.g. Herzberg 1950, King 1964).

One important symmetry property for homonuclear molecules is the symmetry with respect to nuclei exchange. If the nuclei are fermions, the total molecular wavefunctions (including nuclear spin) must be antisymmetric under nuclei exchange. The total wavefunctions may be written $\psi\beta$ where ψ is the molecular wavefunction excluding nuclear spin and β is the nuclear spin wavefunction. As the total wavefunction must be antisymmetric, we may write it as $\psi^{(s)}{}_\beta{}^{(a)}$ or $\psi^{(a)}{}_\beta{}^{(s)}$ where the superscripts denote symmetry(s) or antisymmetry(a) with respect to nuclear exchange. For the $^1\Sigma_g^+$ ground state of H_2 the non-spin (ψ) wavefunctions are symmetric for even J'' and antisymmetric

for odd J´´ (Herzberg 1950). For the nuclear spin wavefunctions, the statistical weights of the symmetric ($\beta^{(s)}$) and antisymmetric ($\beta^{(a)}$) are 3 and 1 respectively (Herzberg 1950). Consequently the statistical weights of the odd J´´ levels ($\psi^{(a)}$) will be three times that of the even J´´.

A similar argument can be used in discussing the electron spin which, for otherwise identical states, gives rise to $^1\Sigma_g^+$ and $^3\Sigma_g^+$ states with statistical weights of 1 and 3 respectively.

As electric dipole transitions between different spin states (electron or nuclear) are forbidden according to the selection rules (Section 2.4.3), we may ignore the triplet states in an absorption process since the H_2 ground state is a singlet. Both nuclear spin species are found in the ground state and due to the above mentioned selection rule, the different spin states cannot combine. This gives rise to the concept of H_2 as consisting of two distinct species called ortho-hydrogen (odd J´´) and para-hydrogen (even J´´). For a general discussion of transitions, however, it is convenient to treat H_2 as a single gas with odd and even J´´ levels having a statistical weight of 3 and 1 respectively (see Section 2.6.2).

2.4 Electric Dipole Transitions

2.4.1 Transition Probability

The probability that a molecule will undergo an electric dipole transition from a lower state n'' to an upper state n' when irradiated by photons of energy $h\nu_{n'n''}$ (the energy difference between the states), is given by the Einstein transition probability of absorption $B_{n'n''}$. This may be written for non-degenerate levels, as (Herzberg 1950)

$$B_{n'n''} = \frac{8\Pi^3}{3h^2c} \left|R_{n'n''}\right|^2 \qquad \ldots\ 2.3$$

where $R_{n'n''}$ is the matrix element of the electric dipole moment

$$\text{i.e.} \qquad R_{n'n''} = \int \psi^*_{n'} P_e \psi_{n''} d\tau \qquad \ldots\ 2.4$$

where $\psi_{n''}$ and $\psi_{n'}$ are the initial and final state wave-functions, P_e is the electric dipole moment of the electrons and $d\tau$ is a volume element of configuration space.

2.4.2 Degenerate Levels

If the levels n'' and n' are degenerate, with substates i and j respectively, the transition probability between these levels will be modified to give (see Nicholls and Stewart (1962) for corresponding case in emission).

$$B_{n'n''} = \frac{8\pi^3 \sum_{ij} |R_{ij}|^2}{3h^2 c\, \omega_{n''}} \qquad \ldots\ 2.5$$

where the summation is over all the degenerate substates i and j and $\omega_{n''}$ is the number of substates i(degree of degeneracy of level n''). This equation holds only if the sublevels i are equally populated (i.e. the molecules are in thermodynamic equilibrium). For a given rotational level in an electronic state, the degeneracy may be written as the product of the electronic and rotational degeneracies. In general $\omega_{n''}$ may be written

$$\omega_{n''} = (2-\delta_{0\Lambda''})(2S''+1)(2J''+1) \qquad \ldots\ 2.6$$

where $(2J''+1)$ is the rotational degeneracy, $(2S''+1)$ is the multiplicity (spin degeneracy) and $(2-\delta_{0\Lambda''})$ is the Λ degeneracy term,

$$\text{i.e. } (2-\delta_{0\Lambda''}) = \begin{cases} 1 \text{ if } \Lambda'' = 0 \\ 2 \text{ if } \Lambda'' \neq 0 \end{cases} \qquad \ldots\ 2.7$$

2.4.3 Selection Rules

In general $|R|^2$ has non-zero values only for transitions between certain states of the molecule. The restrictions governing the nature of the states define the selection rules which, for electric dipole transitions, may be briefly summarized as follows.

I Electronic

1) $\Delta\Lambda = 0, \pm 1$

2) $\Delta S = 0$ i.e. Multiplicity does not change

3) The reflection symmetry does not change. Transitions will therefore be of the types $\Sigma^+ \leftrightarrow \Sigma^+$ or $\Sigma^- \leftrightarrow \Sigma^-$ but $\Sigma^+ \not\leftrightarrow \Sigma^-$.

4) The inversion symmetry changes, i.e. $g \leftrightarrow u$ but $u \not\leftrightarrow u$, $g \not\leftrightarrow g$.

II Rotational

1) $\Delta J = 0, \pm 1$ where $\Delta J = J' - J''$. The exception is $\Delta J \neq 0$ for Σ-Σ transitions. This selection rule gives rise to branches in the rotational spectrum. The branches are designated P, Q, R for $\Delta J = -1, 0, +1$ respectively.

2) Parity must change i.e. $+ \leftrightarrow -$ but $+ \not\leftrightarrow +$, $- \not\leftrightarrow -$.

3) Nuclear symmetry does not change i.e. $s \leftrightarrow s$, $a \leftrightarrow a$ but $s \not\leftrightarrow a$.

There are no selection rules governing vibrational transitions.

2.4.4 Other Transitions

The above discussion and selection rules have dealt only with electric dipole transitions. In cases where the matrix element is zero for electric dipole transitions.

it is still possible to have a finite transition probability for different types of transitions; e.g. magnetic dipole, electric quadrupole etc. The relative probability of these transitions is, however, several orders of magnitude less than a similar electric dipole transition and they are classified under the general category of forbidden transitions. As forbidden transitions will not be considered in this chapter, the term transition will be taken to mean electric dipole transition throughout the text.

2.4.5 Hydrogen Transitions

Applying the dipole selection rules to the ground state of hydrogen, it is evident that only transitions to the states of the type $^1\Sigma_u^+$ and $^1\Pi_u$ can take place. The lowest members of these types of states, as shown in Fig. 2.1, are the $B^1\Sigma_u^+$ state and $C^1\Pi_u$ state, and transitions from the ground state to these states give rise to the well known Lyman and Werner band systems.

i.e. the $B^1\Sigma_u^+ \leftarrow X^1\Sigma_g^+$ Lyman system

and the $C^1\Pi_u \leftarrow X^1\Sigma_g^+$ Werner system

2.5 Transition Strengths

2.5.1 Line Strength

In general, an upward transition will take place from a vibration-rotation level $v''J''$ of an electronic

state n'', Λ'' to another such level v', J' in the upper state n', Λ'. (The convention of denoting the upper state by primed quantum numbers and the lower state by double primed quantum numbers will be used throughout the text). The transition strength is (Nicholls and Stewart 1962)

$$\left|R_{n''v''J''\Lambda''}^{n'v'J'\Lambda'}\right|^2 = \sum_{ij} \sum_{M'M''} \left| \int \psi_j^* \, v'J'\Lambda'M' \, P_e \psi_{iv''J''\Lambda''} d\tau \right|^2 \quad \ldots\ldots \quad 2.8$$

where the summation is over the degenerate electronic states i and j and the rotational degenerate states denoted by the magnetic quantum numbers M'' and M'. The integration is taken over all configuration space, and the wavefunctions ψ refer to the states denoted by the appropriate quantum numbers. P_e is the dipole moment of the electrons. Using the Born-Oppenheimer approximation, equation (2.8) reduces to (Nicholls and Stewart 1962)

$$\left|R_{n''v''J''\Lambda''}^{n'v'J'\Lambda'}\right|^2 = p_{v'v''} S_{J''\Lambda''}^{J'\Lambda'} \quad \ldots\ldots \quad 2.9$$

where $S_{J''\Lambda''}^{J'\Lambda'}$ is called the Hönl-London factor and depends only on the initial and final angular momentum quantum numbers J and Λ. $p_{v'v''}$ is called the band strength and is given by

$$p_{v'v''} = \sum_{ij} \left| \int \psi^*_{v'} R_e^{ij} \psi_{v''} dr \right|^2 \quad .... \quad 2.10$$

where R_e^{ij} is the electronic transition moment.

$$\text{i.e.} \quad R_e^{ij} = \int \psi_j^* P_e \psi_i d\tau \quad .... \quad 2.11$$

where ψ_j and ψ_i are the electronic wavefunctions of the states j and i respectively.

It should be noted that the notation for band strength (equation 2.10) is not universal. A number of authors (e.g. Wolniewicz 1969) use the expression

$$p_{v'v''} = \left| \int \psi^*_{v'} R_e^{ij} \psi_{v''} dr \right|^2 \quad .... \quad 2.12$$

i.e. the band strength is not summed over the degenerate electronic levels. This notation is convenient for theoretical calculations because, with this notation $p_{v'v''}$ depends only on the electronic transition moment and the vibrational wavefunctions. However, to determine the theoretical absorption intensity, we need the value $\sum_{ij} p_{v'v''}$ of equation (2.12) above to make the transition probability consistent with equation (2.5). The notation used in this thesis (equation 2.10) directly relates the band strength to the observed transition probability (equation 2.5) and is therefore a more convenient expression for experimental work.

In the case of H_2, this difference in notation is significant only for the C ← X Werner band system where the C state is doubly degenerate.

2.5.2 Hönl-London Factors

The Hönl-London factors $S_{J''\Lambda''}^{J'\Lambda'}$ are the relative strength factors of the rotational lines within a vibrational band. The exact form of the Hönl-London factors will depend on the type of states involved in the transition, including the coupling of the various angular momenta in both states. Extensive tables and references to tables of Hönl-London factors for transitions between states belonging to Hund's coupling cases (a) and (b), as well as intermediate coupling cases, have been tabulated by Tatum (1967) and Schadee (1964). Both authors have pointed out that many earlier tabulations of Hönl-London factors are incorrect and need to be normalized to the sum rule

$$\sum_{J'} S_{J''\Lambda''}^{J'\Lambda'} = (2J'' + 1) \qquad \ldots. \quad 2.13$$

where the summation is over all transitions originating from a common lower level J'' for absorption. A similar sum rule

$$\sum_{J''} S_{J''\Lambda''}^{J'\Lambda'} = (2J' + 1) \qquad \ldots. \quad 2.14$$

holds for emission, i.e. transitions from a common upper level J'.

2.5.3 Hönl-London Factors for Hydrogen

The ground state of molecular hydrogen is a $^1\Sigma_g^+$ state, consequently only the singlet transitions of the type $^1\Sigma \leftarrow {}^1\Sigma$ and $^1\Pi \leftarrow {}^1\Sigma$ need be considered. Hönl-London factors for singlet transitions have been evaluated on the basis of a symmetric top model of the molecule (Rademacher and Reiche 1927, Kronig and Rabi 1927) and the normalized Hönl-London factors are (Schadee 1964)

$$S_{J''0}^{J'0} = \begin{cases} J''+1 & \text{for R branch} \\ J'' & \text{for P branch} \end{cases} \quad \ldots\ldots \quad 2.15$$

for $^1\Sigma \leftarrow {}^1\Sigma$ transitions ($\Lambda' = \Lambda'' = 0$). For $^1\Pi \leftarrow {}^1\Sigma$ transitions ($\Lambda' = 1$) the Hönl-London factors are

$$S_{J''0}^{J'1} = \begin{cases} \tfrac{1}{2}(J''+2) & \text{for R branch} \\ \tfrac{1}{2}(2J''+1) & \text{for Q branch} \\ \tfrac{1}{2}(J''-1) & \text{for P branch} \end{cases} \quad \ldots\ldots \quad 2.16$$

2.5.4 The Franck-Condon Factor

The electronic transition moment R_e^{ij} generally varies only slightly with varying internuclear separation. Consequently, the mean-value theorem can be applied to the integral in equation 2.10 to give

$$p_{v'v''} = q_{v'v''} \sum_{ij} \left| \overline{R_e}^{ij} \right|^2 \qquad \ldots\ldots 2.17$$

where

$$q_{v'v''} = \left| \int \psi^*_{v'} \psi_{v''} dr \right|^2 \qquad \ldots\ldots 2.18$$

is called the Franck-Condon factor.

If the electronic transition moment varies significantly with internuclear separation, the band strength may still be expressed in terms of the Franck-Condon factor and the electronic transition moment by using the concept of the r-centroid.

2.5.5 The r-Centroid

The transition time is very short compared to the vibration period of the molecule. Therefore, according to the Franck-Condon principle, the transition can be considered as taking place at a constant internuclear distance. The internuclear separation at which a transition v''-v' takes place is called the r-centroid for that transition, and is written $r(v'v'')$. The r-centroid may be considered as being the most probable internuclear separation at which the transition takes place and is given by (Nicholls & Stewart 1962).

$$r(v'v'') = \frac{\int \psi^*_{v'} \, r \, \psi_{v''} \, dr}{\int \psi^*_{v'} \, \psi_{v''} \, dr} \qquad \ldots\ldots 2.19$$

Consequently, we may replace R_e^{ij} by $R_e^{ij}[r(v'v'')]$ for the particular transition. Hence equation (2.10) may be written

$$p_{v'v''} = q_{v'v''} \sum_{ij} \left| R_e^{ij}[r(v'v'')] \right|^2 \quad .... \quad 2.20$$

The range of validity of the r-centroid approximation has been discussed by Fraser (1954).

2.5.6 Rotational Dependence of Band Strengths

It was pointed out in section (2.2) that the vibrational wavefunction for light molecules (e.g. H_2) can have a slight dependence on the rotation. In this case the band strength is dependent on J and may be written (Wolniewicz 1969) $q_{v'v''}^{J'J''}$.

The extent of this J dependence can be seen from Table 2.1 (after Wolniewicz 1969).

A similar variation of the Franck-Condon factor of several Lyman bands has been calculated by Halmann and Laulicht (1968).

In principle, the magnitude of the variation in band strength is large enough to be detected by the present experimental measurement. However, attempts to observe such a variation in the results were unsuccessful due to several limiting factors. These will be discussed in Chapter 6.

TABLE 2.1

J''	$p_{00}^{J'J''}$ (10^{-2} atomic units)	
	P	R
0		0.5955
1	0.6341	0.5701
2	0.6461	0.5413
3	0.6528	0.5100
4	0.6539	0.4769
5	0.6494	0.4428
6	0.6395	0.4083
7	0.6246	0.3741
8	0.6053	0.3408
9	0.5822	0.3090
10	0.5562	

The band strength $p_{00}^{J'J''}$ (0-0 band) of the Lyman bands. (after Wolniewicz 1969)

2.6 The Oscillator Strength

Experimental transition strengths are often expressed in terms of a dimensionless quantity called the oscillator strength. The oscillator strength represents the ratio of the quantum theoretical to the classical value of the transition strength, the classical value being calculated for a single harmonic oscillating electron radiating energy

$h\nu_{n'n''}$. The oscillator strength $f_{n'n''}$ for a transition $n' \leftarrow n''$ is given as (Nicholls and Stewart 1962).

$$f_{n'n''} = \frac{8\pi^2 m \nu_{n'n''}}{3he^2 \omega_{n''}} \sum_{ij} \left| R_{ij} \right|^2 \quad \ldots\ldots \quad 2.21$$

where $\sum_{ij} \left| R_{ij} \right|^2$ is the transition strength, m is mass of the electron and the other symbols have their usual meaning.

2.6.1 Experimental Oscillator Strengths

The oscillator strength can be related to an experimentally measurable quantity (see Chapter 3), the integrated absorption coefficient $\int k d\nu$ by (Herzberg 1950, Nicholls and Stewart 1962)

$$f_{n'n''} = \frac{mc}{\pi e^2 N_{n''}} \int_{n'n''} k d\nu \quad \ldots\ldots \quad 2.22$$

where the integration is over the line (or band) associated with the transition $n' \leftarrow n''$ and $N_{n''}$ is the number density of molecules in initial level n''. $N_{n''}$ may alternatively be written in terms of the molecular number density N and the fractional population $\alpha_{n''}$ of molecules in state n''.

$$\text{i.e.} \quad N_{n''} = N\alpha_{n''} \quad \ldots\ldots \quad 2.23$$

The absorption coefficient is generally defined at S.T.P. in which case the molecular number density is given by N_o (Loschmidt's Number). Since the absorption measurements are taken at room temperature, however, it is convenient to define the absorption coefficient at 1 Atmosphere and room temperature and a corresponding number density N_A (see Chapter 5). Hence we may write equation 2.22 as

$$f_{n'n''} = \frac{mc}{\pi e^2 N_A \alpha_{n''}} \int_{n'n''} k d\nu \qquad \ldots\ 2.24$$

2.6.2 Line Oscillator Strengths

In the case of H_2, we are interested in transitions originating at the various rotational levels of the lowest vibrational level ($v''=0$) of the ground state. We may write the fractional distribution $\alpha_{J''}$ of molecules in rotational level J'' in terms of the Boltzmann distribution and the appropriate statistical weights $G_{J''}$ for each level

$$\text{i.e.}\quad \alpha_{J''} = \frac{G_{J''}}{Q_r} \exp\left[-\frac{\varepsilon_{J''}}{k_B T}\right] \qquad \ldots\ 2.25$$

where k_B is Boltzmann's constant (the symbol k_B has been used to avoid confusion with k, the absorption coefficient), $\varepsilon_{J''}$ is the energy of the J'' level and Q_r is the rotational state sum

$$\text{i.e.} \quad Q_r = \sum_{J''} G_{J''} \exp\left(-\frac{\varepsilon_{J''}}{k_B T}\right) \qquad \ldots \quad 2.26$$

Q_r is alternatively known as the rotational partition function. The statistical weight $G_{J''}$ is determined by the degeneracy of the J'' level and by the relative ortho to para hydrogen ratio (discussed in Section 2.3.2). Consequently we have

$$\alpha_{J''} = \begin{cases} \dfrac{(2J''+1)}{Q_r} \exp\left(-\dfrac{\varepsilon_{J''}}{k_B T}\right) & \text{for even } J'' \\ \dfrac{3(2J''+1)}{Q_r} \exp\left(-\dfrac{\varepsilon_{J''}}{k_B T}\right) & \text{for odd } J'' \end{cases} \qquad \ldots \quad 2.27$$

The corresponding line oscillator strength may be written

$$f^{J'J''}_{v'o} = \frac{mc}{\pi e^2 N_A \alpha_{J''}} \int_{J'J''} k\,d\nu \qquad \ldots \quad 2.28$$

where the integration is over the $(J''J')$ line of the $(v'-0)$ band.

Spectroscopic measurements are generally taken in terms of wavelength rather than frequency, and so the experimental integrated absorption coefficient is generally expressed as $\int k\,d\lambda$, (see Chapter 3) and the line oscillator strength will therefore become

$$f^{J'J''}_{v'o} = \frac{mc^2}{\lambda_0^2 \pi e^2 N_A \alpha_{J''}} \int_{J'J''} k d\lambda \qquad \ldots\ 2.29$$

where λ_0 is the wavelength of the line centre. (This expression is only valid if the line width is very much smaller than λ_0, a condition met for optical and ultra-violet transitions).

CHAPTER 3

3. Gaseous Absorption

3.1 Introduction

Experimentally, integrated absorption coefficients and hence oscillator strengths, can be determined by absorption measurements provided that the line shape is known. The knowledge of line shape is necessary because, in general, laboratory absorption measurements do not yield the correct value for the absorption coefficient as a function of wavelength unless it is constant over a spectral region defined by the resolution of the dispersing instrument. This can be readily seen by determining the observed absorption in terms of the actual absorption.

The transmission T_λ at a given wavelength λ may be expressed in terms of the absorption coefficient k (at wavelength λ) and the amount of absorbing gas $\underline{a}$ by Beer's Law (Goody 1964).

$$\text{i.e.} \quad T_\lambda = \exp(-k\underline{a}) \qquad \ldots\ 3.1$$

For a dispersion instrument of finite resolution we may define a resolution function $F(\lambda-\lambda')$ which depends on the size and shape of the slits and dispersion of the instrument. We may normalize this function such that

$$\int F(\lambda-\lambda') \, d\lambda = 1 \qquad \ldots\ 3.2$$

The function F may be considered as determining the observed fractional intensity of the incident spectrum at wavelength λ when the instrument is set at λ', and is determined only by the wavelength difference $(\lambda-\lambda')$, i.e. it is independent, within reasonable limits, of absolute wavelength setting. The observed intensity I', at apparent wavelength λ', will then be

$$I' = \int F(\lambda-\lambda') \, I_\lambda d\lambda \qquad \ldots\ 3.3$$

where I_λ is the incident intensity at wavelength λ of the source. If we now consider a gas of transmission T_λ the apparent transmission T' will be given by

$$T' = \frac{\int F(\lambda-\lambda') \, I_\lambda \, T_\lambda \, d\lambda}{\int F(\lambda-\lambda') \, I_\lambda \, d\lambda} \qquad \ldots\ 3.4$$

Consequently, only if T_λ (and hence k) is constant over the range of wavelengths over which F is finite, will the observed transmission give the actual transmission, and therefore the correct absorption coefficient.

$$\text{i.e. } T' = T_\lambda = \exp-(k\underline{a}) \qquad \ldots\ 3.5$$

If, on the other hand, k is varying within the range of finite F, (e.g. an absorption line which is narrower than

the resolution full width) the observed absorption will not give the absolute absorption. However, if the variation of k with λ (i.e. the line shape) is known, it is possible to relate the integrated observed absorption, within certain approximations, to the integrated absorption coefficient.

3.2 Curve of Growth

3.2.1 The Equivalent Width

The integrated absorption over a line is called the equivalent width W

$$\text{i.e.} \quad W = \int A_\lambda \, d\lambda$$

$$= \int 1-\exp(-k\underline{a})d\lambda \qquad \ldots\ 3.6$$

(W represents the width of a rectangular line which is a perfect absorber). The equivalent width can be related to the observed integrated absorption under certain restrictions to the intensity variation of the incident spectrum. By imposing the restriction that the source spectrum has a constant intensity in the vicinity of the absorption line, it is possible to show that the equivalent width is equal to the observed integrated absorption. For a constant I_λ, equation 3.4 reduces to

$$T' = \int F(\lambda-\lambda') \, T_\lambda \, d\lambda \qquad \ldots\ 3.7$$

Consequently the integrated observed absorption may be written

$$\int A' d\lambda' = \int d\lambda' \left[1 - \int F(\lambda - \lambda') \, T_\lambda \, d\lambda \right] \qquad \ldots\ 3.8$$

Since the resolution function F depends only on the wavelength difference, we may write equation (3.2) as

$$\int F(\lambda - \lambda') d\lambda = \int F(\lambda - \lambda') d\lambda' = 1 \qquad \ldots\ 3.9$$

The right hand side of equation 3.8 may therefore be written

$$\begin{aligned} \int d\lambda' \left[1 - \int F(\lambda - \lambda') T_\lambda \, d\lambda \right] &= \int d\lambda' \int F(\lambda - \lambda')(1 - T_\lambda) \, d\lambda \\ &= \int d\lambda' \, F(\lambda - \lambda') \int 1 - T_\lambda \, d\lambda \\ &= W \qquad \ldots\ 3.10 \end{aligned}$$

Consequently, the integrated observed absorption is the equivalent width under these conditions. Goody (1964) has shown that this result also holds if the intensity of the source spectrum varies linearly with wavelength in the region of the absorbing line. However, the added condition that the resolution function F be symmetrical is required for the proof of equation 3.10.

$$\text{i.e.} \quad F(\lambda-\lambda') = F(\lambda'-\lambda) \qquad \ldots\ldots 3.11$$

This resolution function may be considered as a combination of the slit function (convolution of entrance and exit slit shapes) and the dispersion linearity of the grating. The slit function will be symmetrical for rectangular slits and the dispersion is approximately linear over the region of interest. Consequently the symmetry condition is generally met experimentally. The integrated observed absorption will therefore yield the correct equivalent width provided that the source spectrum is either constant or varying linearly in the wavelength region near the line.

3.2.2 Small Absorption Region

The manner in which the equivalent width W grows with increasing amounts of absorbing gas a and the absorption coefficient k is known as the curve of growth. This curve of growth depends on the line shape (i.e. the variation of k with wavelength), and a value of $\int k d\lambda$ can only be obtained from a measured W and a if the curve of growth or line shape is known.

The only instance where the equivalent width does not depend on line shape is in the limiting case of small absorption. If $ka \ll 1$, $\exp(-ka)$ may be expanded to give $1-ka$, the higher order terms being vanishingly small. Hence equation (3.6) may be written

$$W = \underline{a}\int k \, d\lambda$$

The range over which this expression is valid defines the linear region of the curve of growth and a measure of W and $\underline{a}$ directly yields the integrated absorption coefficient without a knowledge of the line shape or growth curve. The corresponding value of W is, however, very small in this linear region and, as will be seen in Section 3.4.2 and Fig. 3.2, corresponds to a W value of less than 1mÅ for a typical absorption line of H_2 at room temperature. Experimentally, such small equivalent widths cannot be measured accurately because the peak observed absorption is very small. The monochromator used for the present work had a resolution half width of about 0.3Å and, if a triangular resolution function is assumed, an equivalent width of 1mÅ corresponds to a peak observed absorption of about 0.3%. It will be seen in Chapter 4 that experimental measurements of such small absorption cannot be accurately made.

With the limiting resolution of the present instrument, it is therefore necessary to take equivalent width measurements where the absorption is stronger, and the line shape must be taken into account in relating W to the integrated absorption coefficient.

3.3 Line Shapes

The shape of a spectral line may be attributed to

three main factors giving rise to natural, pressure and Doppler broadening. Although all three forms of broadening occur simultaneously, thus complicating the curve of growth, it is possible to select experimental conditions such that only Doppler broadening need be considered (see Section 3.4.1).

The absorption coefficient may conveniently be expressed in terms of the line shape and a peak absorption coefficient k_o

$$\text{i.e.} \quad k_\lambda = k_o \, f(\lambda,\lambda_o) \qquad \ldots\ldots 3.13$$

where $f(\lambda,\lambda_o)$ is the shape of the line centred at λ_o and is normalized such that

$$f(\lambda_o,\lambda_o) = 1 \qquad \ldots\ldots 3.14$$

3.3.1 Natural Broadening

A molecule in an excited state has a finite lifetime before it decays into a lower level. From the Uncertainty Principle, the finite lifetime of the state must be associated with an energy spread of the excited level. Consequently transitions from the ground state to the excited state will have a spread of energy which is characteristic of the upper level lifetime. The energy spread defines the line shape which, for natural broadening, is

Lorentzian and is given by (Goody 1964)

$$f(\lambda,\lambda_o) = \frac{\Delta_N^2}{(\lambda-\lambda_o)^2 + \Delta_N^2} \qquad \ldots. 3.15$$

where Δ_N is the natural width of the line and is given by

$$\Delta_N = \frac{\lambda_o^2}{4\pi c\tau_N} \qquad \ldots. 3.16$$

where τ_N is the lifetime of the excited state and λ_o is the wavelength of the line centre. The above expressions for line shape and width are only approximate and hold only if the width Δ_N is very much smaller than the wavelength of the line centre λ_o. The above expression for line shape (equation 3.15) and subsequent line shape expressions are also not standard. The expressions differ from the expressions found in most texts (e.g. Goody 1964) because of the particular normalization used (equation 3.14).

3.3.2 Pressure Broadening

The interaction between molecules is, in general, complex and this gives rise to a complex expression for line shape. However, an approximation can be made by considering only collisions which terminate the absorption process by inducing decay. This situation is analogous

to natural broadening where the lifetime is now replaced by the mean time between collisions, and the line shape is similar to equation (3.15). The pressure broadened width is given by

$$\Delta_p = \frac{\lambda_o^2}{4\pi\tau_p c} \qquad \ldots\ldots 3.17$$

where τ_p is the mean time between collisions. Using kinetic theory, this can be expressed as (Goody 1964)

$$\Delta_p = \frac{\lambda_o^2 N\sigma^2}{c}\left(\frac{2RT}{M\pi}\right)^{\frac{1}{2}} \qquad \ldots\ldots 3.18$$

where σ is the diameter of the molecule, and N is the number density. R is the gas constant, T the absolute temperature and M is the molecular weight.

3.3.3 Doppler Broadening

The thermal motion of the molecules gives rise to a Doppler shift of the absorbing frequency for each molecule. The overall observed line profile will therefore be determined by the velocity distribution within the gas. The line shape is Gaussian and is given by (Goody 1964)

$$f(\lambda,\lambda_o) = \exp - \left(\frac{\lambda-\lambda_o}{\Delta_D}\right)^2 \qquad \ldots\ldots 3.19$$

where

$$\Delta_D = \frac{\lambda_o}{c}\left(\frac{2RT}{M}\right)^{\frac{1}{2}} \qquad \ldots\ldots 3.20$$

is the Doppler width of the line. R, T and M are the same as in equation (3.18).

3.3.4 Mixed Profile

As both natural and pressure broadening are Lorentzian in shape, the general line shape may be considered as a mixed Doppler and Lorentz profile. The curve of growth of such a mixed profile cannot be determined analytically; however, a numerical analysis for several combinations of Doppler and Lorentz widths has been given by Van der Held (1931) and the corresponding curves are shown in Fig. 3.1. The parameter d is given by twice the ratio of the Lorentz to Doppler widths,

$$\text{i.e. } d = \frac{2\Delta_L}{\Delta_D}$$

where Δ_L is the total Lorentz width (i.e. $\Delta_L = \Delta_N + \Delta_p$). The curves d=0 and d=∞ represent the curves of growth for a pure Doppler and pure Lorentz line respectively.

These curves, however, are useful only as a guide to the general nature of the curve of growth. In a practical case, the curve of growth is complicated by two important features.

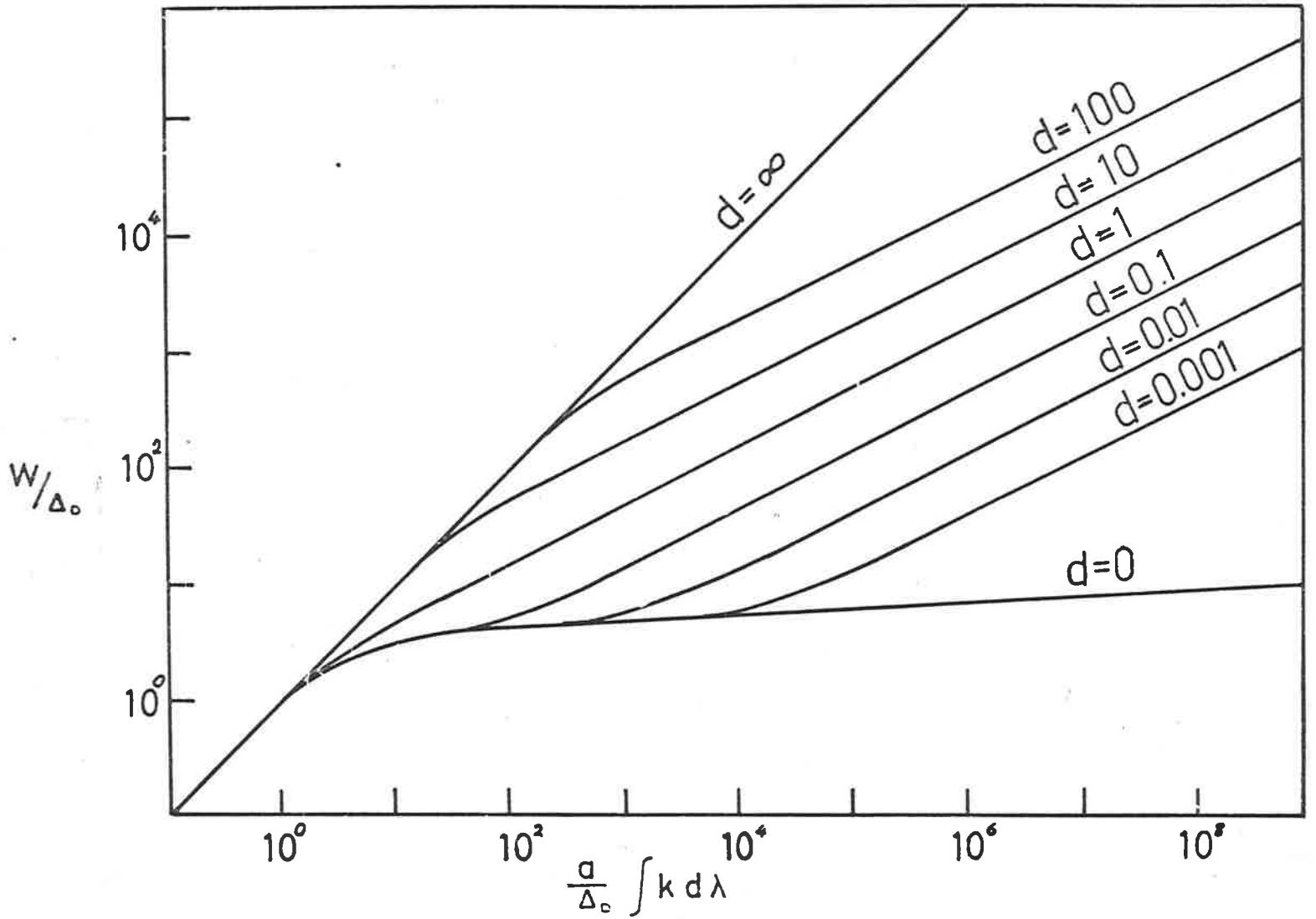

Fig. 3.1 Curves of growth for a mixed Lorentz and Doppler profile. (after Van der Held 1931)

1) The pressure broadening width will itself vary with pressure. Consequently the total Lorentz width will vary with pressure in a way which will depend on the relative magnitudes of the natural and pressure broadening.

2) The above curves only apply to isolated lines. If a pair (or a group) of lines are closely spaced such that there is some overlap between them, the observed curve of growth will, in general, be different from that of an isolated line.

Consequently, before applying a curve of growth analysis, it is necessary to know the relative magnitudes of the different line widths and the proximity of lines to each other relative to their width.

3.4 Curve of Growth for Molecular Hydrogen

3.4.1 The Doppler Approximation

In the case of H_2 the problem is simplified because the lines are quite well separated compared to the line widths. The closest rotational line separation is about 0.1Å which is considerably larger than the line widths, approximate values of which are given below. Furthermore, as will be seen below, a simplification can be made by considering only a Doppler curve of growth for the

analysis. First, we can obtain definite parameters for the curve of growth by considering the magnitude of the Lorentz and Doppler widths under the experimental conditions. The lifetimes of both excited states (B and C) are approximately 10^{-9} sec. (Hesser 1968). Experimental results were taken at pressures of about 10^{-3} torr, where the two Lorentz widths (at $\lambda_o \sim 1000$Å) are

$$\Delta_N \simeq 10^{-4} \text{ Å}$$

$$\Delta_p \simeq 10^{-9} \text{ Å}$$

where the values have been given to an order of magnitude only. Consequently the Lorentz width can be attributed only to natural broadening and is constant under experimental conditions. The Doppler width for H_2 at room temperature ($\sim$300°K) will be approximately

$$\Delta_D \simeq 5.10^{-3} \text{ Å}$$

Consequently the curve d=0.01 in Fig. 3.1 will give an approximate representation of the expected curve of growth for H_2.

Experimentally, it is desirable to obtain equivalent width measurements in a region where the gradient of the curve of growth is as large as practicable (i.e. W is varying

rapidly with $\underline{a}\int kd\lambda$. This is necessary because the reciprocal of the gradient effectively multiplies the error in W. From Fig. 3.1, for example, it can be seen that for a Doppler curve of growth in the region where it is varying slowly ("Doppler saturation" region) an error of, say, 10% in W will give an uncertainty of several hundred percent in $\underline{a}\int kd\lambda$. It therefore becomes necessary to take measurements either below this "Doppler saturation" region (i.e. $\frac{W}{\Delta_D} < 3$) or in the higher pressure region where the Lorentz wings of the natural broadening become important. The latter choice is, however, undesirable because the natural width is not known with great precision, and also the pressure broadening becomes more important and can no longer be ignored. Consequently, measurements of W need to be taken for $\frac{W}{\Delta_D} < 3$ to yield accurate values of $\underline{a}\int kd\lambda$. This procedure has the added advantage of being independent of the Lorentz width provided that $d << 1$ i.e. the curves d=0 and d=0.01 are indistinguishable in the lower region of the curve of growth. It would appear, from Fig. 3.1, that this condition holds for all values of d, however, there are minor differences between the curves which cannot be shown on the log/log scale of the figure. Nevertheless, the differences are negligible for $d < 0.1$, and a Doppler curve of growth can be assumed under the experimental conditions.

3.4.2 Equivalent Width of Doppler Lines

Substituting the Doppler profile into equation 3.6 gives the equivalent width as

$$W = \int 1-\exp\left[-k_o\underline{a}\ \exp-\left(\frac{\lambda-\lambda_o}{\Delta_D}\right)^2\right]d\lambda \qquad \ldots\ 3.21$$

The integral can be expressed as a power series of $k_o\underline{a}$, (Mitchell & Zemansky 1934) giving

$$W = \Delta_D\ \pi^{\frac{1}{2}} \sum_{n=1}^{\infty} (-)^{n+1}\ \frac{(k_o\underline{a})^n}{n!n^{\frac{1}{2}}} \qquad \ldots\ 3.22$$

The integrated absorption coefficient can be expressed in terms of k_o

$$\text{i.e. } \int k d\lambda = k_o \int \exp-\left(\frac{\lambda-\lambda_o}{\Delta_D}\right)^2 d\lambda \qquad \ldots\ 3.23$$

This reduces to (Mitchell & Zemansky 1934)

$$\int k d\lambda = k_o\ \Delta_D\ \pi^{\frac{1}{2}} \qquad \ldots\ 3.24$$

Hence the relationship between W and $\underline{a}\int k d\lambda$ (curve of growth) can be established by expressing $\underline{a}\int k d\lambda$ in terms of $k_o\underline{a}$ (equation 3.23) and substituting into the power series in

equation (3.22). The corresponding curve of growth is shown in Fig. 3.2 (only the experimentally useful region $\frac{W}{\Delta_D} < 3$ is shown). This curve is, in fact, the lower part of the d=0 curve of Fig. 3.1 plotted on a linear scale. A linear curve of growth (i.e. $W = \underline{a}\int k d\lambda$) is shown for comparison by the broken line. From the two curves it is clear that, for Doppler lines, the linear small absorption region (see Section 3.2.2) is approximately valid only for $\frac{W}{\Delta_D} \leq 0.2$ (i.e. $W \leq 1$ mÅ for $\Delta_D \approx 5$ mÅ).

From this curve of growth it is therefore possible to obtain a value of $\int k d\lambda$ from the measured value of W and amount of gas $\underline{a}$ (or pressure and length - see Section 5.2).

From Fig. 3.2 it can be seen that the gradient at $\frac{W}{\Delta_D} = 3$ is small (<0.5) and the error in $\int k d\lambda$ would be more than twice the experimental error in W. An arbitrary upper limit of useful measurements was taken at $\frac{W}{\Delta_D} = 2.5$, where the gradient is about 0.5 and the error in $\int k d\lambda$ is twice the error in W.

3.4.3 Experimental Curve of Growth

The Doppler approximation can be verified by determining an experimental curve of growth. The general procedure consists of measuring W as a function of pressure and verifying that the variation of W with pressure does in

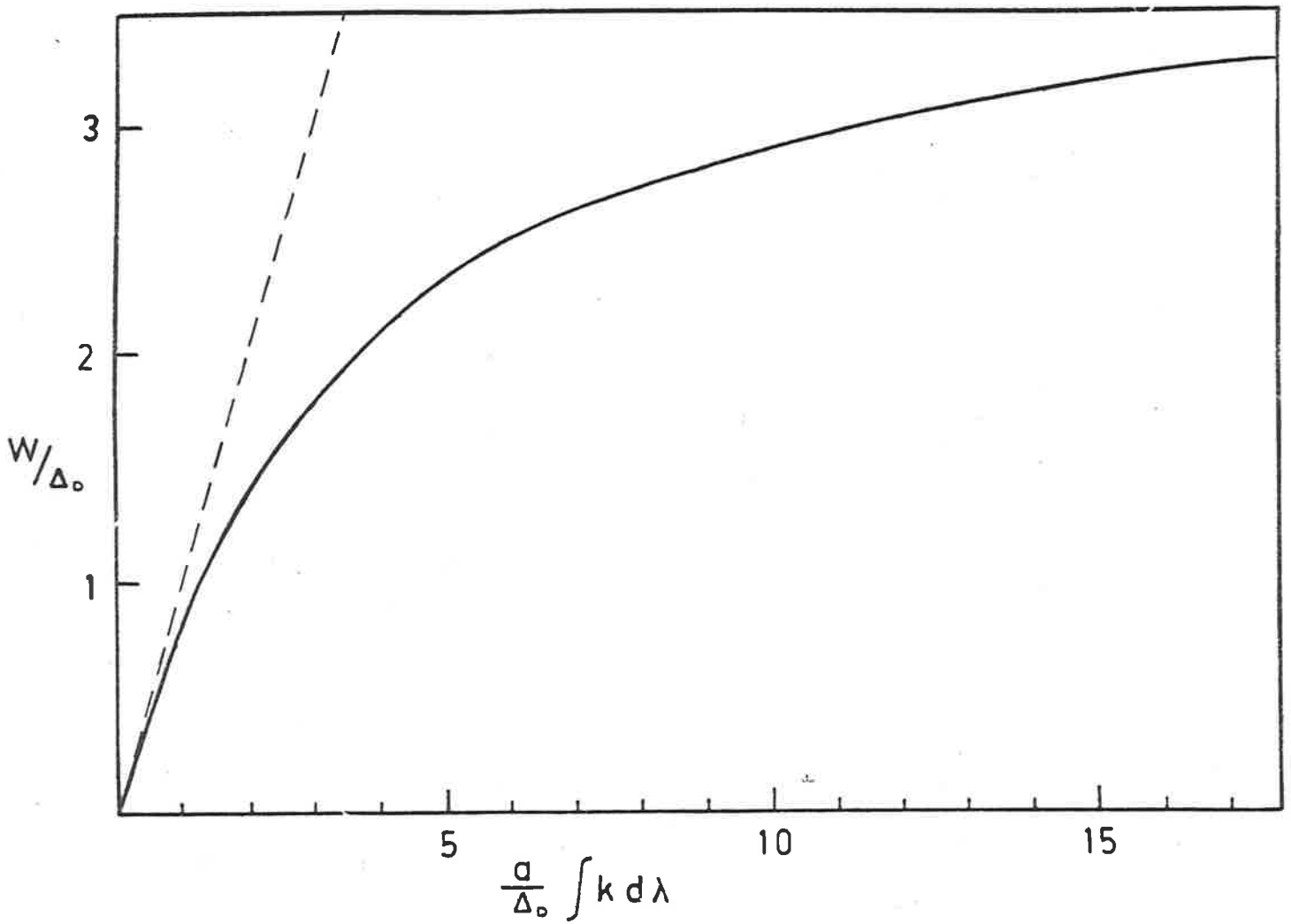

Fig. 3.2 The curve of growth for a Doppler line

fact follow the Doppler curve of growth. Since quite accurate values of W are required to obtain a meaningful curve, however, this procedure is quite slow. It is possible nevertheless, to obtain a relative curve of growth quite rapidly by using an approximation which is valid when the line width is very much narrower than the resolution width of the instrument. Using equation (3.4), the apparent absorption A' may be written

$$A' = \frac{\int F(\lambda-\lambda') \, I_\lambda \, A_\lambda \, d\lambda}{\int F(\lambda-\lambda') \, I_\lambda \, d\lambda} \qquad \ldots\ 3.25$$

For a given wavelength setting λ', the denominator in the above expression is constant and may be written γ^{-1}.

$$\text{i.e.} \quad A' = \gamma \int F(\lambda-\lambda') \, I_\lambda \, A_\lambda \, d\lambda \qquad \ldots\ 3.26$$

The integral is finite only when $A \neq 0$, i.e. over the limits of the absorption line. If the line is centred on wavelength λ_o and if the resolution function is much wider than the line, we may approximate $F(\lambda-\lambda')I_\lambda$ in equation 3.26 by $F(\lambda_o-\lambda')I_{\lambda_o}$ and write

$$A' \simeq \gamma F(\lambda_o-\lambda')I_{\lambda_o} \int A_\lambda \, d\lambda$$

$$\text{i.e.} \quad A' \propto W \qquad \ldots\ 3.27$$

Hence if the wavelength setting is kept constant and the apparent absorption A´ is measured as a function of pressure, the variation of A´ will follow the variation of W, i.e. the curve of growth. Naturally, such a curve will not give the absolute values of W against pressure and therefore reflects only the nature of the curve of growth. However, the experimental values can be normalized by measuring the actual equivalent width at one pressure and fitting it to the unnormalized curve.

An experimental curve of growth has been taken for the R_1 line of the (3-0) Lyman band using this technique. The monochromator was set at a wavelength λ' just greater than the R_1 line centre to avoid interference from the R_o line. (The line separation between the R_o and R_1 is approximately 0.5Å). The corresponding curve of growth is shown in Fig. 3.3. The solid line represents the theoretical Doppler curve of growth for the R_1 line (based on the average strength of the R_1 line from the results in Chapter 6).

Transmission measurements were taken with the photo-absorption system described in Chapter 4 and operated in the mode described in Section 4.6 except that the monochromator wavelength drive was turned off. Transmission measurements

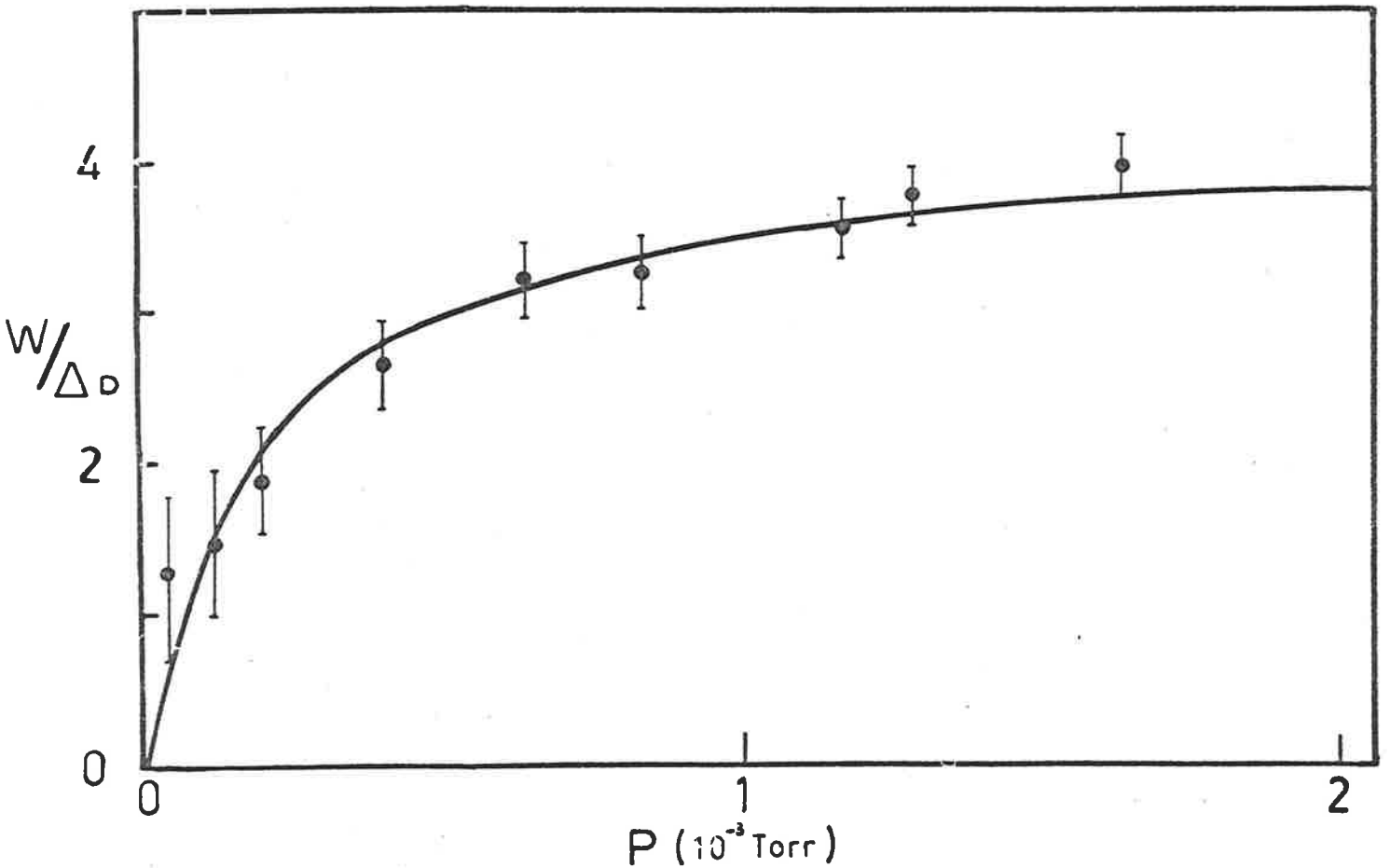

Fig. 3.3 An experimental curve of growth

were repeated a number of times for each pressure until the statistical error for the transmission was about ±0.2%. The corresponding error in the absorption is therefore $\pm \frac{0.002}{1-T}$. The maximum absorption in the Doppler saturation region was about 4% and the error indicated by the error bars in Fig. 3.3 is about ±5% of the absorption in this region. For smaller absorption, the relative error becomes increasingly large. The low absorption measurements also have a larger uncertainty in the absolute pressure than the higher pressure values (see Section 5.2.2); however, pressure error bars have been omitted from Fig. 3.3.

It can be seen from Fig. 3.3 that the experimental points are in excellent agreement with the theoretical Doppler curve of growth.

3.5 Doublet Analysis

One frequent type of measurement that cannot readily be analysed in terms of the simple treatment given so far is the case of unresolved pairs of lines. This occurred quite frequently, in fact, more frequently than isolated lines and was caused by the relatively poor available instrument resolution. In the case where a pair of lines is unresolved (e.g. the R_0 and R_1 lines of the Werner bands which are typically 0.1Å apart) we are able to measure only a total equivalent width W_T for the pair. We know, from the

Hönl-London factors and Boltzmann factors, the ratio of the theoretical line integrated absorption coefficients; but, because of the non-linear curve of growth the ratio of the equivalent widths will be different. If, for example, we have two lines where the values of $\frac{a}{\Delta_D}\int k d\lambda$ are 4 and 2 respectively, the corresponding values of $\frac{W}{\Delta_D}$ are approximately (from Fig. 3.2) 2.1 and 1.4 (i.e. a ratio of 3:2). To obtain correct values of $\int k d\lambda$ for these two lines W_T would therefore need to be split into corresponding components W_1 and W_2 which are in the ratio 3:2. As this ratio will vary, depending on the value of W_T as well as the ratio of the line strengths, a trial and error test would be required to obtain the corresponding correct components W_1 and W_2.

The problem can be overcome by introducing another parameter which is approximately linear with W and is related to the integrated absorption coefficient. If we introduce the function $S(k_o)$

where $$S(k_o) = \sum_{n=1}^{\infty} (-)^{n+1} \frac{(k_o a)^{n-1}}{n!\, n^{\frac{1}{2}}} \qquad \ldots\ 3.28$$

and substitute it into equation 3.22, the integrated absorption coefficient may be expressed as

$$\int k d\lambda = \frac{W}{\underline{a} S(k_o)} \qquad \ldots\ldots 3.29$$

W can also be related to the function $S(k_o)$ by equations (3.22) and (3.28) above

$$\text{i.e. } W = S(k_o)\, k_o \underline{a} \Delta_D \Pi^{\frac{1}{2}} \qquad \ldots\ldots 3.30$$

The above approach is particularly convenient because the values of the function $S(k_o)$ have been tabulated in terms of $k_o\underline{a}$ and $S(k_o)k_o\underline{a}$ by Mitchell & Zemansky (1934) [Mitchell & Zemansky actually use the term ℓ instead of $\underline{a}$ which is consistent with their discussion of absorption in a gas of one atmosphere. It will be shown in Section 5.2.1 that $\underline{a}=\ell$ when the pressure is one atmosphere]. For a given value of W (i.e. $S(k_o)k_o\underline{a}$ from equation 3.30), the corresponding value of $S(k_o)$ can be determined, and the values of W and $S(k_o)$ can then be used to determine the integrated absorption coefficient from equation 3.29.

Furthermore, the relationship between W and $S(k_o)$ turns out to be approximately linear over the range of experimentally useful equivalent widths. Fig. 3.4 shows the relationship between $\frac{W}{\Delta_D}$ and $S(k_o)$ (the parameter Δ_D normalizes the curve to be independent of line width). It can be seen that in the range $\frac{W}{\Delta_D} < 2.5$ (see Section 3.4.2) the relation

$$S(k_o) \simeq 1 - 0.225 \frac{W}{\Delta_D} \qquad \ldots\ldots 3.31$$

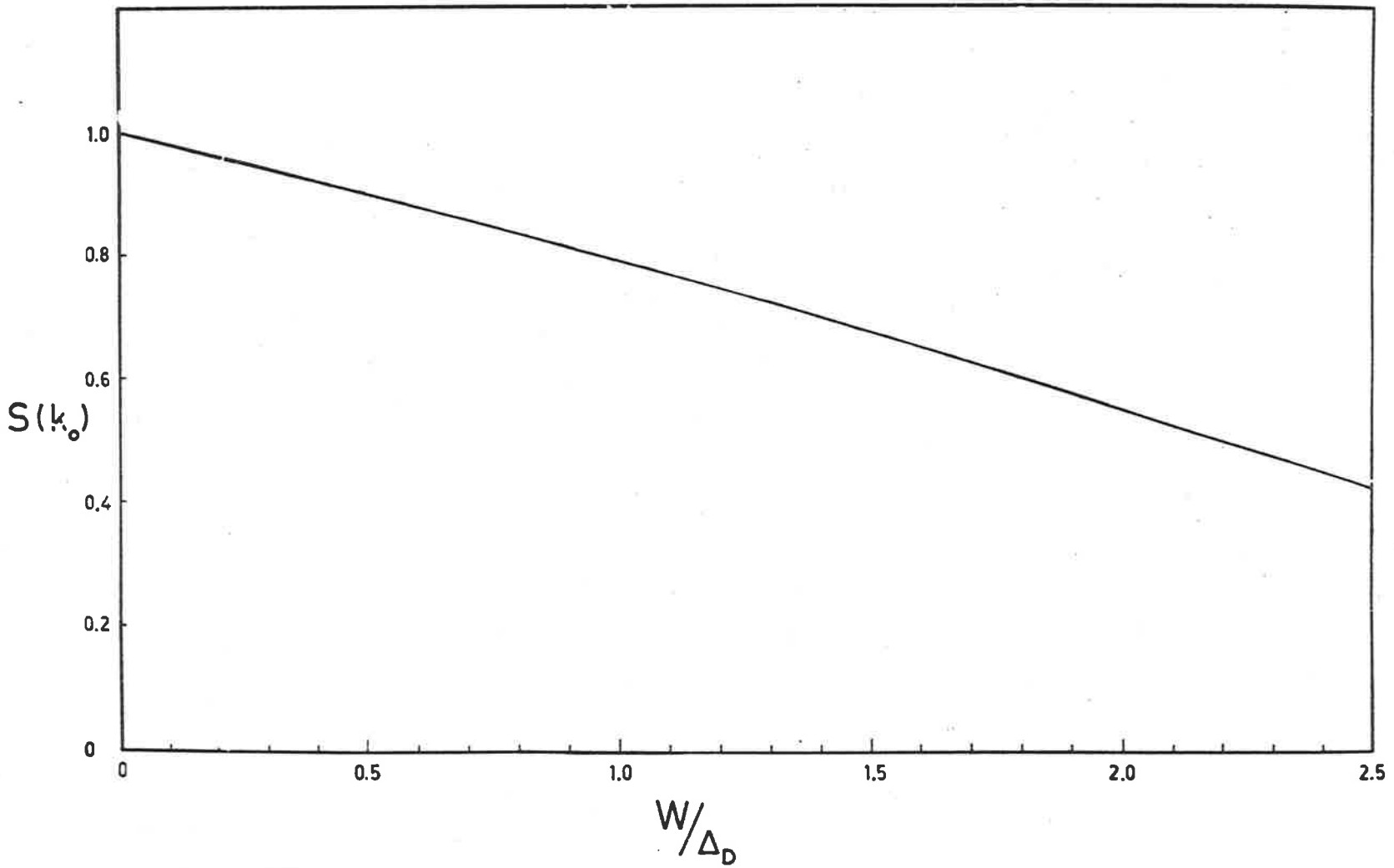

Fig. 3.4 The variation of $S(k_o)$ with $\frac{W}{\Delta_D}$

is approximately valid. This approximately linear relationship enables a given value of W_T to be split into its two components quite accurately by using the relations

$$W_T = W_1 + W_2 \qquad \ldots\ldots 3.32$$

and

$$\frac{W_1}{S(k_o)_1} = L_{1,2} \frac{W_2}{S(k_o)_2} \qquad \ldots\ldots 3.33$$

where the terms $S(k_o)_{1,2}$ refer to the value of $S(k_o)$ for line components 1 and 2, and $L_{1,2}$ is the theoretical ratio of the strengths (integrated absorption coefficients) of lines 1 and 2. $L_{1,2}$ will be determined by the corresponding Hönl-London and Boltzmann factors for the two lines. Using equations (3.31-3.33) it is therefore possible to determine the corresponding components W_1 and W_2 for a given W_T if the line strength ratio $L_{1,2}$ is known.

As the use of the function $S(k_o)$ is equivalent to the Doppler approximation used earlier (Section 3.4.2), it is convenient to adopt this form of analysis for all lines. It will be shown in Section 5.5.4 that the use of $S(k_o)$ also lends itself to an accurate error analysis by relating the error in W to an error in $\int k d\lambda$.

Using equation 3.29 we can express the line oscillator

strength (equation 2.29) directly in terms of W and $S(k_o)$

i.e. $$f_{v'o}^{J'J''} = \frac{mc^2 W}{N_A \alpha_{J'-} \Pi e^2 \lambda^2 S(k_o)\underline{a}} \quad \ldots\ldots 3.34$$

CHAPTER 4.

4. The Photoabsorption System

It was pointed out in the previous chapter that the main limitation in determining equivalent widths accurately, is the necessity to measure relatively small apparent absorption. Experimentally, this poses a problem because it is, in fact, the transmission that is measured. With conventional analogue techniques it is quite easy to measure transmissions to within say, 5%. However, if the absorption being measured is only 5% the relative error in the absorption will be 100%. If, therefore, accurate equivalent widths are to be determined it is necessary to use a technique whereby the transmission can be measured more accurately, or a multiple scanning system which repeats the measurement a large number of times and therefore improves the statistical accuracy. The present system is of the former variety and, in principle, the accuracy is limited only by data accumulation time (i.e. by counting statistics).

4.1 General Description

The following is a broad outline of the complete experimental system shown in Fig. 4.1. The various elements in the system and their functions will be described in greater detail in subsequent sections. Basically the system consists of a differentially pumped cell, two detectors,

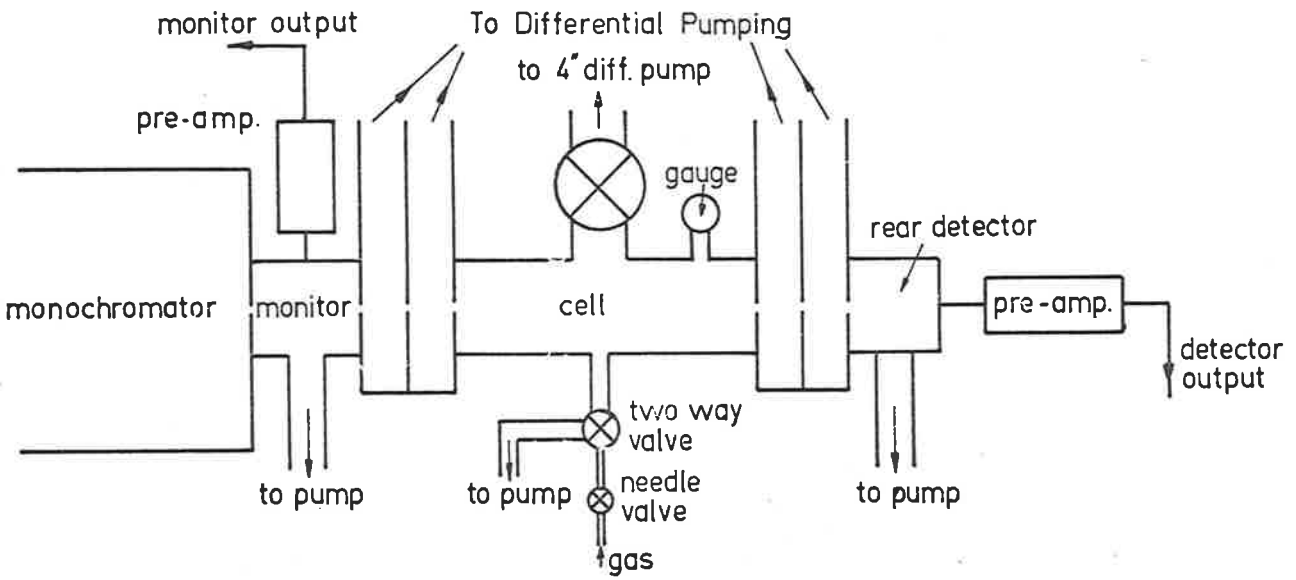

Fig. 4.1 A schematic of the photoabsorption system

one for measuring the incident flux and the other for measuring the transmitted flux through the cell, and a monochromator as the photon source. Near monochromatic light from the monochromator is sampled by the partially transparent incident flux monitor, the output count rate of which is proportional to the flux incident on the cell. A second detector at the other end of the cell measures the transmitted flux, and the outputs from these two detectors are used to determine the relative transmission. Normalization of the detector gains is achieved by alternatively measuring the transmission with the cell "full" and "empty". (As the cell is differentially pumped, a high pressure can only be maintained by leaking gas into the cell. Hence the terms "full" or "empty" refer to the case of the gas leaking into the cell or not). The "empty" pressure was considerably less than the "full" pressure, hence, defining the transmission ratio for the "empty" as equal to unity enables the "full" transmission ratio to be normalized such that it is in fact the absolute transmission. (The term "absolute transmission" will, for brevity, be taken to mean the absolute transmission integrated over the wavelengths defined by the instrument resolutions).

In practice, it is impossible to evacuate the cell completely, hence, there will be some absorption

associated with the "empty" transmission measurement. However, this absorption is small, and certainly much smaller than that associated with the "full" measurements; consequently, the error introduced is small and certainly much smaller than the statistical error.

The transmission ratio is obtained as a binary number from a digital divider and stored on magnetic tape. The data handling and reduction, as well as the operation of the system such as wavelength advance, emptying and filling the cell, is controlled electronically.

4.2 The Monochromator

A McPhersons model 225 1 metre near normal incidence vacuum ultra-violet monochromator was used as the dispersing instrument. The monochromator was fitted with a 1200 line per m.m. grating blazed for 1200Å and giving a reciprocal dispersion of 8.3Å per m.m. in the first order. The monochromator was operated with a resolution of about 0.3Å corresponding to an entrance and exit slit size of about 30μ. Narrower slits with correspondingly improved resolution could not be used conveniently because the entrance slits became rapidly clogged by sputtered material from the lamp cathode (see Section 5.5.1).

The wavelength drive of the monochromator was modified with a stepping motor which enabled the wavelength to be

incremented in small predetermined steps. Increments of 2.5 mÅ or any multiple thereof could be obtained by feeding a command pulse into the stepping motor control unit. Absorption measurements were taken as normalized transmission measurements for each step position and the final spectrum consisted of a large number of measurements taken at regular intervals (see Section 4.6). A typical line absorption spectrum is shown in Fig. 4.2.

For most absorption measurements a wavelength increment of 10 mÅ was used. The use of such a small step served two purposes. First, the statistical error associated with the equivalent width (integrated or summed absorption over the line) is less than that of a single measurement. Second, minor irregularities in the magnitude of the wavelength increment are insignificant if the increments are much smaller than the apparent width of the line.

4.3 The Light Source

A water cooled capillary discharge tube operated in a pulsed discharge mode was used as the light source. The lamp was pulsed by a thyratron modulated power supply and operated at a repetition rate of 2KHz with a pulse voltage of 7 K.V. and an average current of 20m.A. The circuit and description of the power supply are given in Appendix I.

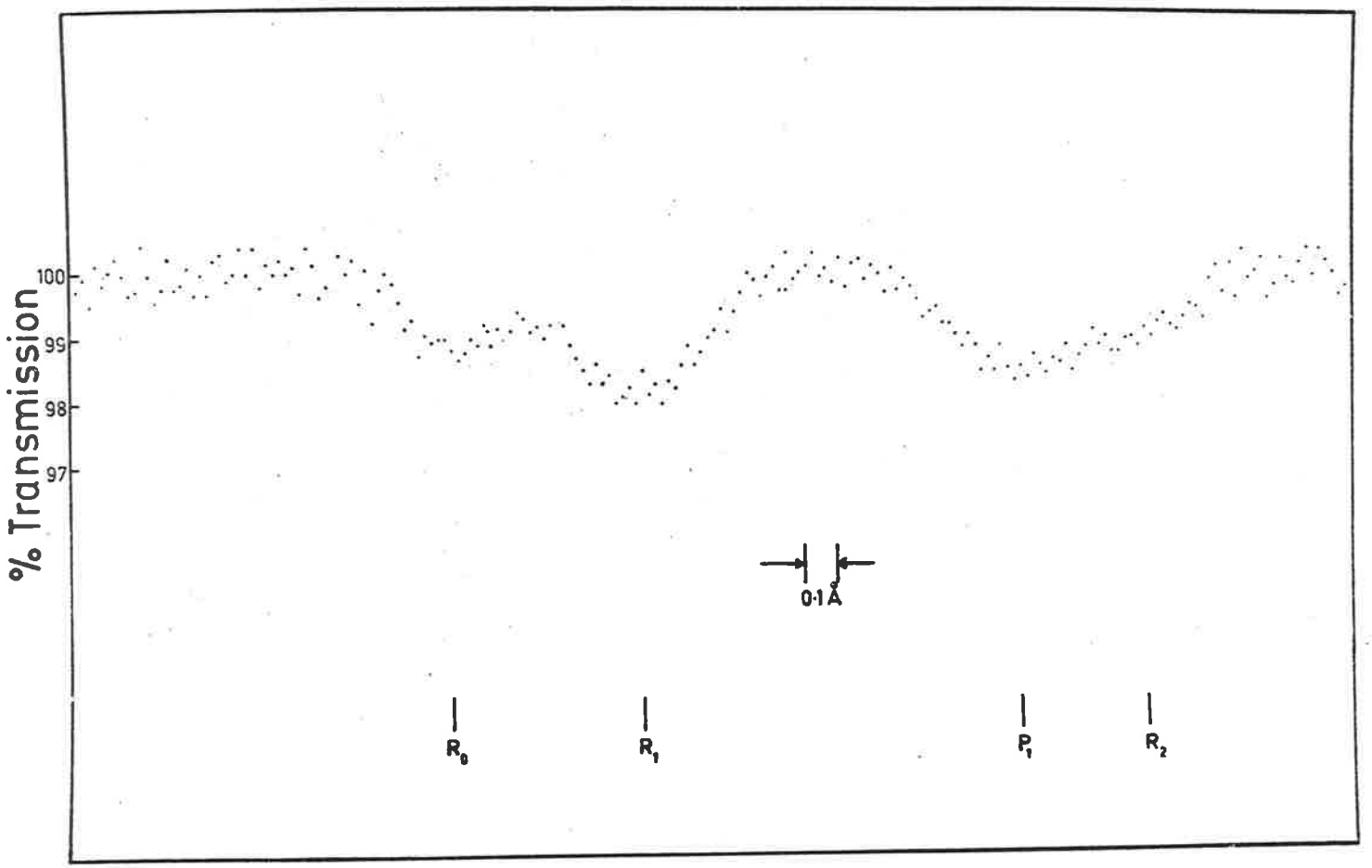

Fig. 4.2 A typical spectrum of a part of the (3-0) Lyman band taken with a resolution of ∿ 0.5 Å and a wavelength increment of 20 mÅ between measurements

The lamp construction was basically the same as the capillary discharge tube described by Newburgh et al. (1962) and consisted of a hollow aluminium cathode and a pre-slit adjacent to the entrance slit of the monochromator as anode. The windowless lamp was isolated from the monochromator vacuum chamber by a two stage differential pumping system consisting of a high speed Roots blower first stage and a high speed oil booster second stage. Both pumps were backed by conventional rotary vacuum pumps.

4.3.1 Rare Gas Continua

The lamp was used with either argon or helium, the continua of which have been investigated by many authors (e.g. Huffman et al. 1963, 65(a), Wilkinson & Byram 1965). In the case of argon, the two broad resonance lines at 1048Å and 1066Å were also used as "continua" because the lines are sufficiently wide compared to the resolution width of the monochromator, to allow the equivalent width of absorption lines in the wings of the resonance lines to be measured. Maximum intensity of these resonance lines was obtained when the lamp was operated at a pressure of about 5 torr. The maximum intensity of the argon continuum is obtained at lamp pressures of about 200 torr (Zaidel & Schreider 1970). However, the differential pumping did not permit such high lamp pressures to be maintained and the

lamp was operated at a pressure of about 60 torr.

The helium continuum was used for the absorption measurements below 980Å. The continuum intensity above 980Å was too low to enable sufficiently accurate line measurements to be made within a reasonable time (see Section 5.5.1). The maximum flux from this continuum was obtained when a gas pressure of about 100 torr was used in the lamp.

4.3.2 Gas Purity

It has been pointed out by many workers (e.g. Huffman et al. 1965(a), Wilkinson & Byram 1965) that the rare gas continua can only be excited when the impurity level in the gas is very low. This arises from the fact that the rare gases have a high ionization potential and the presence of lower ionization potential impurities can quench the continuum discharge.

For the present work commercial grade bottle helium and argon were used. Surprisingly, purification with liquid nitrogen traps and a molecular sieve (type 13X) did not produce a noticeable change in the intensity of the continua. In the case of unpurified helium, the low intensity of the observed impurity emission lines suggested that the impurity level was small. Purification reduced the intensity of these lines but did not completely remove them. However, the continuum intensity did not rise

noticeably.

As there was no gain in the continuum intensity, the only benefit that could have been gained from using the molecular sieve would have been the removal of impurity emission lines and an increase in the amount of useable continuum for absorption measurements. According to the discussion in Section 3.2, the integrated observed absorption is equal to the equivalent width only if there is no structure such as an emission line superimposed on the continuum. The molecular sieve purification, although reducing the intensity of the impurity emission lines, did not reduce them sufficiently to allow absorption measurements to be taken, and therefore did not warrant its use. The commercial grade argon also exhibited a minimal effect when purified by the molecular sieve. Therefore no purification was employed for the lamp gases.

4.4 Detectors

Both detectors were Mullard type B419BL channel electron multipliers (C.E.M.) operated in a pulse counting mode. These detectors are ideally suited for far ultra-violet work as they have an extremely low noise of less than one count per second and are insensitive to scattered light above 1600Å. The rear detector was used as a photon detector, the quantum efficiency being about 7% at 1000Å and the photoelectric response curve in this region is similar to tungsten (Evans 1965).

The front detecting system consisted of a tungsten grid photo-cathode and a C.E.M. Photo-electrons from the grid were accelerated towards the C.E.M. entrance cone which was at a positive potential relative to the grid. This accelerating potential, which was adjustable, was set to give the maximum count rate. The optimum accelerating voltage was found to be about 200V which is in agreement with the results of Frank et al. (1969), who found a peak electron collecting efficiency for a Bendix C.E.M. to be ∿85% at 200eV incident electron energy. A more detailed description of this detecting system and its associated vacuum chamber is given in Appendix II.

4.4.1 Gain Stability

The maximum operating pressure for the C.E.M. quoted by the manufacturer is about 10^{-3} torr. As the absorption measurements were made at pressures of about 10^{-3} torr or less, the detectors could be safely operated without any precautions. However, the gain of a C.E.M. was found to be slightly sensitive to ambient pressure (see Section 5.4.1). To maintain gain stability, it was therefore essential that the detector chamber pressures be kept constant; consequently the cell was differentially pumped at all times, even when cell pressures of about 10^{-4} torr were used.

Relative variations of the gains of the two detectors due to power supply instability was overcome by operating both detectors from the same power supply (Fluke model 408B). The slightly different operating voltages and the electron accelerating voltage for the front detector were obtained from simple resistive voltage dividers and the multiplier voltages were about 3 K.V.

However, even with these precautions the gain of the two detectors did not remain constant. There was a slow gain change due to a gradual degradation of the C.E.M. as well as a gain change caused by pressure variations between the "empty" and "full" cell. The slow gain drifts were corrected for by an averaging technique which is described in Section 4.6.2 and the pressure induced gain changes were allowed for in the analysis of results (see Section 5.4.1).

4.4.2 Detector Outputs

The outputs of the two C.E.M.'s were amplified by preamplifiers mounted adjacent to the vacuum system. (see Appendix III). The preamplifier output pulses of approximately 40 n s width and several hundred mV height were fed into a dual discriminator (E.G. and G type TR104S) and then into fast three bit prescalers (E.G. and G type S100) which interface between the discriminators and the rest of the data handling system. This interface was needed because

the integrated circuitry used cannot handle the narrow output pulses from the discriminator.

For convenience, and brevity, the outputs from these scalers will be referred to as the monitor and detector outputs.

4.5 The Absorption Cell

The absorption cell consists of a tube, approximately 41 c.m. in length, with parallel narrow differential pumping slits at each end. The gas flow into the cell was via a needle valve coupled to the inlet of a small electrically controlled two-way valve which will be referred to as the gas admittance valve. One outlet of this valve was connected to the cell, the other to a pump such that the gas flow through the needle valve would be either into the cell or into the pump. The use of this pump prevented the gas pressure between the needle valve and the admittance valve from building up when the cell was isolated (i.e. "empty").

The cell pressure was determined by the needle valve leak rate which was reasonably constant for a given needle valve setting. The pressure stability and reproducability was as good as the reading accuracy of the pressure gauges (i.e. within a few percent). As the absolute pressure calibration (see Section 5.2.3) was only accurate to within 5%, the error due to pressure variations was negligible compared to the absolute pressure accuracy.

Emptying the cell was achieved by shutting the gas admittance valve and simultaneously opening a second electrically controlled valve coupling the cell to a 4" diffusion pump. Filling the cell was similarly achieved by shutting the diffusion pump valve and opening the gas admittance valve.

Water vapour was pumped out of the cell by a small liquid nitrogen trap connected to the cell via a 1" butterfly valve. This relatively small aperture enabled any water vapour in the system to be pumped out readily without affecting the average gas temperature in the cell due to the large remaining surface area of the cell at room temperature.

Between the cell and both the front and rear detectors there were two differential pumping chambers (see Fig. 4.1) which could be connected to a 4" diffusion pump or a larger differential pumping system identical to that used for the lamp. The 4" diffusion pump was used for all absorption measurements as these involved cell pressures of about 10^{-3} torr or less (see Section 5.3.1), and the larger differential pumping system was used for preliminary high pressure scans of up to 0.1 torr for location of the absorption lines.

4.6 Digital Data Handling System

The mechanical operation and data handling are

incorporated into the same basic electronic control system and their operation will therefore be considered together.

Fig. 4.3 shows a simplified schematic of the basic control and data reduction system. The principle of operation may be summarized as follows. The ratio of the transmitted flux for a "full" cell and an "empty" cell is obtained by using a digital divider. By ensuring that the incident flux is the same for both measurements, this ratio will be the absolute transmission. The constant flux condition is met by controlling the data accumulation times (i.e. total recorded flux) from the incident flux monitor.

The various elements and their function in the system are (see Fig. 4.3)

1. The reference scaler.
   The binary scaler used to accumulate the monitor counts is referred to as the reference scaler. When this scaler has accumulated 2^n counts (where n can be set between 10 and 19), it generates a pulse which is used to trigger the other electronics in the system.
2. The digital divider.
   The digital divider consists of two 16 bit binary scalers which we call X and Y, an arithmetic binary dividing unit and a 16 bit count down scaler at

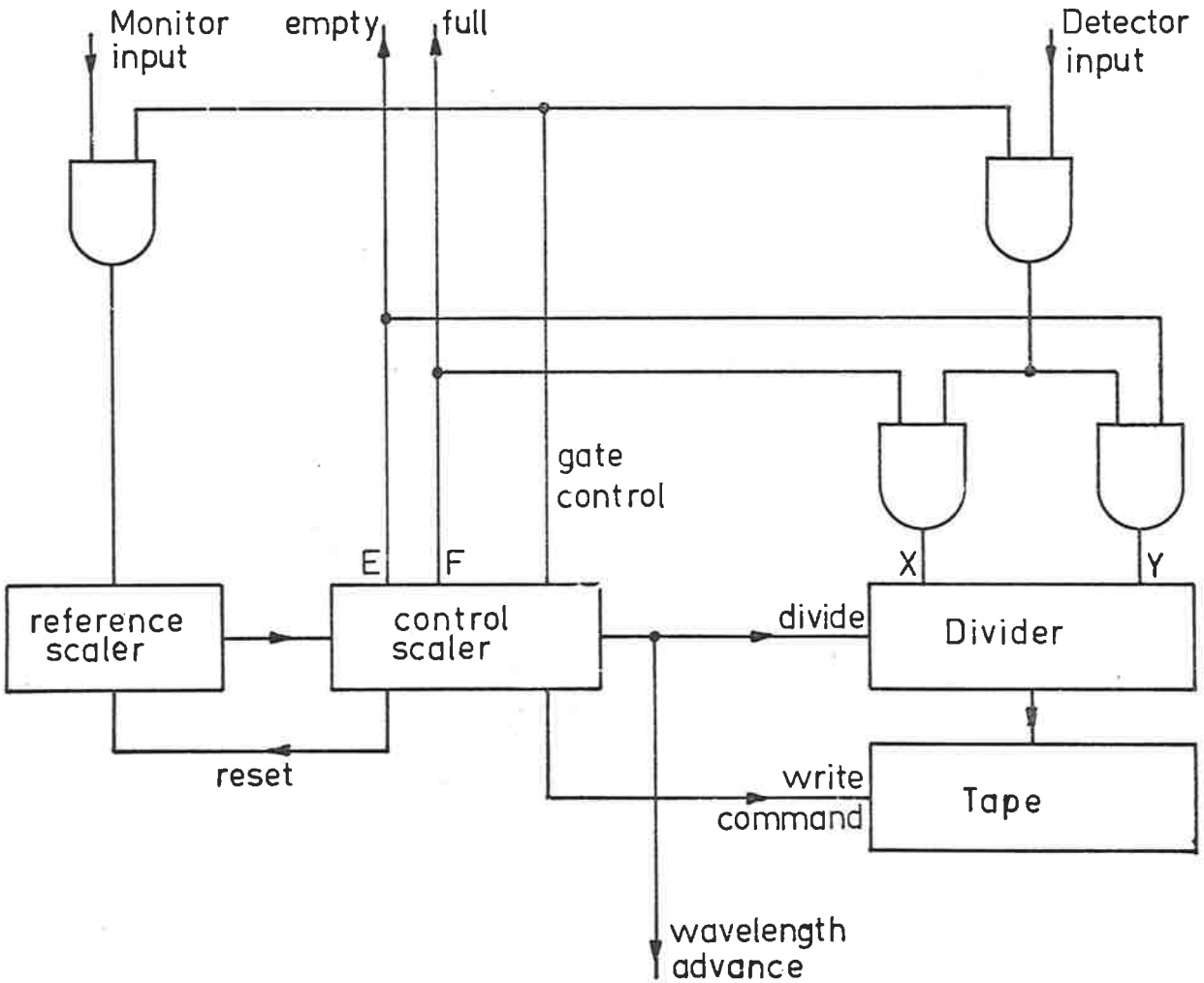

Fig. 4.3 The schematic of the digital data reduction and recording system

the output. On a command pulse, the binary ratio of X and Y is obtained and presented as a series of pulses from the count-down scaler.

3. A magnetic tape storage system.
   The tape storage system consists essentially of three scalers for data accumulation and one scaler used as a channel number (or data recognition channel). On a write command pulse, the contents of these scalers are transferred to the tape and the channel number advanced by one.

4. The control scaler.
   A simple two bit scaler is used to control the various stages of operation of the system. The four distinct states of this scaler are decoded to control the operation of the entire system which has four measurements associated with each complete cycle (see next section).

Details of the operation and circuits of the various sections of the data handling system are given in Appendix IV.

4.6.1 Operation

The control and data handling system is a recycling system, each cycle giving two transmission values. The overall operation of the system can be understood from

the operations contained within a single cycle, which, from a cell "full" condition, consist of the following sequence.

1. Cell "full" (gas admittance valve open)
   The reference scaler (initially reset) accumulates the monitor counts and the rear detector is gated into the X scaler of the divider.
2. When the reference scaler fills (i.e. reaches 2^n), the rear detector is gated off, the gas admittance valve shuts (and 4" diffusion pump valve opens).
3. After a delay of about ½ minute during which time the cell pressure reaches equilibrium, the rear detector is gated into the Y scaler of the divider while the reference scaler again accumulates the monitor output.
4. When the reference scaler again reaches 2^n, the following operations take place.
   a. The Y scaler gate closes.
   b. A divide command pulse is fed into the divider, giving the ratio X/Y out. The scalers X and Y are automatically cleared after this operation.
   c. The wavelength of the monochromator is incremented by a preset amount (typically 0.01Å).

5. After a short delay (approximately 3 secs) the contents of the tape scaler (X/Y) is written on tape. The Y scaler gate opens again and another "empty" measurement is made.
6. After the "empty", another "full" measurement is made (with a suitable delay for gas pressure to reach equilibrium). At the end of the "full", operation 4 is repeated (except 4(a), X scaler closes).

The reason why the "empty" and "full" measurements are alternated in pairs is discussed in the next section.

4.6.2 System Stability

The time taken to obtain a single absolute transmission measurement was less than 10 minutes. It had been noticed that the relative gain drift between the two detectors was small and the gain fluctuations had longer periods than 10 minutes. Gain drifts with periods considerably longer than 10 minutes were eliminated by using an alternating technique described below. In considering the operation, there is a time lag between the accumulation in the X and Y scalers of the divider. Hence, if there is a slow change in the gain of one detector relative to the other the ratio X/Y is not a correctly normalized transmission ratio. If, for example, the gain in the rear detector is

slowly increasing and the accumulation order is X, then Y, the ratio X/Y will be slightly smaller than it should be. A suitable technique to overcome this error consists of reversing the order of accumulation for the next transmission measurement, (i.e. the accumulation sequence is X, Y, Y, X, X etc.). A slow gain change will therefore give ratios of X/Y which will be alternatively higher and lower than the correct value, giving close to the correct average value.

4.6.3 Statistical Accuracy

Most transmission measurements were made to constant statistical accuracy. This condition could be met over a large range of photon fluxes by varying the wavelength increment and the reference scaler, always keeping the complete "empty" and "full" measurements to less than 10 minutes, e.g. a typical spectrum may be obtained with an increment of 1/50Å and reference scaler set for 2^{16} counts. If the flux level drops to a level such that 2^{16} counts would take more than 10 minutes, the spectrum can be obtained at 2^{15} counts and 1/100Å steps, i.e. half as many counts/data point with twice as many steps for the same spectrum. Total accumulated counts and accuracy are the same in both cases. Hence by suitably varying the reference scaler and magnitude of increment, the same total accuracy can be obtained with

each transmission measurement restricted to less than 10 minutes. Typical scanning accuracies will be discussed in the next chapter.

4.6.4 Absolute Transmission

The divider output X/Y represents the absolute transmission as is evident from the following. Since the data accumulation time is controlled by the accumulated monitor counts, the recorded rear detector counts will be $2^n \frac{D}{M}$*, where 2^n is the total monitor counts registered by the reference scaler, and $\frac{D}{M}$ is the ratio of detector to monitor count rates. Hence the X scaler of the divider contains $2^n \frac{D_F}{M_F}$ counts where the subscript F denotes cell "full". Similarly Y contains $2^n \frac{D_E}{M_E}$ counts, E denoting "empty". Hence X/Y represents $\frac{D_F}{M_F} \Big/ \frac{D_E}{M_E}$, i.e. the "full" detector ratio normalized by the "empty" detector ratio. As the pairs D_F, M_F and D_E, M_E are measured simultaneously, the result was also independent of any variations in flux.

---

* Assuming that the relative gain of both detectors is constant

CHAPTER 5

5. Procedure and Data Analysis

5.1 Introduction

Equivalent width measurements were taken with the system described in Chapter 4 for as many lines of the Lyman and Werner bands as possible within the experimental limitations which will be discussed in this chapter.

The wavelengths of the rotational lines were obtained from the data of Dieke (1958) and Namioka (1964 a) and were located by calibrating the wavelength drive of the monochromator from observed emission lines. For the argon continuum, the wavelengths of the two broad resonance lines were used, and for the helium, the large number of impurity emission lines served as a reference. The wavelengths of the emission lines were taken from the tables of Kelly (Report UCRL-5612).

This chapter describes the preliminary measurements and assumptions required for the correct analysis of the experimental data. The experimental limitations are briefly discussed also. The analysis of the data to give band oscillator strengths is discussed, and a typical example of an absorption spectrum and the appropriate calculations are given.

5.2 Preliminary Measurements

5.2.1 Measurement of a

The determination of the integrated absorption coefficient from W needs one other measured parameter, namely a the amount of absorbing gas present. This is determined by the average number density (pressure) and the length of the absorbing column. In a static gas column a will be given by (Goody 1964)

$$a = \ell p \qquad \ldots 5.1$$

where ℓ is the length of the gas column and p is the pressure (in atmospheres).

Although the absorption cell was differentially pumped, the value of a was assumed to be given by the static cell expression above, where the length was taken as the distance between the differential pumping slits. At the experimental operating pressures of about 10^{-3} torr, the above approximation should hold because the rectangular differential pumping slits ($\sim$ 3×15 mm) are very much smaller than the mean free path which is approximately 160 mm at 10^{-3} torr for H_2 (C.R.C. Handbook 1968).

The validity of the above approximation can be tested by measuring a as a function of pressure. We may write Beer's Law in the form

$$\ln T = -k\underline{a} \qquad \ldots 5.2$$

Consequently, for a region where the absorption coefficient is constant (i.e. a continuum), the variation of $\underline{a}$ with measured pressure can be determined from the variation of the transmission with measured pressure. When k is constant, we also have the added advantage that the transmission is independent of resolution and can be measured directly (see equation 3.5).

Ideally, it would be best to take such a series of transmission measurements with H_2, as they could then be directly related to the experimental work. Unfortunately, the H_2 continuum is weak and has a superimposed band structure, and an alternative gas had to be used. Oxygen was chosen as a suitable alternative because it has a strong ionization continuum with several regions of approximately constant absorption coefficient. One such region ($\lambda \sim 745$Å) is particularly useful because the helium continuum is quite intense in this region, thus enabling rapid transmission measurements of high statistical accuracy to be made.

Transmission measurements were taken with the photo-absorption system operated as described in Section 4.6 except that the wavelength advance was off (i.e. the measurements were made at a constant wavelength). About 20 measurements

were taken for each pressure, with a statistical error of about 1% per transmission measurement, thus giving a final transmission accuracy of about 0.2% for each pressure. When sufficient measurements were taken, the wavelength was advanced by about 2Å and several measurements were repeated and found to give the same transmission within the statistical error. This then served to verify that the absorption coefficient was approximately constant in this spectral region.

The values of ln T against pressure are shown in Fig. 5.1. The best fit straight line suggests that the proportionality

$$\underline{a} \propto p \qquad \ldots 5.3$$

holds over the appropriate pressure range. The proportionality may be written in terms of an effective cell length ℓ'

$$\text{i.e.} \qquad \underline{a} = \ell' p \qquad \ldots 5.4$$

We may therefore express the gradient of the line in Fig. 5.1 as

$$\frac{d(\ln T)}{dp} = -k\ell' \qquad \ldots 5.5$$

Expressing p in atmospheres, this gradient has the value 22,200, and the absorption coefficient k in this region is

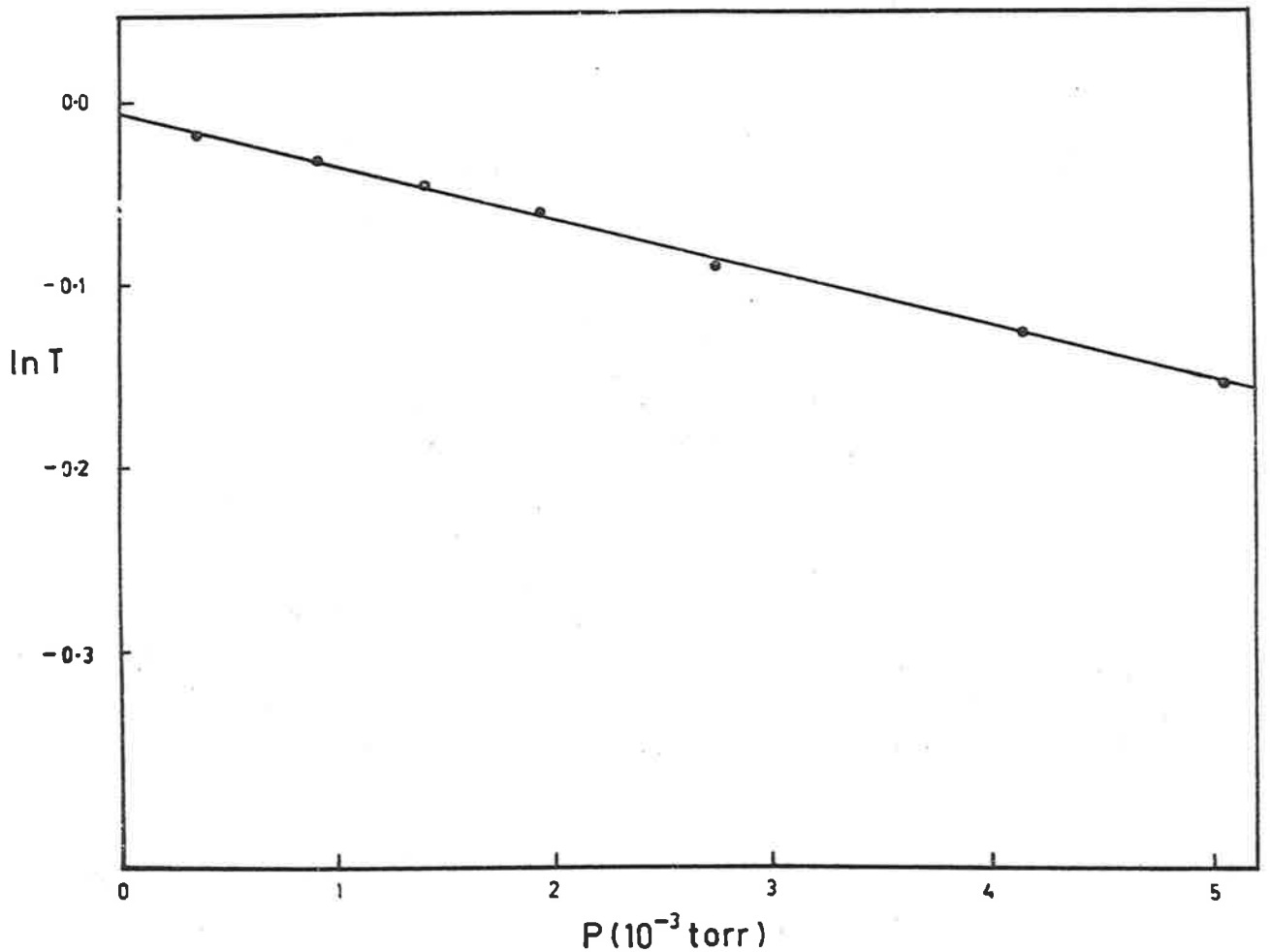

Fig. 5.1 The transmission as a function of pressure for 0_2 at $\lambda \sim 745$ Å

about 545 cm^{-1} at S.T.P. (Cook & Ching 1965). At the temperature at which the measurements were made ($22^{o}C$), this gives $k \simeq 505\ cm^{-1}$ and $\ell' = 44.0$ cms. The measured cell length was 41 cms. In view of the present experimental error, as well as the 10-15% error in k quoted by Cook & Ching, the value of ℓ' may therefore be assumed to be the same as the cell length (i.e. 41 cms).

There is no obvious reason why H_2 should behave differently from O_2 at comparable pressures, because the mean free path is much greater than the slit size for both O_2 and H_2. It is therefore expected that the above result will be valid for H_2 as well as O_2. Consequently, a constant cell length of 41 cms was assumed for the H_2 absorption measurements. An arbitrary uncertainty of 5% in this length was also assumed.

It will be noticed from Fig. 5.1 that the best fit line does not pass through the origin (T=1 when p=0). This "zero offset" is due to an experimental inadequacy which is discussed in detail in Section 5.4.1.

5.2.2 Pressure of the Absorbing Gas

The absolute pressure of the absorbing gas p_g was taken as proportional to the difference between the "full" and "empty" pressure readings.

$$\text{i.e. } p_g = C(p_F - p_E) \qquad \ldots 5.6$$

where p_F and p_E are the "full" and "empty" pressure gauge readings and C is a calibration scale factor (see Section 5.2.3). As p_E was about 5.10^{-6} torr, the differencing procedure can be ignored for "full" pressures above 10^{-4} torr. This differencing procedure was necessary for the lower operating pressures because p_E did not, in fact, correspond to the partial pressure of the residual hydrogen in the "empty" cell. A mass spectrometer (A.E.I. minimass) was fitted to the cell and it was found that, when the cell was "empty", the partial pressure of H_2 was very small ($\sim 10^{-7}$ torr) and the larger "empty" pressure reading was mainly due to water vapour and some N_2. Moreover, when the cell was "full", the partial pressure of water vapour and the other impurities did not appear to change. It was therefore assumed that the "full" pressure reading corresponded to the partial pressure of hydrogen plus that of the impurities which corresponded to the "empty" pressure reading. Accordingly, the measured partial pressure p_m of the absorbing gas is given by

$$p_m = p_F - p_E \qquad \ldots 5.7$$

The measured pressure can then be related to the absolute pressure p_g by a calibration factor C (see Section 5.2.3).

$$\text{i.e.} \quad p_g = Cp_m = C(p_F - p_E) \qquad \ldots 5.8$$

This differencing approximation was also tested by relative partial pressure measurements with the mass spectrometer and found to be valid. The mass spectrometer was not used for absolute partial pressure measurements throughout the experiment because its operating pressure upper limit ($\sim 10^{-5}$ torr) would have restricted its use to a few of the strongest lines.

It is interesting to note that, under the experimental conditions, the presence of the water vapour (plus other impurities) does not affect the measured transmission. From Section 4.6.4, it can be seen that the transmission can be written in terms of the separate "full" and "empty" measured transmissions T_F and T_E.

$$\text{i.e.} \quad T = \frac{T_F}{T_E} \qquad \ldots 5.9$$

If there is no interaction between the hydrogen and the impurities, the transmission will be given by the product of the hydrogen and impurity transmissions, (Goody 1964) which can be written $T(H_2)$ and T(Imp) respectively.

$$\text{i.e.} \quad T = \frac{T(H_2)_F \cdot T(\text{Imp})_F}{T(H_2)_E \cdot T(\text{Imp})_E} \qquad \ldots 5.10$$

As the impurity level does not change between the "empty" and "full" cell conditions, and the "empty" H_2 partial pressure is very low, we may write equation (5.10) as

$$T = T(H_2)_F \qquad \ldots 5.11$$

Hence the presence of the impurities does not affect the accuracy or reliability of the hydrogen transmission measurements, provided that the partial pressure of the absorbing gas can be measured.

5.2.3 Pressure Calibration

Cell pressures were measured by an ionization gauge (Edwards Speedivac model 3B) for pressures less than 10^{-3} torr and a Pirani gauge (Edwards model 7/2B) for pressures above 10^{-3} torr. Both gauges were calibrated absolutely with hydrogen and oxygen (for the cell length determination) against a McLeod gauge. The ionization gauge calibration was limited to pressures between 10^{-4} torr and just above 10^{-3} torr because the McLeod gauge was not sufficiently accurate at lower pressures and the ionization gauge could not be operated above 10^{-3} torr. However, the observed linearity in this range was used to extrapolate the calibration to lower pressures. The accuracy of the pressure calibration was estimated to be about 5%. Although

the Pirani gauge calibration was more extensive and covered a larger pressure range, the absolute calibration error was also taken as about 5%. Both gauges exhibited a linear variation of reading with absolute pressure, and the gauge pressure could therefore be directly related to the absolute pressure by an appropriate scaling factor C.

In the case of the ionization gauge reading, however, a temperature dependence must be taken into account. The ionization gauge reading p_m depends on the gas ionization potential and the gas number density, not the pressure

$$\text{i.e.} \quad p_m \propto N$$

From the gas equations this proportionality can be written

$$p_m = A \frac{p_g}{T'} \qquad \ldots 5.12$$

where A is an arbitrary constant, p_g is the absolute gas pressure and T' is the temperature at which the reading was taken. For the temperature T_c at which the gauge was calibrated, the absolute pressure can be related to the gauge reading by equation (5.8), giving

$$A = \frac{T_c}{C} \qquad \ldots 5.13$$

where C is the scale factor relating the gauge pressure to the absolute pressure at the appropriate temperature T_c. Hence

equation (5.12) can be written,

$$p_g = C\left(\frac{T'}{T_c}\right) p_m \qquad \ldots 5.14$$

i.e. the absolute gas pressure is related to the gauge reading by a scale factor C and the ratio of the calibration temperature to the temperature at which the measurement was made.

The oscillator strength, however, depends on $(N_A\ p_g)^{-1}$ (from equations 3.34 and 5.1), where N_A is the number density of the gas at one atmosphere and at temperature T' at which the absorption measurement was made. Substituting for p_g from equation (5.14), we can write,

$$N_A\ p_g = N_A\left(\frac{T'}{T_c}\right) C p_m \qquad \ldots 5.15$$

From the gas equations, $N_A\left(\frac{T'}{T_c}\right)$ will be the number density of the gas at one atmosphere and temperature T_c, and can be written N_c.

$$\text{i.e. } N_A\ p_g = CN_c\ p_m \qquad \ldots 5.16$$

Consequently, the value of $(N_A\ p_g)$ will depend only on the gauge reading and will be independent of temperature.

The same relationship does not hold for the Pirani gauge; however, the error introduced by the approximation that the measurements can be taken as independent of room temperature is not significant.

The pressure calibration was made at 22°C at which temperature the number density at 760 torr is about $2.487.10^{19}$ molecules per cm^3. Taking a cell length of 41 cms, and substituting for the various constants, the oscillator strength can be written (from equation 3.34)

$$f_{v''0}^{J'J''} = \frac{0.084\ W}{\alpha_{J''}\ p\lambda^2\ S(k_o)} \qquad \ldots\ 5.17$$

where W is expressed in mÅ, λ in Å and the approximate pressure $p = Cp_m$ in torr.

5.2.4 Gas Purity

The gas used for the absorption measurements was unpurified commercial grade hydrogen. Mass spectrometer tests failed to reveal any impurity in the gas which registered a change in the residual impurity level of the cell. In other words, although some impurities (e.g. H_2O, N_2, O_2 etc.) were present in the gas, their partial pressures were very low compared to the residual impurity level. It was pointed out (Section 5.2.2) that the residual impurity level does not affect the absorption measurement. If, on the other

hand, the incoming impurities are to have a noticeable effect, their absorption coefficients would need to be extremely large compared to H_2.

A heated palladium (diffusion type) purifier was used in an attempt to verify whether the gas impurities had any effect or not. There did not appear to be any difference; however, this result was not conclusive because the flow through the purifier was not constant (i.e. the pressure was not reproducible). This was, in fact, the main reason why it was not used throughout the experiment.

5.3 Equivalent Width Measurements

Prior to taking any equivalent width measurements, a lamp spectrum was obtained (over the required wavelength range only). This spectrum was then used to select the wavelength regions where the equivalent width measurements could be taken. (According to the discussion in Section 3.2, regions where there are emission lines, or other rapid intensity variations, do not yield a correct measure of W, and therefore cannot be used).

A second criterion for rejecting some regions is the absorption line spacings. Within a given separation (determined by the instrument resolution), adjacent rotational lines cannot be resolved. If these lines belong to the same band system, they can be treated as an unresolved doublet

(see Section 3.5). If, however, they belong to different band systems, they cannot be conveniently analysed unless one of the lines is very much weaker than the other, in which case it can be ignored.

5.3.1 Operating Pressures

When the lines which could be studied in a particular region had been selected on the basis of the foregoing section, approximate operating pressures were determined from estimates of the oscillator strength (from other experimental and theoretical values). The optimum operating pressure was chosen as that which yielded an equivalent width of $\sim$ 10 mÅ. (In the case of line doublets, the criterion that the stronger line contribution to the total equivalent width be about 10 mÅ was used).

The initial pressures selected were modified by trial and error until the above condition was met. As the trend of the results became obvious, however, it was possible to estimate appropriate operating pressures quite reliably. The maximum operating pressure used was $\sim 5.10^{-3}$ torr. Although the large differential pumping system could easily handle higher pressures, the length calibration could not be taken with the same reliability because the gas mean free path is comparable to the slit dimensions at pressures above 10^{-3} torr. As the mean free path of O_2 and H_2 are different

by $\sim$ 50% (C.R.C. Handbook 1968), the correlation between H_2 and an O_2 calibration at these higher pressures would not be as reliable as the low pressure calibration.

This upper pressure limit restricted work in most cases, to lines with $J'' \leq 3$.

5.3.2 Measuring Limits in W

It has already been pointed out (Section 3.4.2) that the useful upper limit of W is $\sim$ 12 mÅ $\left(\frac{W}{\Delta_D} \sim 2.5\right)$. The corresponding lower limit can also be determined from the acceptable error in W. This lower limit was arbitrarily taken as W $\sim$ 5 mÅ. Hence the operating range was taken as $1 < \frac{W}{\Delta_D} < 2.5$. Most measurements, however, were aimed at an optimum W $\simeq$ 10 mÅ $\left(\frac{W}{\Delta_D} \simeq 2\right)$ which gave a reasonable relative error and yet left enough margin for error (i.e. ±20% of 10 mÅ was still a useful and accurate value of W).

5.3.3 Line Scans

Equivalent widths were obtained from a transmission scan over a line; a scan consisting of normalized transmission measurements at regular wavelength intervals (typically 0.01Å). For convenience, each transmission measurement will be referred to as a channel (corresponding to a channel of data). With a resolution of $\sim$ 0.3Å (half width) we therefore need about 60 channels of data to define the complete observed absorption line.

A typical scan was started approximately 1Å before the line centre, thus allowing for a margin of error (the wavelength calibration of the monochromator was not exact) and also enabling a reference background level (no absorption) to be obtained before the line (provided that the region before the absorption line in question is free from other absorption lines). The need for this background measurement is discussed in Section 5.4.1.

During the scan, the temperature and both the "empty" and "full" pressures were noted. The pressures in particular, were noted regularly to obtain an average value of the pressure reading difference (see Section 5.2.2). These pressures were generally found to be quite reproducible and most observed variations, in fact, appeared to be in the gauge units rather than the pressure itself. (This was inferred from the lack of correlation between two different gauges during these variations).

A typical scan over a line is shown in Fig. 5.2. This scan was over the P_3 line of the (3-0) Lyman band. The wavelength increment was 0.01Å, the resolution $\sim$ 0.4Å and the reference scaler was set at 2^{17}. The analysis of the equivalent width and oscillator strength for this line will be given as a typical example in Section 5.4.3. The accuracy of this scan will also be discussed in Section 5.5.

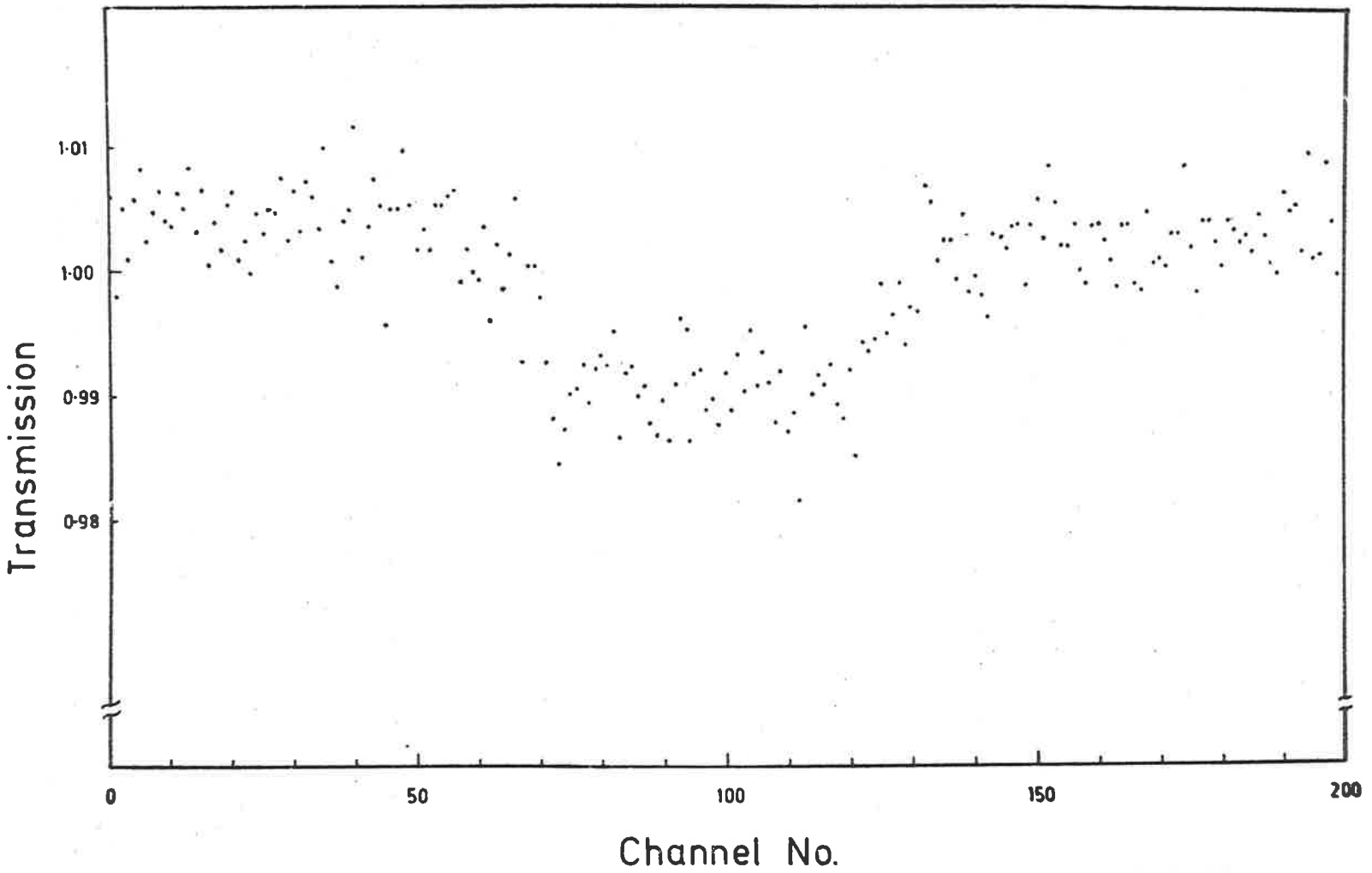

Fig. 5.2 A scan over the P_3 line of the (3-0) Lyman band. The resolution was $\sim$ 0.4 Å and the wavelength increment was 10 mÅ

5.4 Data Analysis

On completion of a scan, the contents of the tape were read into a multi channel analyser (R.I.D.L. model 34-12B) which served both as a convenient visual display of the data and a buffer to a printer (Hewlett-Packard model H23562A). The printed information was in the form of a channel number (corresponding to wavelength) and the channel content (corresponding to transmission ratio). A visual inspection of the displayed data was then used to determine the limits between which the data should be summed. The average transmission on either side of these limits was taken as a background reference level (see next section) from which the summed transmission was subtracted to yield the summed absorption. Multiplying this absorption sum by the wavelength increment Δ_λ then yields the equivalent width.

$$\text{i.e.} \quad W \simeq \Delta_\lambda \sum_{1}^{N} A_i \qquad \ldots 5.18$$

where the summation is over the N channels defining the absorption line.

5.4.1 Background Correction

It has been mentioned on several occasions that the measured transmissions for no absorption (referred to as background level) is not always unity [e.g. the typical

spectrum (Fig. 5.2) and measurement of a (Fig. 5.1)]. However, this effect could not be attributed to absorption because it did not change with cell pressure, and was often above 1.

The most likely explanation which appears to be consistent with observation is that this offset was caused by gain changes in the detectors due to small pressure variations in the detector chambers between the "full" and "empty" cell conditions. The ultimate pressure of the diffusion pumps appeared to be lower when no gas was being pumped (cell "empty"), than when gas was being pumped (cell "full"), giving rise to a small pressure change in the detector chambers. However, the pressure in the latter case did not appear to depend greatly on the cell pressure (within reasonable limits), possibly due to the high pumping speed.

The most direct evidence of the cause of this offset came from tests with the discriminators. The amount of offset from unity could be changed by changing the discriminator setting, suggesting that the pressure variation shifted the pulse height distribution slightly. It was also noted that for old C.E.M.s (for which the pulse height distribution was at a lower voltage level) the offset became worse. When new C.E.M.s were installed, the apparent transmission was close to unity, or just above, and over several months (at the

same operating conditions etc.) the level gradually fell to a few percent below unity.

As this effect could not be corrected without redesigning the entire system, a measure of the reference level (background) was required for each measurement. As the offset was small, and approximately reproducible over a scan, the relative effect on the integrated absorption is small and can be ignored. The equivalent width can be written (from equation 5.18).

$$W = \Delta_\lambda \sum_i^N \left(\frac{T_B - T_i}{T_B} \right) \qquad \ldots 5.19$$

where T_i is the value of a transmission measurement in the line and T_B is the background level.

5.4.2 Oscillator Strength Calculation

From the experimental value of W the corresponding value of $S(k_o)$ was determined from Fig. 3.4. This then enabled the line oscillator strength to be calculated using equation (5.17). Of more interest, however, is the band oscillator strength. The individual rotational line strengths are related to the band strength by the Hönl-London factors (see Equation 2.9), and therefore yield no more information about the system than the band oscillator strength. Consequently, the line oscillator strengths need not be

evaluated; instead each measurement was used to determine the band oscillator strength directly. From equations 2.21 and 2.9, the line oscillator strength may be written in terms of the band oscillator strength.

$$\text{i.e. } f^{J'J''}_{v'o} = \frac{S^{J'\Lambda'}_{J''\Lambda''}}{(2J''+1)} f_{v'o} \qquad \ldots 5.20$$

Therefore, from a given line equivalent width measurement, the band oscillator strength can be written (from equation 5.17)

$$f_{v'o} = \frac{0.084\ W(2J''+1)}{\alpha_{J''}\ p\lambda^2\ S(k_o)\ S^{J'\Lambda'}_{J''\Lambda''}} \qquad \ldots 5.21$$

5.4.3 A Typical Example

The data analysis can be demonstrated by considering the determination of the oscillator strength of the P_3 line of the (3-0) Lyman band shown in Fig. 5.2 as a typical example. The background transmission level T_B was determined from the transmission averaged over channels 0 to 50 and 150 to 200, while the line absorption was determined from this background level and the transmission summed over channels 50 to 150. The total summed absorption was

0.84 and, with a wavelength increment Δ_λ of 0.01Å, the corresponding equivalent width W is 8.4 mÅ. The measurements were made at a pressure of $1.35 \cdot 10^{-3}$ torr and a temperature of 23°C. The line centre $\lambda_o \simeq 1070$Å and the Doppler width was 5.58 mÅ, giving a value of 0.67 for $S(k_o)$ from Fig. 3.4. The fractional distribution $\alpha_{J''}$ in the J'' rotational level of the ground state was about 0.09 and the Hönl-London factor is 3 (i.e. J'' for P branch). Substituting the above parameters into equation (5.21), the corresponding band oscillator strength reduces to $1.8 \cdot 10^{-2}$. The error associated with this calculated value will be discussed in Section 5.5

5.5 Error Analysis

The error in a calculated line oscillator strength is determined by the statistical error associated with the measured equivalent width and the error associated with the determination of the parameter a. The error in a can be attributed to the 5% uncertainty in the cell length (see Section 5.2.1) and a 5% uncertainty in the absolute pressure calibration (Section 5.2.3) as well as the error associated with the pressure measurement (the reading accuracy of the gauge scale). Associated with the error in W, there is also a corresponding error in $S(k_o)$. This error is, however,

directly related to the error in W since $S(k_o)$ is a function of W (equation 3.30).

The band oscillator strengths are determined from weighted means of a number of individual line oscillator strength measurements. The errors can therefore be separated into the statistical and measurement errors, from which the weighting factors are determined, and the systematic 10% uncertainty in a.

5.5.1 Scanning Accuracy

It was mentioned in Chapter 4 (Section 4.6.3) that scans of constant statistical accuracy could be obtained by varying the reference scaler and wavelength increment according to the available photon flux. In practice, however, it was found that scans over low flux regions, especially with narrow monochromator slits, could not be taken with high statistical accuracy because the scanning time involved was long (over 24 hours) and satisfactory results could not be obtained. This was caused by a slow clogging of the entrance slits by the lamp when the slits were narrow. This clogging effectively changed the resolution function $F(\lambda-\lambda')$ during a scan (see Section 3.2) and rendered the equivalent width approximation invalid.

Consequently, scans over the lines in such regions were taken with poorer statistics than lines in higher flux regions.

This was compensated for by repeating the line measurement several times. Alternatively, if the line was sufficiently well separated from adjacent lines, a scan was taken with poorer resolution (i.e. wider slits and hence higher photon flux). This also reduced the clogging problem.

5.5.2 Transmission Accuracy

The statistical error associated with a single transmission measurement can be determined from the total number of accumulated counts for the "empty" and "full" transmission ratios. From Section 4.6.4 the transmission T can be written as

$$T = \frac{D_F}{D_E} \cdot \frac{M_E}{M_F} \qquad \ldots 5.22$$

where D_F, D_E, M_F and M_E are the detector and monitor "full" and "empty" total accumulated counts. The accumulated monitor counts were determined from the reference scaler setting and can be written

$$M_F = M_E = 2^n$$

when the reference scaler is set on 2^n. The corresponding C.E.M. output counts were, however, 2^{n+3}. The factor of 2^3 arises from the 3 bit prescalers used to divide both C.E.M. outputs prior to accumulation. From counting statistics,

the relative error in M_E and M_F is therefore $\left(2^{n+3}\right)^{-\frac{1}{2}}$.

Since the absorption was small, D_F and D_E were about equal and can be written as a fraction $\frac{1}{r}$ of the monitor counts, i.e. $D_E \simeq D_F \simeq \frac{2^n}{r}$. The error in transmission can therefore be written

$$\frac{\sigma_T}{T} = \left(\frac{2r}{2^{n+3}} + \frac{2}{2^{n+3}}\right)^{\frac{1}{2}}$$

$$= \left(\frac{r+1}{2^{n+2}}\right)^{\frac{1}{2}} \qquad \ldots 5.23$$

For example, the P_3 line of the (3-0) Lyman band shown in Fig. 5.2 was taken with the reference scaler set at 2^{17} and the ratio r=3. The corresponding relative error (from equation 5.23) is about 0.28% per transmission measurement. As the absorption is small, (i.e. $T \simeq 1$), the error for all transmission channels in either the line or the background is approximately the same.

5.5.3 Error in W

The equivalent width (equation 5.19) may conveniently be expressed as

$$W = \Delta_\lambda N\left[1 - \frac{\sum^{N} T_i}{NT_B}\right] \qquad \ldots 5.24$$

As the background level T_B is determined by averaging over N' channels, the error in the value of T_B will be $N'^{-\frac{1}{2}}\sigma_T$. Similarly the statistical error in $\frac{\sum_{N}^{N} T_i}{N}$ will be $N^{-\frac{1}{2}}\sigma_T$. The corresponding statistical error in W will be

$$\sigma_W = N\Delta_\lambda \sigma_T \left(\frac{1}{N} + \frac{1}{N'}\right)^{\frac{1}{2}} \qquad \ldots 5.25$$

For the P_3 line of the (3-0) Lyman band (Fig. 5.2), the background level was determined from the average of 50 channels on either side of the line (i.e. $N'=100$) and line full width was about 100 channels (i.e. $N=100$). With an increment of $\Delta_\lambda = 0.01$Å and a value of $\sigma_T \simeq 0.28\%$ (previous section), the error in W is

$$\sigma_W \simeq 0.40 \text{ mÅ}$$

The corresponding value of W is 8.4 mÅ. Consequently, the relative error in W is about 5%.

5.5.4 The Error in $\frac{W}{S(k_o)}$

An error in W will have a corresponding error in $S(k_o)$ because $S(k_o)$ is a function of W (i.e. equation 3.30). The standard deviation in $\frac{W}{S(k_o)}$ can therefore be written

$$\sigma_{W,S} = \sigma_W \frac{\partial}{\partial W}\left[\frac{W}{S(k_o)}\right]$$

$$= \sigma_W \left[S(k_o)^{-1} - \frac{W}{S(k_o)^2} \frac{\partial S(k_o)}{\partial W}\right] \quad \ldots 5.26$$

where $\sigma_{W,S}$ is the standard deviation of $\frac{W}{S(k_o)}$.

The relative error in $\frac{W}{S(k_o)}$ can therefore be written

$$\sigma_{W,S}\left[\frac{S(k_o)}{W}\right] = \frac{\sigma_W}{S(k_o)W}\left[S(k_o) - W \frac{\partial S(k_o)}{\partial W}\right] \quad \ldots 5.27$$

This equation can be simplified by using the approximate linear relationship between W and $S(k_o)$ (i.e. equation 3.31)

$$\text{i.e. } \frac{\partial S(k_o)}{\partial W} = \frac{-0.225}{\Delta_D} \quad \ldots 5.28$$

Consequently, the bracketed term on the right hand side of equation (5.27) can be written from equations (3.31) and (5.28) as

$$\left[S(k_o) - W \frac{\partial S(k_o)}{\partial W}\right] \simeq \left[\left(1 - \frac{0.225_W}{\Delta_D}\right) - W\left(\frac{-0.225}{\Delta_D}\right)\right]$$

$$= 1 \quad \ldots 5.29$$

Thus the relative error in $\frac{W}{S(k_o)}$ is given by $\frac{\sigma_W}{W(Sk_o)}$, i.e. the relative error in W divided by the value of $S(k_o)$.

Consequently, if we apply this correction to the typical example of the P_3 line of the (3-0) band, the relative error of 5% in W gives an error of about 7% in $\frac{W}{S(k_o)}$ $[S(k_o) \simeq 0.7]$.

5.5.5 Error in Doublets

For a doublet, this treatment is not valid because the value of $S(k_o)$ applies only to each line component and not the total W_T. The foregoing analysis is still valid for determining the total error σ_{W_T} in W_T. If the errors in each component W_1 and W_2 were proportional to the value of W (i.e. the same relative error), the different $S(k_o)$ values would give different errors in $\frac{W}{S(k_o)}$ for each line. However, as W_1 and W_2 are derived from the same W_T the relative error in $\frac{W}{S(k_o)}$ must be the same for both lines. Consequently, the error in W_T(i.e. σ_{W_T}) was split into components σ_{W_1} and σ_{W_2} which gave the same relative errors in $\frac{W}{S(k_o)}$

i.e. $$\frac{\sigma_{W_1}}{W_1 S(k_o)_1} = \frac{\sigma_{W_2}}{W_2 S(k_o)_2} \qquad \ldots 5.30$$

However, the values of W_1 and W_2 and the corresponding values of $S(k_o)$ are related by the theoretical absorption coefficient ratio $L_{1,2}$ (equation 3.33), which can be written

$$\frac{W_1}{W_2} = L_{1,2} \frac{S(k_o)_1}{S(k_o)_2} \qquad \ldots 5.31$$

Consequently the ratio of the errors σ_{W_1} and σ_{W_2} can be written

$$\frac{\sigma_{W_1}}{\sigma_{W_2}} = L_{1,2} \left(\frac{W_1}{W_2}\right)^2 \qquad \ldots 5.32$$

The total error in W_T (i.e. σ_{W_T}) can therefore be split into two components by equation (5.32) such that the relative errors in the oscillator strength are the same for both lines.

5.5.6 Pressure Uncertainty

Apart from the uncertainty in the absolute pressure calibration (Section 5.2.3), there is an uncertainty in the pressure measurement due to the finite precision of reading the pressure gauge. This error can be represented by a constant absolute reading error; consequently the relative error is smaller for large scale readings than for small scale readings. There is also a dependence on the

absolute pressure because the reading error in the "empty" pressure can be ignored if the "full" pressure is very much larger than the "empty" pressure. The ionization gauge scale was estimated to have a reading error of about 1% of the full scale. For example, the ionization gauge pressure (not corrected for the calibration factor of about 3) for the $P_3(3\text{-}0)$ Lyman band was $P_F=(4.8 \pm .1) \cdot 10^{-4}$ torr; the "empty" pressure was very much smaller ($\sim 5.10^{-6}$ torr) and the corresponding error can be ignored. The relative error in the pressure reading is therefore $\sim$ 2%.

The relative values of the calculated oscillator strengths, therefore, are accurate to within the relative errors in $\frac{W}{S(k_o)}$ and the pressure. For the absolute values, however, the systematic 10% uncertainty in the cell length and pressure calibration must be taken into account.

CHAPTER 6

6. RESULTS AND DISCUSSION

6.1 Previous Measurements

It has been pointed out in Chapter 1 that the only previous band oscillator strength measurements for molecular hydrogen have been the photoabsorption results of Haddad et al. (1968) and Hesser et al. (1968) for a number of Lyman bands, and the inelastic electron scattering results of Geiger et al. (1964, 66, 69) for both the Lyman and Werner systems. Only the most recent electron scattering results (Geiger & Schmoranzer 1969) will be considered for comparison with the present and other photoabsorption results.

The previous photoabsorption results have been expressed in terms of absolute band oscillator strengths; however, the electron scattering results have been given in terms of relative band strengths $\left\{\frac{p_{v'o}}{|\bar{R}_e|^2}\right\}$ and dipole strengths D from which the absolute band oscillator strength can be determined. The mean dipole strength is given by (Geiger & Schmoranzer 1969)

$$\bar{D} = |\bar{R}_e|^2 \qquad \ldots 6.1$$

Geiger & Schmoranzer approximate the mean dipole strength to

the dipole strength at the equilibrium internuclear separation $D(r_e)$ and quote their results as such. The dipole strengths for the B and C states (D_B and D_C) are given as 0.98 and 0.89 (atomic units) respectively. The absolute band strengths may be written

$$p_{v'o} = D\left(\frac{p_{v'o}}{|\bar{R}_e|^2}\right) \qquad \ldots 6.2$$

The band strength can be related to the oscillator strength (equation 2.21) which reduces to

$$f_{v'o} = \frac{303.8}{\lambda} p_{v'o} \qquad \ldots 6.3$$

where the band strength is in atomic units and λ is in $\mathring{A}$.

6.2 Present Results

The results for the Lyman and Werner bands are presented in Tables 6.1 and 6.2 respectively. The results are given in terms of the band oscillator rather than the line oscillator strengths (see Section 5.4.2) for the various lines measured. The relative errors associated with each value (excluding the 10% uncertainty in the absolute calibration of a) are also given.

The results represent most of the lines in both band systems which could be conveniently measured. No measure-

ments were taken in the region between 980 Å and 1040 Å [the (0-0) Werner and (5-0) to (10-0) Lyman bands] due to insufficient flux from the lamp. Of the remaining spectral region below 980 Å, a large number of lines from both systems could not be measured due to overlap of bands of both systems (see Section 5.3). This overlap criterion restricted Lyman band measurements more severely than Werner band measurements because the Lyman bands in this region are considerably weaker than the Werner bands. Lines of the Werner system (especially the strong R_0, R_1 or Q_1 lines), which were close to weaker Lyman lines (i.e. lines with $J'' \geq 2$) could be studied since the weaker Lyman lines could be ignored. On the other hand, only lines of the Werner system with $J'' \geq 4$ could be ignored if they were near strong (R_0, R_1 or P_1) lines of a Lyman band. A further limitation in this spectral region was caused by the presence of a number of impurity emission lines in the helium discharge. (see Section 5.3).

Below 900 Å the overlap problem was further complicated by the presence of the $B' \leftarrow X$ and $D \leftarrow X$ band systems and no measurements were taken in this region.

6.2.1 Lyman Bands

It can be seen from Table 6.1 that the band oscillator strengths for different lines in a band are, in

general, the same within the quoted standard deviations. The largest variations in a given band are about two standard deviations from the weighted mean value. Although measurements for a given band were taken under similar conditions, the standard deviations for different lines differ due to the numbers of scans used to determine the oscillator strengths. For example, the oscillator strengths for the lines in the (13-0) band were obtained from one scan over the P_2 line and two over the R_2 line, and the corresponding standard deviation for the R_2 line is about $2^{\frac{1}{2}}$ times smaller than that of the P_2 line. The band to band variations in the standard deviations were due to different numbers of scans as well as differences in scanning accuracies necessitated by variations in incident photon flux (see Section 5.5.1).

The mean band oscillator strengths will be given and compared against the other experimental and theoretical values in Table 6.3.

TABLE 6.1

Measured band oscillator strengths for several rotational lines of the Lyman bands

Band	Line(s)	$f_{v'o}$ $\times 10^{-3}$	Standard deviation $\times 10^{-3}$	Band	Line(s)	$f_{v'o}$ $\times 10^{-3}$	Standard deviation $\times 10^{-3}$
0-0	R_0 R_1	1.6	0.3	13-0	R_2	11.9	0.9
	P_1 R_2	1.7	0.3		P_2	12.2	1.2
	P_2 R_3	1.7	0.5				
				15-0	R_2	8.5	1.0
1-0	R_0 R_1	5.3	0.8		P_2	8.7	1.1
	P_1 R_2	6.0	1.3		R_3	13.1	1.6
					P_3	10.7	1.6
2-0	R_0 R_1	16	3.6				
	P_1 R_2	12	2.1	16-0	R_1 P_1	7.7	0.7
	P_2 R_3	13	1.8		R_3	7.6	0.8
3-0	R_0 R_1	17.2	1.0	17-0	R_0	5.2	0.5
	P_1 R_2	18.1	1.6		R_1 P_1	4.5	0.6
	P_3	18.3	1.1		R_2	8.4	1.2
					P_2	7.0	0.7
4-0	R_0 R_1	28	2.0		R_3	7.0	0.7
	P_1 R_2	24	2.0				
	P_3	24	6.0	19-0	R_1 P_1	3.8	0.4
					P_2	3.9	0.6

6.2.2 Werner Bands

The Werner band results are given in Table 6.2. As can be seen from the table, oscillator strength measurements for all the measured bands have been restricted to only a few lines per band due to band overlap and the presence of impurity emission lines mentioned previously. In the case of the (3-0) and (4-0) bands, for example, only measurements of the unresolved R_0, R_1 pair of lines were taken. However, a high accuracy for the band oscillator strengths was maintained by repeating the measurements a number of times. For example, the R_0, R_1 pair of the (3-0) band was measured eight times, giving an accurate weighted mean band oscillator strength with standard deviation lower than most other line measurements of bands where more than one line (or one line pair) measurement was possible. The (4-0) band was treated similarly. Unfortunately, the individual results for the R_0, R_1 line pair in this band had an abnormally large spread of values between $2.5 \cdot 10^{-2}$ and $5.4 \cdot 10^{-2}$. The weighted mean value was therefore subject to the accurate choice of standard deviations for the individual measurements.

Although the standard deviations of the individual measurements were accurately calculated according to Section 5.5, the large spread in values (the largest value of $5.4 \pm 0.8 \cdot 10^{-2}$ was 3 standard deviations from the mean value) suggests that the weighted mean is less accurate than the calculated standard deviation implies.

TABLE 6.2

Measured band oscillator strengths for several rotational lines of the Werner bands

Band	Line(s)	$f_{v'o}$ $\times 10^{-2}$	Standard deviation $\times 10^{-2}$	Band	Line(s)	$f_{v'o}$ $\times 10^{-2}$	Standard deviation $\times 10^{-2}$
1-0	R_0 R_1	5.5	0.8	4-0	R_0 R_1	2.8	0.1
	Q_1	6.8	1.4				
	R_0 R_1) R_2 Q_1)	5.8	0.6	5-0	R_0 R_1	2.4	0.3
					Q_1 R_2	2.0	0.3
2-0	P_2	5.3	0.6				
	Q_3	7.4	1.0	6-0	R_0 R_1	1.6	0.2
	P_3	6.9	0.8		Q_1 R_2	1.8	0.3
3-0	R_0 R_1	4.1	0.2				

The only other Werner band measurement which needs comment is the group of four lines (R_0, R_1, R_2, Q_1) of the (1-0) band. The lamp flux in this region was relatively low, and it was difficult to obtain accurate equivalent width measurements without encountering problems with the monochromator entrance slits clogging during the long scanning time. Consequently, of the large number of measurements attempted, only a few yielded results. However, by opening the entrance slits

and thus minimizing the clogging problem, satisfactory measurements were obtained. The increased flux also considerably reduced the time taken to obtain a measurement of sufficient accuracy (less than 20%). Unfortunately, the corresponding drop in resolving power did not allow the first four lines (the R_0, R_1, R_2 and Q_1) to be resolved, and only an equivalent width representing the total equivalent width of the group could be obtained. The group of lines was analysed by splitting the total equivalent width into two nearly equal parts corresponding to the R_0 and R_1 pair and the R_2 and Q_1 pair. As the R_1 and Q_1 line strengths are equal and larger than the R_0 or the R_2 line strengths, splitting the total equivalent width into the ratio of the strengths of the R_0 and R_1 pair and the R_2 and Q_1 pair and analysing these two pairs as doublets (see Section 3.5) gave approximately consistent results. The final band strength value was taken as the average of the two determinations. The results of this analysis were consistent with the separately determined R_0, R_1 pair and Q_1 line values (Table 6.2).

6.3 Comparison with Other Results

Average band oscillator strengths have been obtained from the weighted means of the band oscillator strengths presented in Tables 6.1 and 6.2. The mean values of the

oscillator strengths have been tabulated and compared against the other experimental values and the theoretical values of Allison & Dalgarno (1970) in Tables 6.3 and 6.4 for the Lyman and Werner bands respectively.

6.3.1 The Lyman Bands

It can be seen from the results shown in Table 6.3 that the present experimental oscillator strengths are in good agreement with the electron scattering results of Geiger & Schmoranzer (1969) and the theoretical values of Allison & Dalgarno (1970), but do not agree, in general, with the results of Haddad et al. (1968) and, to a lesser extent, Hesser et al. (1968). The differences between the various results can be readily seen from Fig. 6.1, which shows the band oscillator strength as a function of the upper state vibrational quantum number v′. The (3-0) band result of Haddad et al. has not been included because it is beyond the scale of the figure. From the figure it can be seen that both the present and electron scattering results approximately fit the solid (theoretical) curve of Allison & Dalgarno. The results of Haddad et al., although agreeing with the $v' = 0$ band, show a much more rapid increase in $f_{v'0}$ for increasing v′ than the present results. Hesser's results, on the other hand, show a more rapid decrease in $f_{v'0}$ for $v' \geq 16$ than the present results.

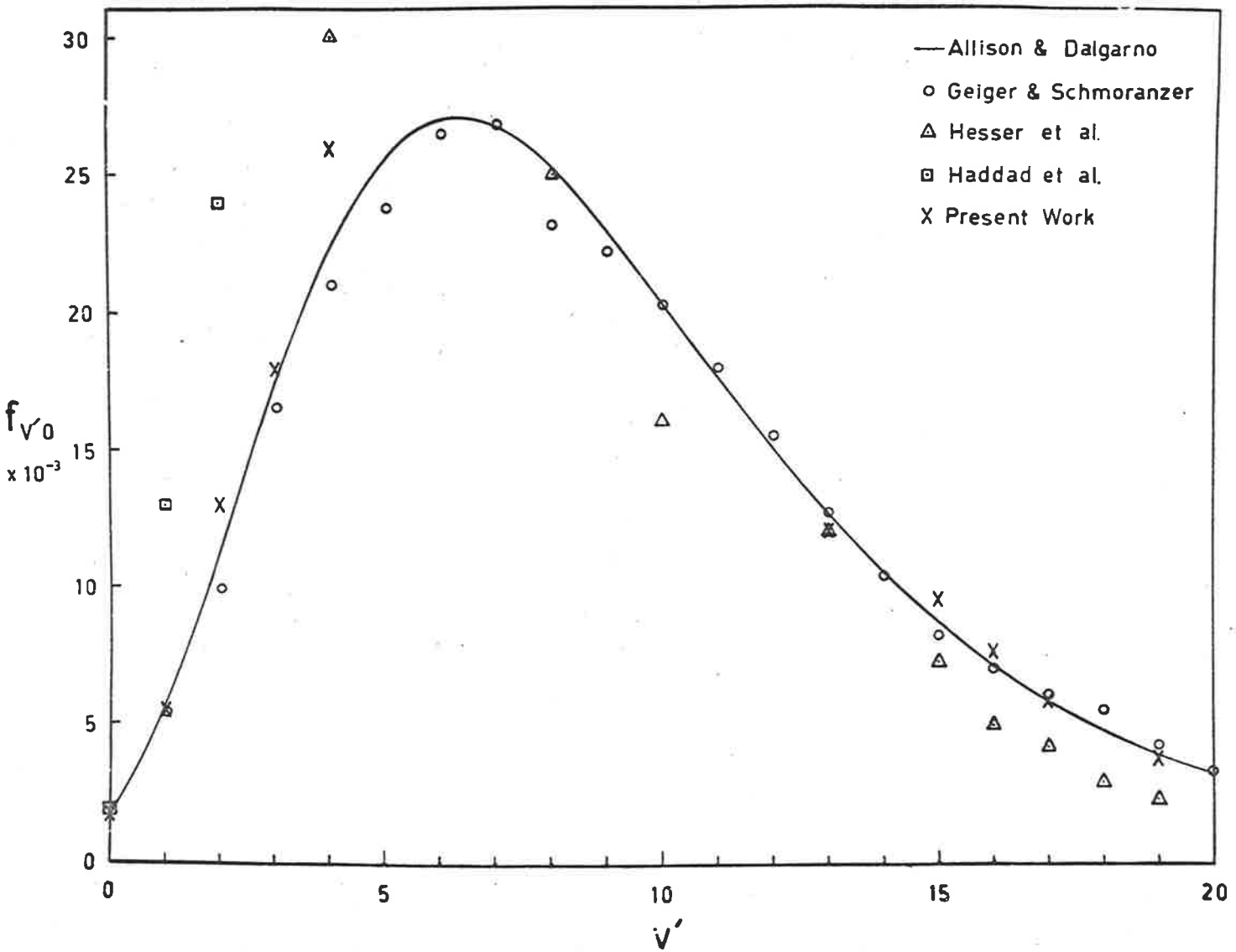

Fig. 6.1 $f_{v'0}$ as a function of v' for the Lyman bands

TABLE 6.3

Comparison of band oscillator strengths for the Lyman bands

v′	$f_{v'o} \times 10^{-3}$				
	Present	Haddad et al.	Hesser et al.	Geiger & Schmoranzer	Allison & Dalgarno
0	1.7	1.9			1.69
1	5.5	13		5.4	5.79
2	13	24		9.9	11.56
3	18	37		16.5	17.55
4	26		30	21.0	22.5
13	12		12	12.7	12.66
15	9.6		7.3	8.24	8.73
16	7.7		5.0	7.04	7.19
17	5.9		4.2	6.12	5.89
19	3.8		2.3	4.25	3.94

6.3.2 Electronic Transition Moment

The experimental and theoretical results can alternatively be compared in terms of the electronic transition moment as a function of the internuclear separation (i.e. the r-centroid). For transitions between non-degenerate Σ states, we may write

$$\sum_{ij} \left| R_e^{ij}[r(v'o)] \right|^2 = \left| R_e[r(v'o)] \right|^2$$

and the transition moment may be written (from equation 2.20)

$$\left| R_e[r(v'o)] \right| = \left(\frac{p_{v'o}}{q_{v'o}} \right)^{\frac{1}{2}}$$

where the band strength can be related to the oscillator strength by equation (6.3). The Franck-Condon factors $q_{v'o}$ were taken from Allison & Dalgarno (1970). The resulting electronic transition moments have been compared against the theoretical curve of Wolniewicz (1969). The r-centroids were taken from the tables of Halmann & Laulicht (1966).

Fig. 6.2 shows the experimental $|R_e|$ values compared against the theoretical transition moment variation with internuclear separation (Wolniewicz).

6.3.3 Lyman Band Discussion

It can be seen from the oscillator strengths (Fig. 6.1) and the electronic transition moments (Fig. 6.2), that the present results are in harmony with the electron scattering results and the theoretical values of Allison & Dalgarno and Wolniewicz. The only exception appears to be the high (4-0) band result. It can be seen from Table 6.1 that the large value can be attributed to the large value

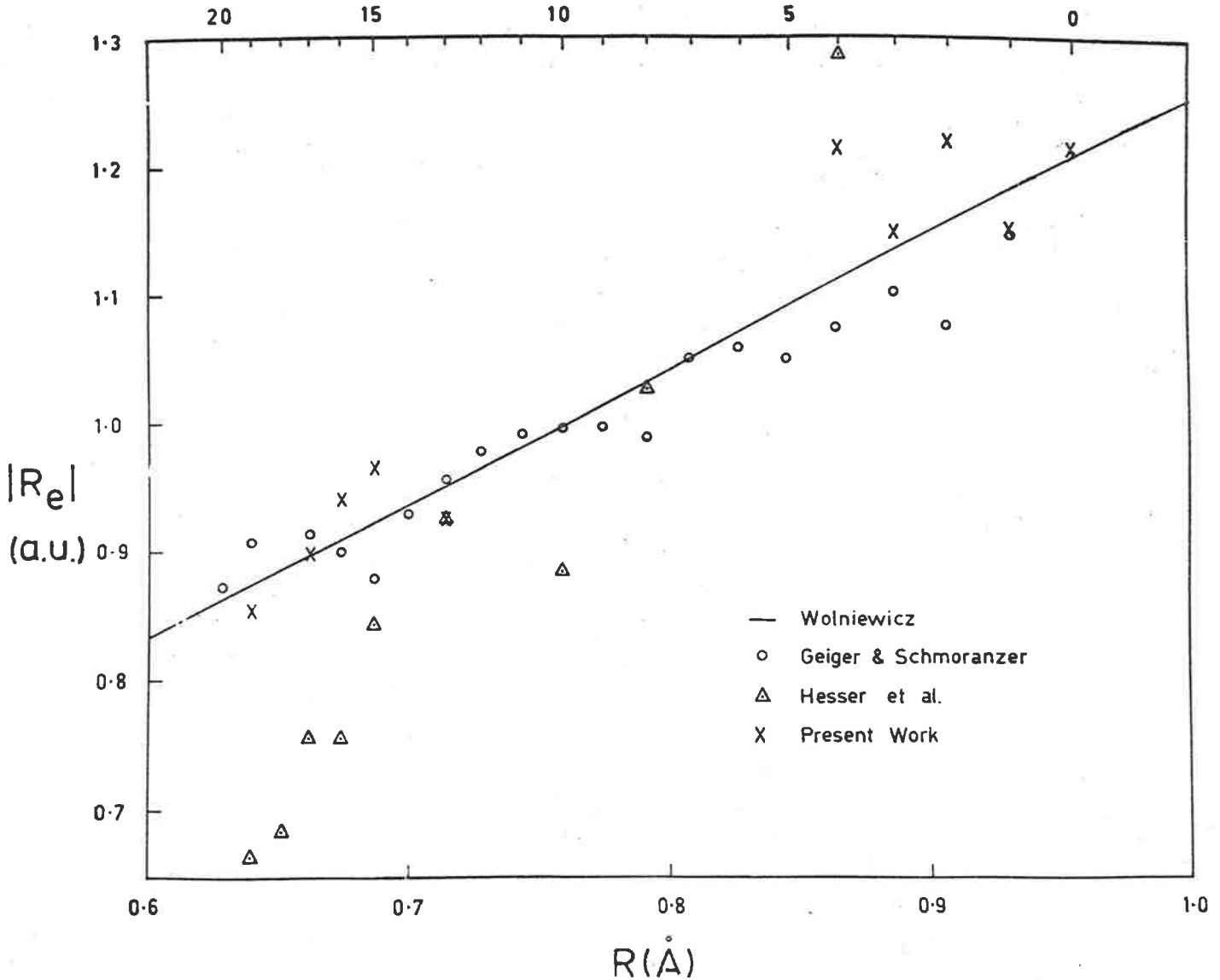

Fig. 6.2 The electronic transition moment as a function of the internuclear separation for the Lyman bands

for the R_0, R_1 pair. Hesser et al. have pointed out that their results do not contain a measure of the R_1 line because the presence of underlying structure in the wings of the argon resonance line would give rise to an error in the equivalent width. Although no such structure was observed in the present work, it was possibly due to lack of resolution rather than lack of structure. Consequently, it is possible that the present R_0, R_1 line pair measurement is less accurate than the results imply. The other photoabsorption measurements of Haddad et al. and Hesser et al., however, do not show good agreement with any of the above, even though a similar equivalent width measuring technique and a Doppler curve of growth analysis were used. In the case of the results of Haddad et al., the discrepancy could possibly be accounted for by the nature of the analysis used. Unlike the present weighted mean averaging technique, Haddad et al. summed their line strengths to determine a band strength and computed the band oscillator strengths from them. This technique places undue weight on the stronger lines in the band, especially the R_1 line. Consequently, in spite of accurate measurements of other lines, the error in the R_1 line dominates the band strength error. The operating pressures used for these measurements were all $\geq 10^{-3}$ torr with a cell length of 60 cm. (Haddad 1967). The present

results suggest that for a 60 cm. path length, pressures of 10^{-3} torr would give equivalent widths well beyond the Doppler saturation region for the R_1 lines of all the bands studied by Haddad et al. except the (0-0) band. Consequently, the R_1 line strengths and hence the band oscillator strengths for the remaining three bands would be subject to very large errors.

The discrepancy in the results of Hesser et al. (1968) are more difficult to account for due to lack of experimental detail and unreliability of their analysis. The authors have quoted an expression containing an incorrect factor of $2(\ln 2)^{\frac{1}{2}}$ in the reduction of line oscillator strengths from peak absorption coefficients k_o. While the authors acknowledge that this factor is incorrect (Lawrence 1971), they are unable to determine whether the published error was used in the actual analysis or not. If this term was included in their analysis, their values would be too low by a factor of $2(\ln 2)^{\frac{1}{2}}$ (~ 1.7) which would bring their (16-0) to (19-0) results into line with the present values. However, the other values, especially the already high (4-0) band result would be increased to well beyond the present and theoretical values. As can be seen from Fig. 6.2, the results of Hesser et al. suggest a much more rapid variation of electronic transition moment with internuclear separation than

the present or theoretical results; a difference which cannot be accounted for by a constant scaling factor.

6.3.4 The Werner Bands

The weighted mean Werner band oscillator strength results are given in Table 6.4 as are the values derived from the electron scattering results of Geiger & Schmoranzer (1969) and the theoretical values of Allison & Dalgarno. The results are also graphically displayed in Fig. 6.3. It can be seen from both Table 6.4 and Fig. 6.3

TABLE 6.4

Comparison of band oscillator strengths for the Werner bands

v'	$f_{v'o} \times 10^{-2}$		
	Present	Geiger & Schmoranzer	Allison & Dalgarno
1	5.8	5.92	7.28
2	6.1	5.55	6.98
3	4.1	4.37	5.47
4	2.8	3.37	3.87
5	2.2	2.10	2.60
6	1.6	1.53	1.70

that the present and electron scattering results are consistently lower than the theoretical values. Although the

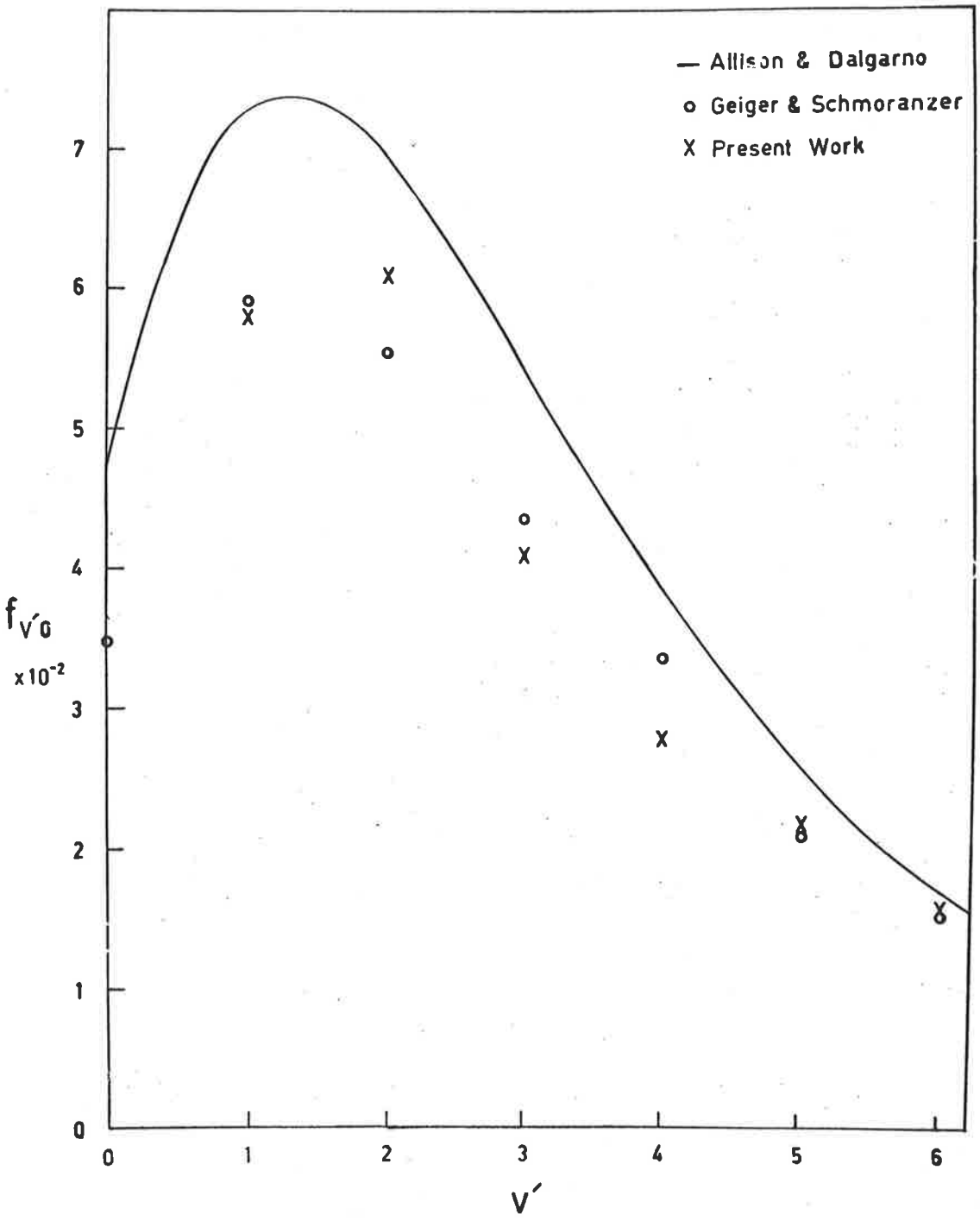

Fig. 6.3 $f_{v'o}$ as a function of v' for the Werner bands

10% systematic uncertainty in a could be used to raise the present values by about 10%, thus minimizing the discrepancy between the present and theoretical values, the good agreement between the theory and present results for the Lyman bands suggests that this uncertainty is considerably less than 10%. Furthermore, the approximate agreement between the present results and the electron scattering results for both band systems suggests that the discrepancy is real and not an experimental error.

The electronic transition moment for the Werner bands can be computed from the experimental band oscillator strengths as in the case of the Lyman bands, except that the upper ($C^1\Pi_u$) state is two-fold degenerate

$$\text{i.e. } \sum_{ij} \left|R_e\right|^2 = 2\left|R_e\right|^2$$

and the electronic transition moment is given by

$$R_e[r(v'o)] = \left(\frac{p_{v'o}}{2\, q_{v'o}}\right)^{\frac{1}{2}}$$

The experimental electronic transition moments are compared to the theoretical electronic transition moment variation with internuclear separation of Wolniewicz (1969). The r-centroids were taken from Halmann & Laulicht (1966).

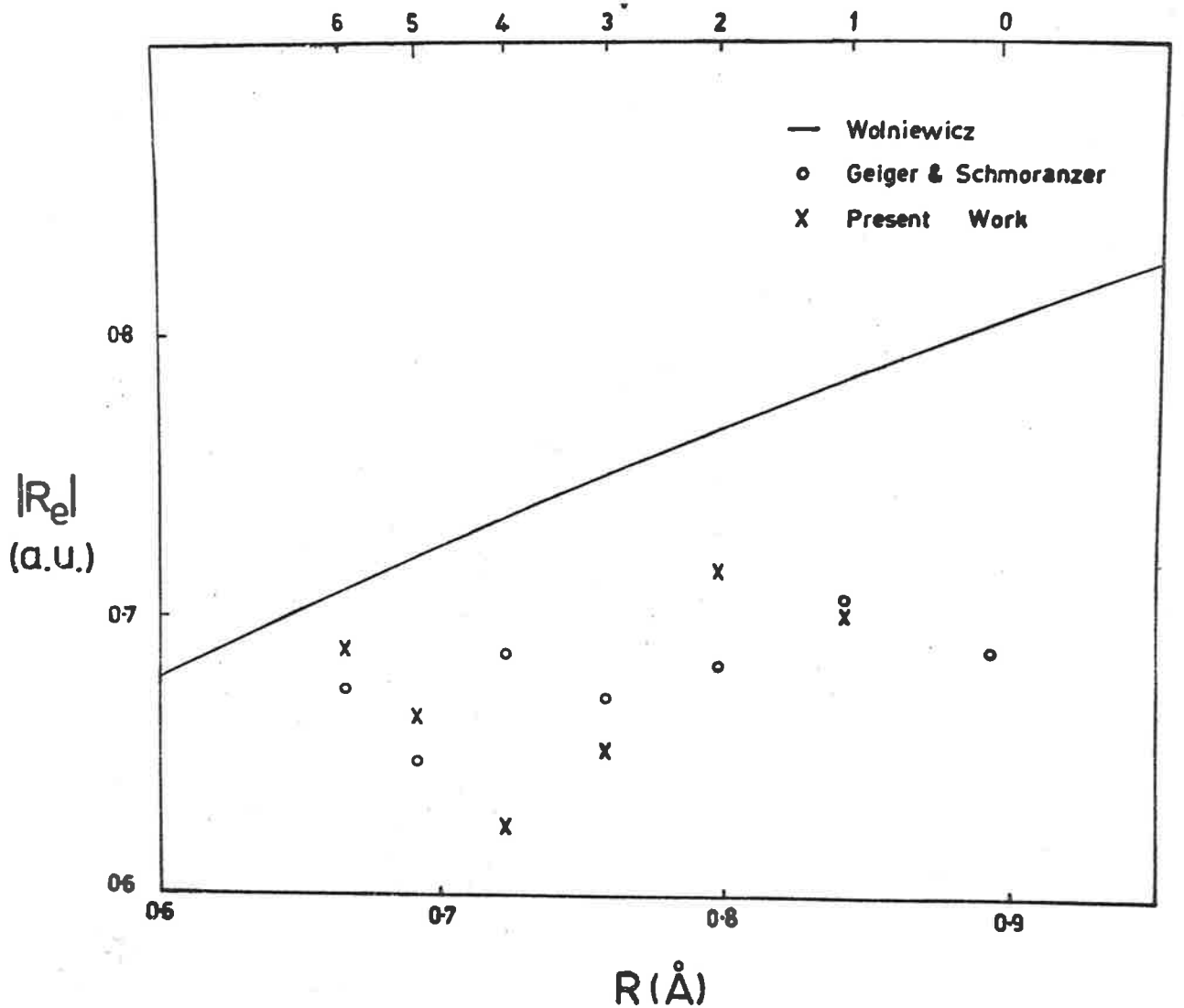

Fig. 6.4 The electronic transition moment as a function of the internuclear separation for the Werner bands

It can be seen from Fig. 6.4 that the experimental (both present and electron scattering) electronic transition moments exhibit a less rapid variation with changing internuclear separation than the theoretical curve.

It is difficult to suggest a likely source for this discrepancy. Inaccuracies in either the Franck-Condon factors or the electronic transition moment could account for the high theoretical values. However, the Franck-Condon factors of Allison & Dalgarno which are based on the theoretical potential curves of Kolos & Wolniewicz (1965, 66, 68) are in close agreement with the Franck-Condon factors derived from empirical R.K.R. potential curves (Halmann & Laulicht 1966). This suggests that the Franck-Condon factors are reliable and the corresponding vibrational wavefunctions and potential curve are accurate.

On the other hand, the electronic transition moments published by Miller & Krauss (1967) and Rothenberg & Davidson (1967), although larger than the experimental values, are sufficiently different from the values of Wolniewicz to suggest that the transition moments are not as reliable as the Franck-Condon factors. In particular, the results of Rothenberg & Davidson show a large discrepancy ($\sim$ 10%) between dipole "length" and "velocity" transition moments. Although Wolniewicz shows good agreement between "length"

and "velocity" calculations. Rothenberg & Davidson have pointed out that such an agreement is not a sufficient condition to establish the accuracy of the wavefunctions used. It therefore appears that inaccuracies in the transition moments for the Werner system are the most likely source of the disagreement between the theoretical and experimental oscillator strengths.

6.3.5 Summary of Results

From the present results, we may conclude that the inelastic electron scattering results of Geiger & Schmoranzer (1969) yield accurate optical oscillator strengths for both the Lyman and Werner band systems. The theoretical calculations for the Lyman bands are also reliable. However, for the Werner band systems, the theoretical values are larger than both the photoabsorption or electron scattering results, suggesting further theoretical study of the $C^1\Pi_u$ state, in particular, the electronic wavefunction.

6.4 Suggestions for Further Work

The present results suggest that there are several extensions and modifications of the experimental work which would yield added information about the two band systems.

One of the most valuable improvements to the present system would be an increase in power of the light source such

that the helium continuum in the region above 980 Å would be sufficiently intense to allow absorption measurements to be taken. Of particular value would be a measure of the oscillator strength of the (0-0) Werner band to determine whether the value of $|R_e|$ follows the electron scattering results or not. It would also be an advantage, with a greater lamp flux, to take measurements of the (1-0) Werner band with an improved resolution and improved statistical accuracy. It would also be of interest to repeat and improve several of the present measurements [eg. the (4-0) Werner band].

The second obvious reason for taking measurements in this region is to complete the information in the missing region [(5-0) to (10-0) bands] of the Lyman system. However, this is less vital since the agreement with the electron scattering results suggests that the electron scattering values are reliable.

It would also be valuable to extend the work to the region below 900 Å. This would reveal more information about the higher v′ transitions of both systems, and would also give a better overall picture of the $|R_e|$ variation with r-centroid for the Werner bands. With the present dispersion instrument, however, this region cannot be studied under the experimental conditions described in this thesis

because of overlap between the Lyman and Werner bands as well as the $B' \leftarrow X$ and $D \leftarrow X$ systems. However, this spectral region can be satisfactorily studied with the present dispersion instrument if the gas is cooled to liquid nitrogen temperature. At this low temperature, only the $J'' = 0$ and $J'' = 1$ rotational levels have an appreciable population; consequently we need only consider three lines in each band (the R_0, R_1 and P_1, for Σ-Σ transitions and the R_0, R_1 and Q_1 for Σ-Π transitions). This simplification of the observed spectrum would then enable a number of bands to be studied that cannot be studied at room temperature with the present available resolution.

Probably the most useful extension of the present work would be a detailed study of the strengths of individual lines in one particular band in an attempt to measure centrifugal distortion effects on the Franck-Condon factors (see Section 2.5.6). Although the experimental system is sufficiently accurate to measure the band strength to within a few percent if enough measurements are taken, the present results are not extensive enough to observe such an effect. The largest variation is between the P and R branches for bands with small v', eg. the (0-0) Lyman band. The lines in these bands are, however, closely spaced and, in the Lyman bands, they occur in pairs such as P_1R_2, P_2R_3 etc.

which, with the present instrument resolution, cannot be separately resolved. Consequently, a detailed study of a particular band is not possible with the present resolution. However, it should be possible to verify the existence of such an effect and determine the approximate magnitude by comparing the average strength of an R_0, R_1 pair with the strength of a P_3 line. The R_4 line intensity is only 5% of the P_3 line at room temperature, consequently its effect on the measured P_3 line strength is small and can be approximately accounted for. The P_3 line was not studied in the (0-0) to (2-0) Lyman bands due to structure in the continuum and the lowest Lyman band for which a P_3 line measurement was taken was the (3-0) band. It has been pointed out that a large number of measurements for this band were taken and it can be seen from Table 6.1 that the band oscillator strength of the P_3 line is larger than that of the R_0, R_1 pair. However, the standard deviations for the measurements are not, at present, sufficiently low to attribute the difference to centrifugal distortion effects, and a large number of additional measurements would be required. The theoretical difference in band strength between the R_0, R_1 line pair and the P_3 line is about 8% (Wolniewicz 1969), and hence it would be necessary to reduce the standard deviations of the experimental measurements to less than 4% before it would be possible to verify that such a difference exists.

APPENDIX I

Lamp Power Supply

The lamp described in Section 4.3 was powered by a thyratron triggered capacitor discharge system. The circuit is shown in Fig. I. This circuit is a simplified version of the pulsed discharge circuit described by Huffman, Larrabee & Chambers (1965).

Briefly, the operation is as follows. The capacitor (0.001 μf) is charged via the 100k resistor to the positive H.T. supply (approx. 5 k.v.) and the inductor to ground (parallel to lamp). When triggered, the thyratron (Philips type 5C22) starts conducting rapidly (with a risetime of less than 1 μs), causing a negative high voltage pulse to be generated on the cathode of the lamp. The lamp breaks down (by ionization of the gas in it) and discharges the capacitor. (As the risetime of the negative voltage pulse is very fast, the impedance of the parallel inductor is high and practically all the discharge current goes through the lamp). When the thyratron current falls below a critical level (capacitor discharged), the thyratron turns off and the capacitor slowly charges up again.

The trigger pulse for the thyratron is generated by a blocking oscillator which is essentially a transformer

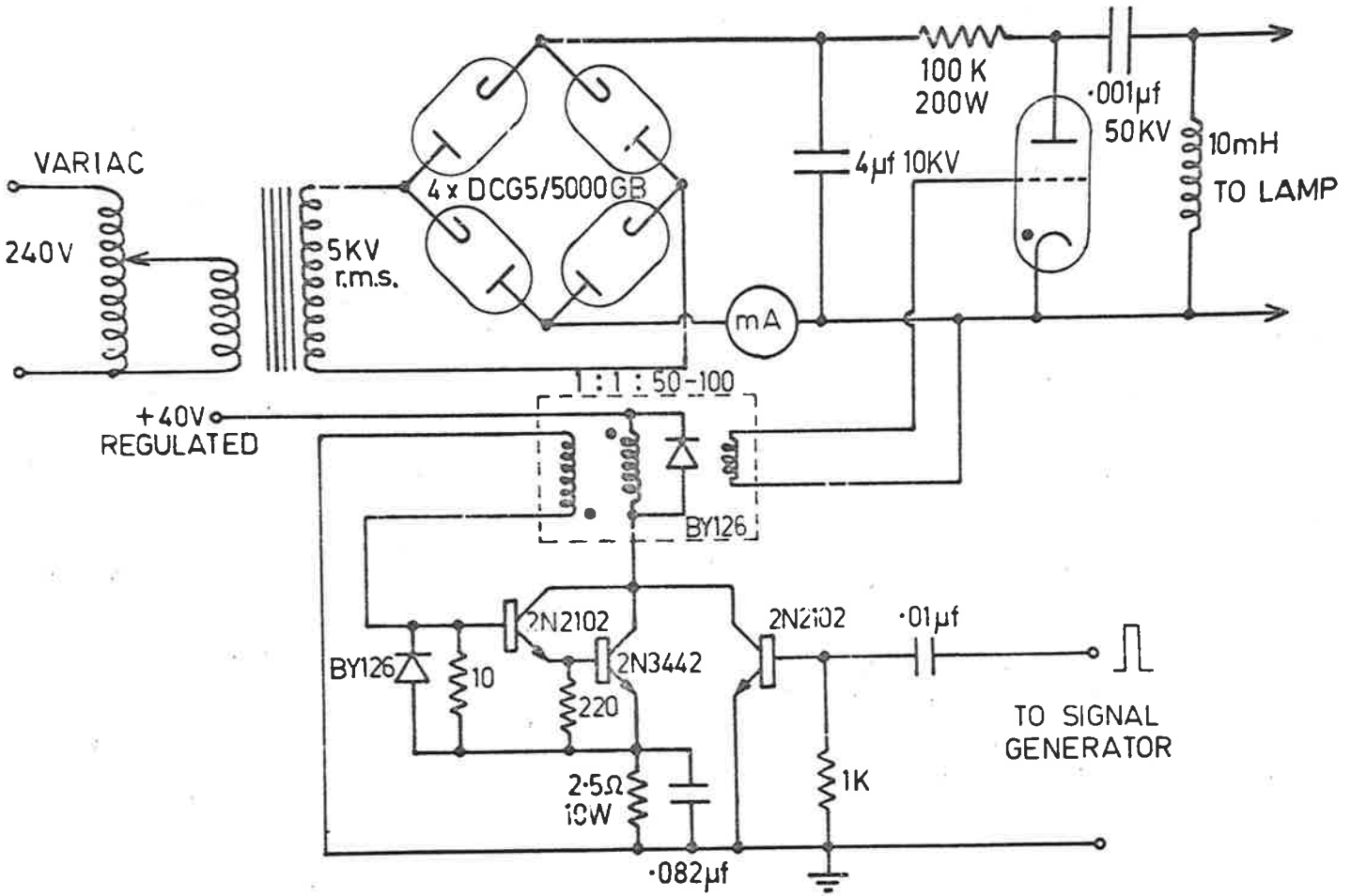

Fig. I Circuit for the lamp power supply

coupled oscillator which is prevented from oscillating by a diode across the collector winding of T_2. Transistors T_1 and T_2 are a Darlington pair (for higher gain) which are coupled to a bifilar wound toroid. The oscillator is triggered by a pulse into T_3 from a signal generator. As T_3 turns on, the collector voltage on T_2 drops, thus inducing T_1 to turn on (due to positive feedback via the transformer), which in turn biases T_2 on. The positive feedback gives rise to a rapid risetime pulse ($\sim$ 1 μs). The pulse width is determined by the inductance of the toroid and in this circuit, the width is $\sim$ 5 μs). A secondary, wound on the coupling toroid, supplies the high trigger voltage ($\sim$ 200 V) required for the thyratron.

APPENDIX II

Beam Monitor and Chamber

The incident flux monitor consists essentially of a semitransparent tungsten grid acting as a photocathode and a C.E.M. as the electron multiplier (see Section 4.4). However, the layout within the chamber (see Fig. II) is a little more elaborate due to the beam optics and the differential pumping slits on either end of the cell.

The radiation emerging from the exit slits of the monochromator is in the form of an approximately 4 degree divergent beam, and, due to the size of the differential pumping slits, the rear detector is able to view only a small fraction of the total beam. It was desirable to monitor only the section of the beam passing through the cell itself, hence a narrow collimator was placed between the exit slits of the monochromator and the grid. The grounded baffle just after this collimator prevented photoelectrons generated at the collimator from reaching the C.E.M.

A second baffle (exit baffle) was used to ensure that only photoelectrons generated at the grid were detected. Without this baffle, a portion of the photon beam illuminated the first differential pumping slits (due to the lengthwise spread of the beam), giving rise to photoelectrons which could be detected by the C.E.M. The exit baffle was at a

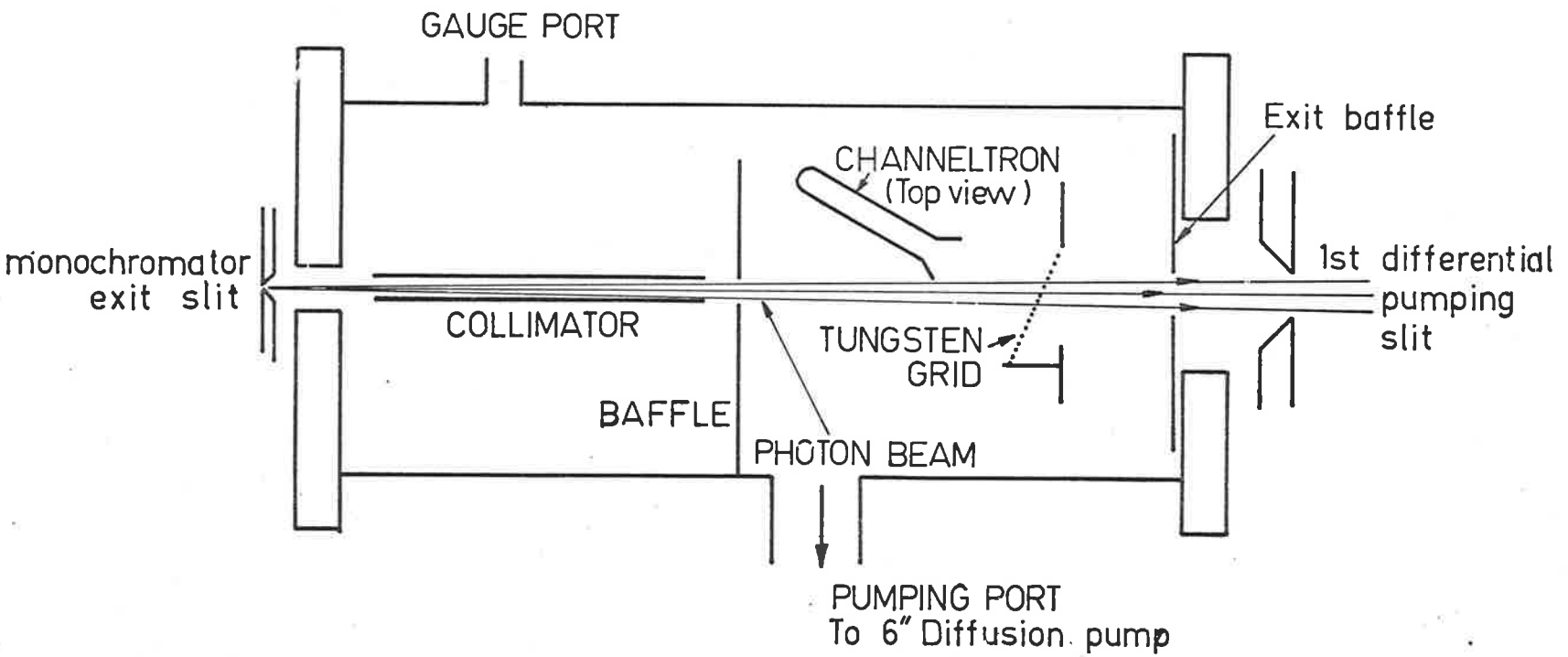

Fig. II A cross-section of the incident flux monitor

potential equal to the C.E.M. cone potential ($\sim$ 200 V) and therefore removed this source of photoelectrons. It was sufficiently far from the grid (further than the C.E.M.) not to affect the electrons generated at the grid.

The C.E.M. output represents, therefore, as accurately as possible, the incident flux into the cell (as sampled by the grid).

APPENDIX III

C.E.M. Preamplifiers

The gain of a C.E.M. is typically 10^7 (i.e. each detected photon or electron gives rise to about 10^7 electrons at the output). This current pulse is amplified and converted to a voltage pulse suitable for the discriminators (E.G. & G. type TR104S) by a very simple two stage amplifier, the circuit of which is shown in Fig. III. Due to the simplicity, the amplifier is stable against oscillation and has a speed (risetime) limited only by the transistors used. It was found that the C.E.M.'s when operated in a saturated gain mode, had a relatively slow risetime ($\sim$ 10 ns) and pulse width of about 40 ns which enabled relatively slow transistors (type 2N 3646) to be used without degrading the risetime or width of the amplified pulse. The output pulse height was just less than 1 volt which adequately covered the discriminator input range (100-600 mV).

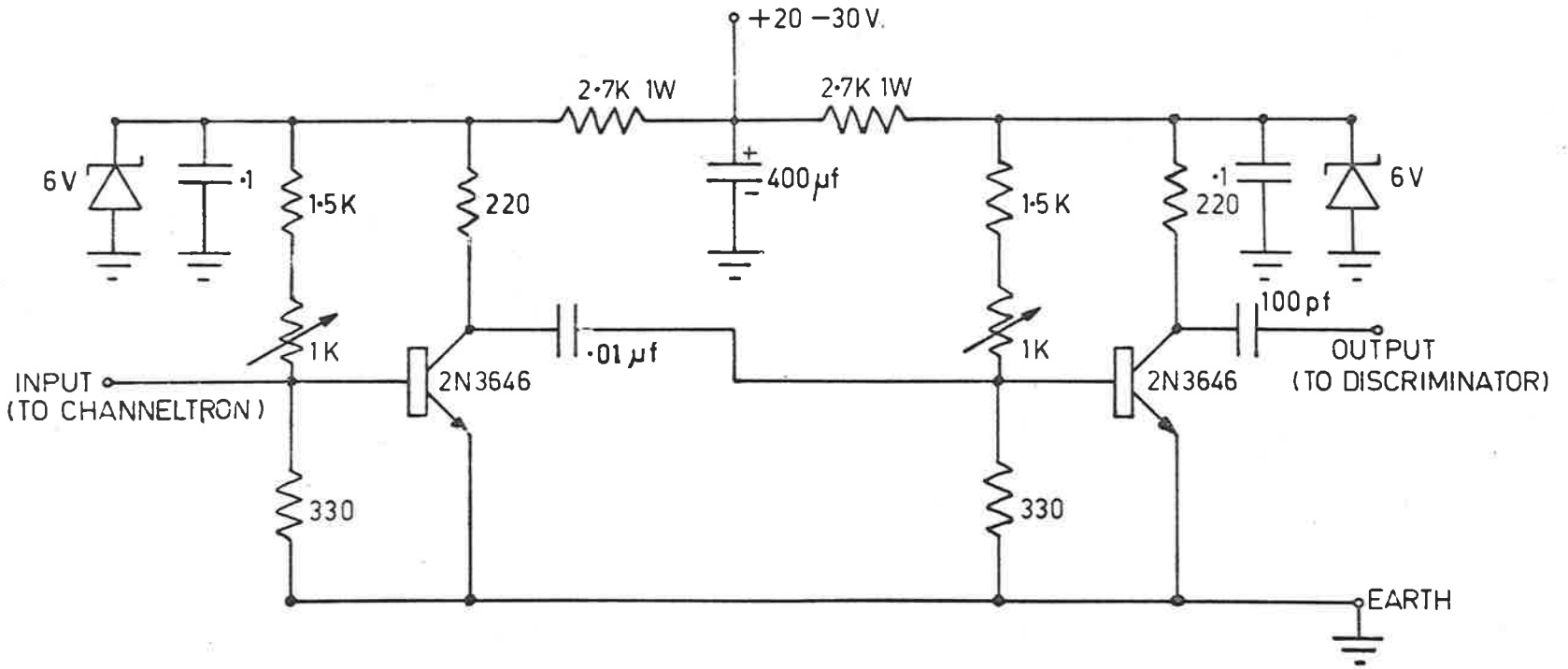

Fig. III The C.E.M. preamplifier circuit

APPENDIX IV

Digital Data Handling Electronics

The logic circuits and a brief description of the operation for the control scaler and data recording system are given in this Appendix.

IV. (1) Control Scaler

The data acquisition system was controlled by a simple two bit subtract scaler called the control scaler. A schematic diagram of the circuit is shown in Fig. IV(a). The scaler was clocked by the output of the reference scaler and the various operations associated with each phase of the data accumulation (see Section 4.6.1) were obtained by appropriate decoding of the different states of the scaler, and generating appropriate command pulses at each change of state.

The operation can be followed from the timing sequence diagram [Fig. IV(b)]. The outputs of the two J-K flip-flops (the two bit scaler) are denoted Q_1 and Q_2. If Q_1 and Q_2 are both initially low, the reference scaler output pulse changes the state of both Q_1 and Q_2 to a high state. Also triggered by the reference scaler pulse is a change of state of the gate control R-S flip-flop which controls the input gates (both monitor and detector inputs). Corresponding

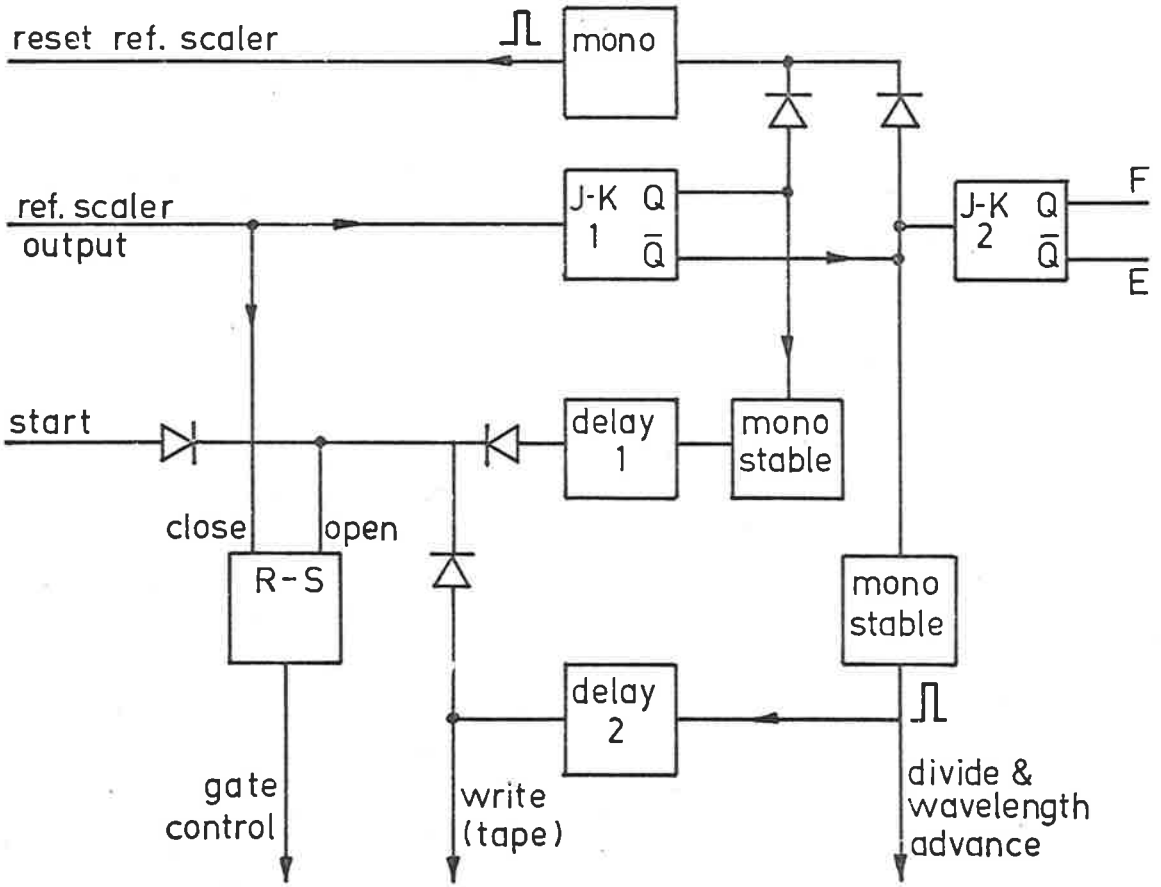

Fig. IV(a) Schematic of the control scaler circuit

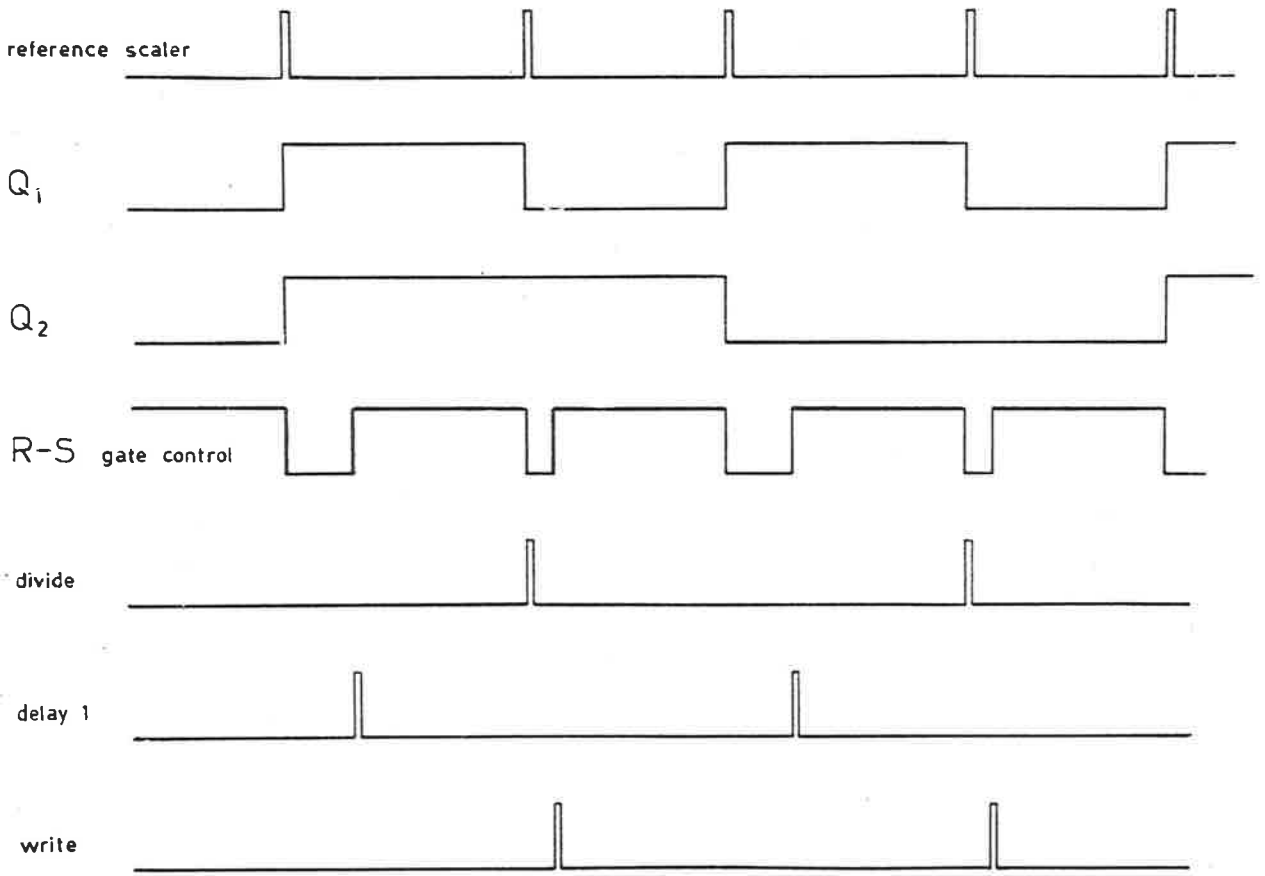

Fig. IV(b) Operating sequence of the control scaler

to the change in Q_1, a pulse is generated by a monostable which resets the reference scaler. A second monostable generates another pulse, which, after a delay of about ½ minute (delay 1) resets the R-S flip-flop (i.e. opens the data accumulation gates). The corresponding change in Q_2 changes the cell from "full" to "empty" and also changes the corresponding divider input from X to Y (see Fig. 4.3). The cell pressure is allowed to reach equilibrium during the ½ minute delay (delay 1) before data accumulation starts again.

The next reference scaler output pulse again changes the R-S and Q_1 but not Q_2. Hence the cell remains "empty". The corresponding change in Q_1 initiates a reference scaler reset pulse and a divide command and wavelength advance pulse. After a short delay (delay 2) during which time the divider output is transferred to the tape scalers (see next section) a tape write command pulse is generated. This pulse also resets the gate control R-S. The next reference scaler output pulse again changes Q_1 and Q_2 and the operation is similar to the first step, except that the cell changes from the "empty" to "full" state and the corresponding divider gates change from Y to X.

IV. (2) Tape System

Both the "empty" and "full" detector outputs as well as the divider ratio (X/Y) were recorded on tape by a relatively simple recording system. The recorder consisted of three scalers for serial information as well as an internal address or channel number scaler. Data was stored on tape as words corresponding to 80 bits or 20 decades of B.C.D. information (i.e. the 3 scalers and channel No. of 5 decades each).

The recording unit was designed around a domestic 2 track tape deck (Revox model A77) which was converted to operate in a semi-incremental mode. The tape transport was modified such that it could be rapidly engaged or disengaged on a command pulse. Just prior to recording a word on tape, the tape transport mechanism was engaged, advancing the tape at a rate of 1 i.p.s. At the end of the 80 bit word, which was written as two trains of 40 coincident pulses on each track, the transport mechanism was disengaged. A begin and end of word pulse was also recorded before and after the 80 bits of information, and served as a reliability check on play back. The bits were recorded on tape as bidirectional pulses for both a binary "0" and "1" [see Fig. IV(f)].

A schematic of the write circuit is shown in Fig. IV(c).

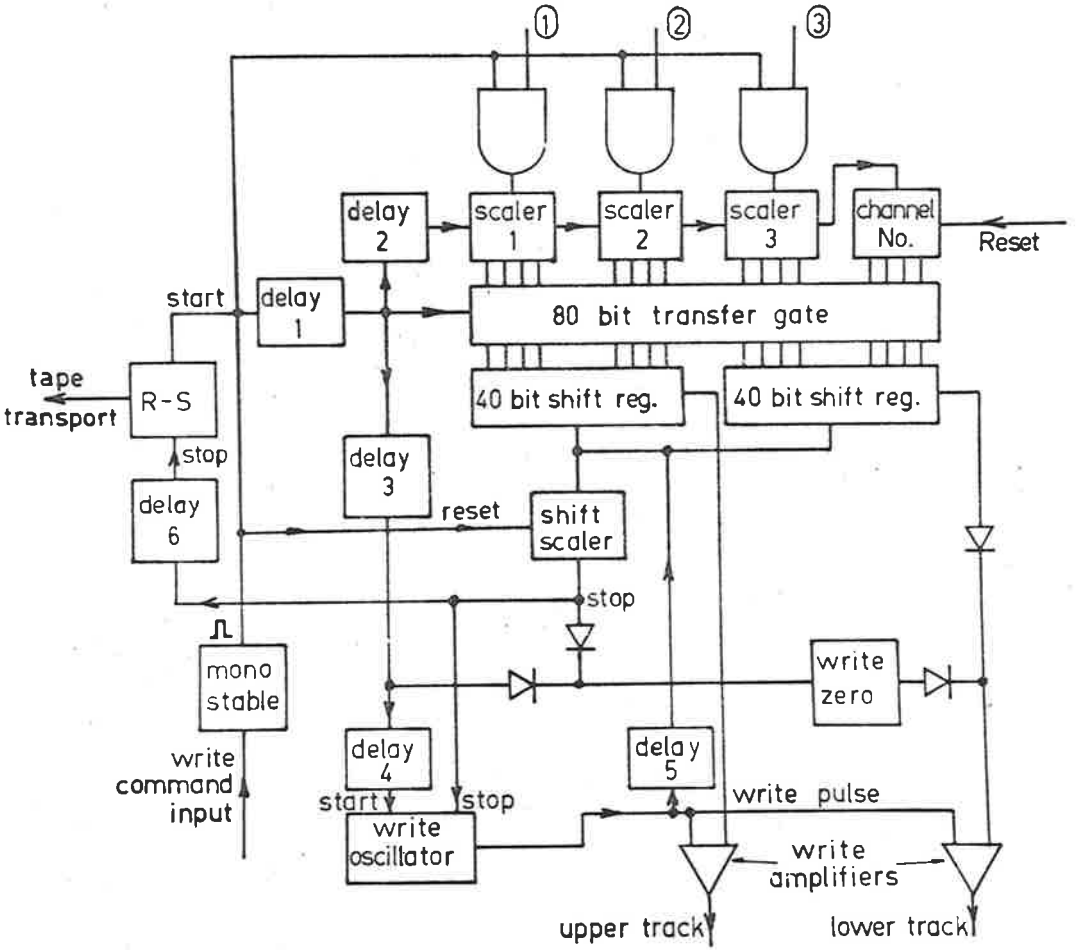

Fig. IV(c) Schematic of the tape recording circuit

An operation sequence diagram showing the essential operating features is given in Fig. IV(d). Serial data is accumulated in the three data scalers (1, 2 and 3) via appropriate input gates. On the write command, a monostable pulse is generated which initiates the following,

1) closes the input gates to the scalers,
2) sets an R-S flip-flop which activates the tape transport,
3) resets the shift scaler,
4) after a brief delay (delay 1) the contents of the three data scalers and the channel number are transferred in parallel (80 bit transfer gates) to two 40 bit shift registers,
5) a short delay after the transfer (delay 2), the data scalers are reset and one is added to the channel number scaler (i.e. advances the channel number by 1).

By this time (approx. 2 μsec. after initial write command) the monostable pulse ends and opens the gates to the 3 scalers.

After a long delay of about 0.1 secs (delay 3), during which time the tape transport mechanism has engaged and reached the correct speed, the actual tape writing procedure is started. The output of delay 3 is used to write a pulse (corresponding to a zero) on the lower track as an identi-

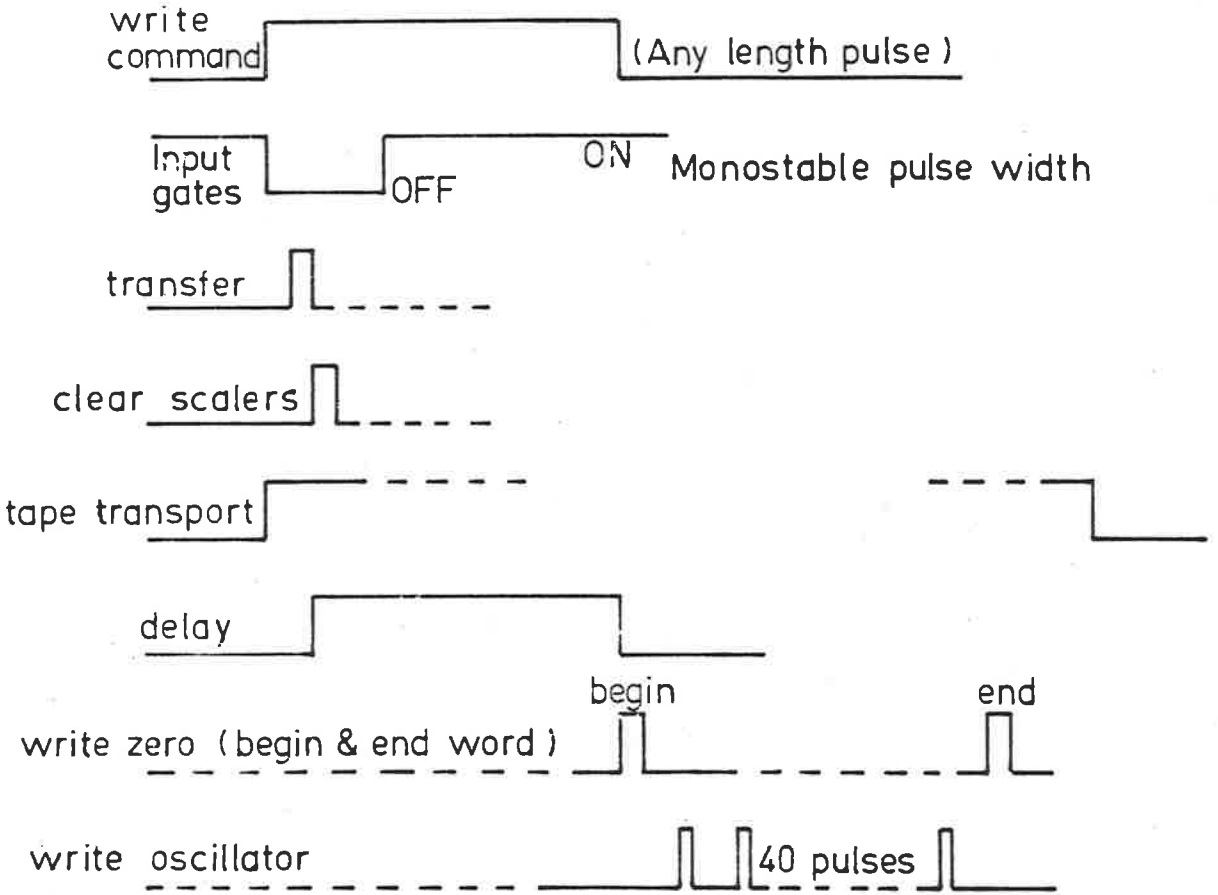

Fig. IV(d) The essential operations of the recording circuit

fication marker (begin word) after which (delay 4) the write oscillator starts. The write oscillator sends a write command pulse to both write amplifiers which write the state of the last bit of both shift registers onto the tape. This is followed (delay 5) by a shift of the shift register ready for the next write pulse from the write oscillator.

When all 40 bits have been shifted through the shift register and transferred onto tape, the shift scaler fills and sends a pulse which stops the write oscillator and writes a zero onto the lower track as an end of word recognition pulse. Finally after delay 6, the tape transport stops (R-S changes state).

The tape play back was designed to transfer the information from the tape into a multichannel analyser (R.I.D.L. model 34-12B), and its readout characteristics were therefore restricted to the mode particularly suitable to the analyser. Apart from transferring information, it was convenient to add scans in the analyser and this necessitated the use of a semi-serial output since the analyser did not have parallel add or subtract facilities. Also the use of the analyser restricted the play back of information to 40 bits corresponding to the channel number and 1 of the 3 input scalers at a time.

The most important feature of any tape reading system

is the check of correctness of the recorded information (i.e. checking against dropouts or spurious pulses on the tape). With only 2 tracks it was not possible to include a parity check; however, the read circuit was designed such that a word would only be accepted as correct provided that it consisted of 40 coincident pulses on both tracks as well as a begin and end of word recognition pulse.

A schematic of the tape read circuit is shown in Fig. IV(e) and the essential operational sequences in Fig. IV(f). The tape was played continuously at 15 i.p.s. and pulses from both tracks were amplified and fed into a pulse recognition circuit which essentially controlled the entire read sequence. The beginning of word pulse starts the read in R-S flip-flop which opens the shift gate and sets the exclusive OR gate to gate the lower track information into the lower 40 bit shift register. Subsequent pulses are read into the shift registers by setting appropriate high or low states at the shift register inputs and then generating shift pulses to clock the information into the shift register. After 40 coincident pulses, the end of word pulse changes the state of the read in R-S, which changes the exclusive OR gate such that it couples the two shift registers in series. The end of word pulse also transfers the last 4 bits (1 B.C.D. decade) into a count-down scaler, and after a brief delay

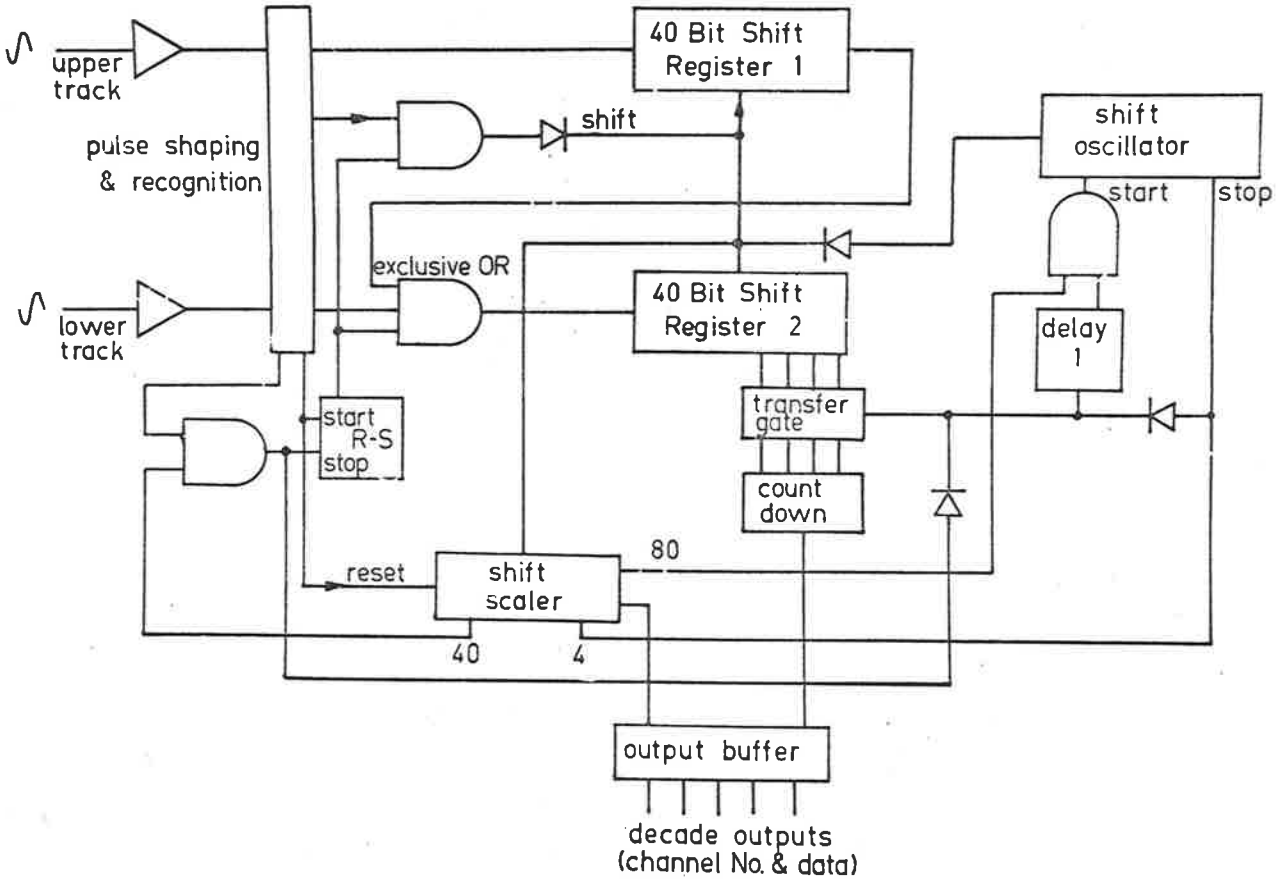

Fig. IV(e) Schematic of the tape playback circuit

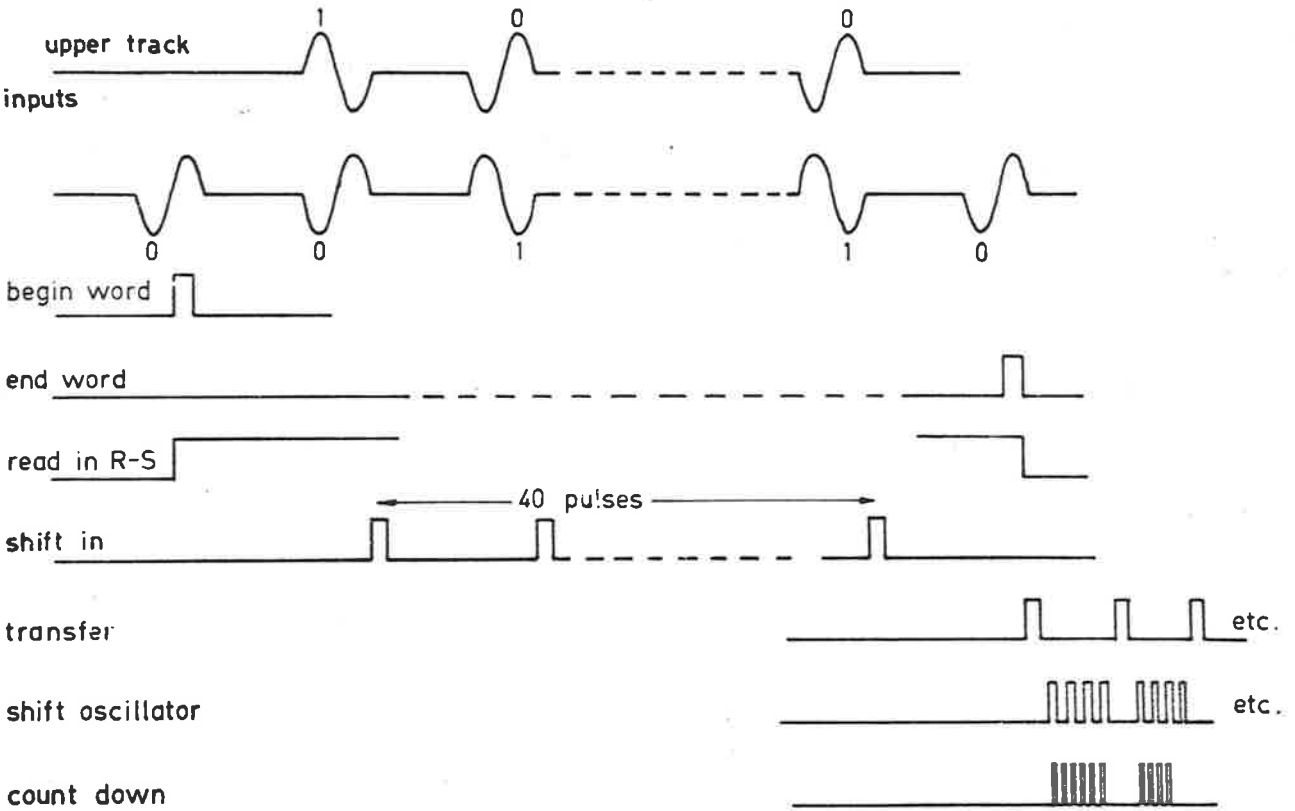

Fig. IV(f) Playback and readout sequence showing the essential operations

($\sim$ 1 μs), initiates a shift oscillator. This shifts the contents until stopped by a suitable command pulse. The command pulse comes from the second bit of the shift scaler and gives out a pulse for every 4 counts. Hence the shift is by 4 bits or 1 decade. The stopping pulse also initiates the transfer gate which transfers the contents into the count-down scaler. This process is repeated until all 80 bits have been shifted through the shift register and read out. After the 80^{th} bit, the shift scaler output (denoted by 80) inhibits the shift oscillator start.

The 4 bit count-down scaler, after receiving parallel information via the transfer gate, counts out the appropriate number of pulses and transmits them to an output buffer which consists of a number of gates which are controlled by the state of the shift scaler. Consequently the output serial information is channelled according to its position on the shift register or which section of the original tape written information it represented. The buffer can be set to transmit whichever section of the data is desired.

BIBLIOGRAPHY

Allison, A.C. & Dalgarno, A.
(1969) J.Q.S.R.T. 9, 1543.
(1970) Mol. Phys. 19, 567.

Bethke, G.W.
(1959a) J. Chem. Phys. 31, 662.
(1959b) J. Chem. Phys. 31, 669.

Born, M. & Oppenheimer, J.R.
(1927) Ann. Phys. 84, 457.

Browne, J.C.
(1969) Astrophys. J. 156, 397.

Ching, B.K., Cook, G.R. & Becker, R.A.
(1967) J.Q.S.R.T. 7, 323.

Cook, G.R. & Ching, B.K.
(1965) Report TDR-469 (9260-01)-4
(Aerospace Corporation).

C.R.C. Handbook of Chemistry & Physics
(1968) The Chem. Rubber Co. ed. Weast.

Dieke, G.H.
(1958) J. Mol. Spec. 2, 494.

Dieke, G.H. & Hopfield, J.J.
(1927) Phys. Rev. 30, 400.

Ehrenson, S. & Phillipson, P.E.
(1961) J. Chem. Phys. 34, 1224.

Evans, D.S.
(1965) Rev. Sci. Inst. 36, 375.

Frank, L.A., Henderson, N.K., Swisher, R.L.
(1969) Rev. Sci. Inst. 40, 685.

Fraser, P.A.
(1954) Can. J. Phys. 32, 515.

Geiger, J.
(1964) Z. Phys. 181, 413.

Geiger, J. & Schmoranzer, H.
(1969) J. Mol. Spec. 32, 39.

Geiger, J. & Topschowsky, M.
(1966) Z. Naturfor. 21a, 626.

Goody, R.M.
(1964) "Atmospheric Radiation I. A Theoretical Basis". (Oxford, Clarendon Press).

Haddad, G.N.
(1967) Ph.D. Thesis. (University of Adelaide).

Haddad, G.N., Lokan, K.H., Farmer, A.J.D. & Carver, J.H.
(1968) J.Q.S.R.T. 8, 1193.

Halmann, M. & Laulicht, I.
(1966) J. Chem. Phys. 46, 2684.

Halmann, M. & Laulicht, I.
(1968) J.Q.S.R.T. 8, 935.

Herzberg, G.
(1950) "Spectra of Diatomic Molecules". Second edit. (Van Nostrand: Princeton).

Herzberg, G. & Howe, L.L.
(1959) Can. J. Phys. 37, 636.

Herzberg, G. & Monfils, A.
(1960) J. Mol. Spec. 5, 482.

Hesser, J.E.
(1968) J. Chem. Phys. 48, 2518.

Hesser, J.E., Brooks, N.H. & Lawrence, G.M.
(1968) J. Chem. Phys. 49, 5388.

Hopfield, J.J.
(1930) Nature. 125, 927.

Hori, T.
(1927) Z. Phys. 44, 838.

Huffman, R.E., Larrabee, J.C. & Chambers, D.
(1965) App. Optics. 4, 1145.

Huffman, R.E., Larrabee, J.C. & Tanaka, Y.
(1965a) App. Optics. 4, 1581.

Huffman, R.E., Tanaka, Y. & Larrabee, J.C.
(1963) App. Optics. 2, 617.

Jeppesen, C.R.
(1933) Phys. Rev. 44, 165.
(1938) Phys. Rev. 54, 68.

Kelly, R.L.,
Report No. UCRL-5612 "Vacuum Ultra-Violet Emission Lines".
(Uni. of Calif.) Lawrence Radiation Lab.

King, G.W.
(1964) "Spectroscopy and Molecular Structure".
(Holt, Rinehart and Winston, Inc.).

Kolos, W.
(1968) Int. J. Quant. Chem. 2, 471.

Kolos, W. & Wolniewicz, L.
(1965) J. Chem. Phys. 43, 2429.
(1966) J. Chem. Phys. 45, 509.
(1968) J. Chem. Phys. 48, 3672.
(1969) J. Chem. Phys. 50, 3228.

Kronig, R. DeL. & Rabi, I.I.
(1927) Phys. Rev. 29, 262.

Lawrence, G.M.
(1965) J.Q.S.R.T. 5, 359.
(1971) Private communication.

Lurio, A., de Zafra, R.L. & Goshen, R.
(1964) Phys. Rev. 134a, 1198.

Lyman, T.
(1911) Astrophys. J. 33, 98.

Miller, K.J. & Krauss, M.
(1967) J. Chem. Phys. 47, 3754.

Mitchell, A.C.G. & Zemansky, M.W.
(1934) "Resonance Radiation & Excited Atoms".
(Cambridge U.P.).

Monfils, A.
(1961a) Bull. Acad. Roy. Belg. (Sciences) 47, 599.
(1961b) Bull. Acad. Roy. Belg. (Sciences) 47, 816.
(1965) J. Mol. Spec. 15, 265.

Namioka, T.
(1964a) J. Chem. Phys. 40, 3154.
(1964b) J. Chem. Phys. 41, 2141.
(1965) J. Chem. Phys. 43, 1636.

Newburgh, R.G., Heroux, L. & Hinteregger, H.W.
(1962) App. Optics. 1, 733.

Nicholls, R.W. & Stewart, A.L.
(1962) "Atomic and Molecular Processes"
ed. D.R. Bates. (Academic Press).

Pauling, L. & Wilson, E.B.
(1934) "Introduction to Quantum Mechanics".
(McGraw-Hill).

Peek, J.M. & Lassettre, E.N.
(1963) J. Chem. Phys. 38, 2392.

Pekeris, C.L.
(1934) Phys. Rev. 45, 98.

Rademacher, H. & Reiche, F.
(1927) Z. Phys. 41, 453.

Richardson, O.W.
(1930) Proc. Roy. Soc. A126, 482.
(1934) "Molecular Hydrogen and its Spectrum".
(Yale Uni. Press).

Roscoe, R.
(1941) Phil. Mag. 31, 349.

Rothenberg, S. & Davidson, E.R.
(1967) J. Mol. Spec. 22, 1.

Samson, J.A.R.
(1967) "Techniques of Vacuum Ultra-Violet Spectroscopy".
(John Wiley & Sons Inc. N.Y.).

Schadee, A.
(1964) Bull. Astronom. Inst. Netherlands. 17, 311.

Sharp, T.E.
(1971) Atomic Data. 2, 119.

Spindler, R.J. Jr.
(1969a) J.Q.S.R.T. 9, 597.
(1969b) J.Q.S.R.T. 9, 627.
(1969c) J.Q.S.R.T. 9, 1041.

Takezawa, S.
(1970) J. Chem. Phys. 52, 2575.

Tatum, J.B.
(1967) Astrophys. J. Supplement Series 14, 21.

Van der Held, E.F.M.
(1931) Z. Phys. 70, 508.

Varsavsky, C.M.
(1966) Space Sci. Rev. 5, 419.

Villarejo, D., Stockbauer, R. & Inghram, M.G.
(1968) Chem. Phys. Letters. 2, 11.
(1969) J. Chem. Phys. 50, 1754.

Werner, S.
(1927) Proc. Roy. Soc. A113, 107.

Wilkinson, P.G. & Byram, E.T.
(1965) App. Optics. 4, 581.

Witmer, E.E.
(1926) Proc. Nat. Acad. Sci. 12, 238.

Wolniewicz, L.
(1966) J. Chem. Phys. 45, 515.
(1969) J. Chem. Phys. 51, 5002.

Zaidel, A.N. & Schreider, E. Ya.
(1970) "Vacuum Ultra-Violet Spectroscopy".
(Ann Arbor - London).